THE UNIVERSITY
of EDINBURGH

Exploring the Parameter Space of Warm Inflation

Nico Kronberg

A thesis submitted in fulfilment of the requirements
for the degree of Doctor of Philosophy
to the
University of Edinburgh
August 2016

Abstract

Warm inflation is an implementation of exponential early-universe expansion that incorporates interactions between the inflaton field and its environment. These interactions allow the inflaton to dissipate some of its energy into other fields, which may then thermalise and form a radiation bath. A radiation bath present throughout inflation changes the inflaton dynamics and introduces thermal fluctuations that enhance the spectrum of primordial density perturbations. In the models we consider, the inflaton decays into the light particles of the radiation bath via heavy mediator particles. Warm inflation is subject to a complicated set of constraints which typically requires a large number of such mediator fields to be included in the model. The motivation for this work was to use the parametric dependence of the full low-temperature dissipation coefficient to uncover regimes where this number can be reduced.

Previous studies have examined primarily the low-momentum regime of the dissipation coefficient, where inflaton dissipation occurs via off-shell mediator particles. In the low-temperature regime, the production of on-shell mediators in the so-called pole regime suffers from Boltzmann suppression and was therefore thought to be negligible. It has been found, however, that the exponential suppression can be compensated by a sufficiently small effective coupling between the mediator fields and the light fields.

In this thesis, we present a numerical code that scans the parameter space of warm-inflation models including both the low-momentum and the pole contribution to the dissipation coefficient. We generate random values for the parameters of the model and the initial conditions of the field and the radiation density; we then solve the full equations of motion for the radiation density and the inflaton field using the general low-temperature dissipation coefficient. Our search includes chaotic, hybrid, and hilltop models, each of which inhabits

different regions of warm-inflation parameter space.

Our main finding is that the pole contribution to inflaton dissipation significantly extends the parameter ranges accessible to warm inflation. Specifically, we can achieve 50 e-folds of inflation and a spectral index compatible with Planck data with fewer mediator fields and smaller coupling constants. For instance, while low-momentum-dominated dissipation typically requires $\mathcal{O}(10^6)$ mediator fields, we find pole-dominated solutions with as few as $\mathcal{O}(10^4)$ for the quadratic hilltop potential. It is clear that the inclusion of the pole contribution opens up interesting model-building possibilities and that the parametric dependence of the full dissipation coefficient holds promise for achieving even greater reductions of the field content.

Lay Summary

In particle-physics models of inflation, the accelerated expansion of the very early universe is driven by the potential energy of a scalar field, the inflaton. In traditional models, the inflaton's interactions with other fields are negligible until the end of inflation, at which point they mediate the reheating of the universe. Warm inflation generalises this approach by considering the effects of inflaton interactions throughout the inflationary era.

In warm-inflation models, the inflaton is coupled to a set of heavy mediator particles that in turn interact with a set of light particles, which we will refer to as radiation. These interactions allow for the production of a thermalised radiation bath and lead to an additional friction term in the equation of motion of the inflaton field.

In this work, we have used a numerical code to examine the comparatively un-explored pole regime of warm inflation. Our code scans the parameter space of a set of monomial, hybrid, and hilltop potentials whilst taking into account both the pole and the more traditional low-momentum regime of warm inflation.

For most of the inflaton potentials under consideration, we have found parameter ranges that are compatible with Planck observations for the tilt of the primordial power spectrum and for the tensor-to-scalar ratio. Additionally, we were able to show that the inclusion of pole-dominated dissipation can significantly reduce the number of mediator fields that have to be introduced into the model. Whilst low-momentum-dominated dissipation typically requires $\mathcal{O}(10^6)$ mediator fields, we have found parameter regions that can sustain warm inflation with as few as $\mathcal{O}(10^4)$ extra fields. The inclusion of the pole contribution thus opens up interesting model-building possibilities that promise great reductions of the field content of warm-inflation models.

Declaration

Except where otherwise stated, the research undertaken in this thesis was the unaided work of the author. Where the work was done in collaboration with others, a significant contribution was made by the author.

N. Kronberg
August 2016

Acknowledgements

I would like to thank Martin Evans and Andrew Liddle for good advice and helpful interventions, Jane Patterson for support in all matters emotional and administrative, and Mar Bastero-Gil and my supervisor, Arjun Berera, for many useful conversations and contributions without which this thesis would not have been possible.

Publications

The work presented in this thesis is based on the following publication:

> Bastero-Gil, M., Berera, A., and Kronberg, N., *Exploring the Parameter Space of Warm-Inflation Models* (2015), accepted for publication in JCAP, arXiv:1509.07604.

Contents

List of Figures

Chapter 1

Introduction

1.1 Overview

The inflationary paradigm is part of the programme in theoretical physics that aims, at various levels, to understand the origin of our universe. Since the first models of inflation were introduced in the 1980s, they have made enormous progress explaining not only the remarkable uniformity of the observable universe but also the origins of the structures that we do see within it. Both uniformity and structure manifest themselves in the temperature distribution of the cosmic microwave background, which is isotropic down to 1 part in 10^5 and yet displays fluctuations with characteristic statistical properties. This level of uniformity is easily accomplished by inflating the universe so dramatically that what we can see of it was originally part of just one very small, fairly smooth and homogeneous region. Furthermore, inflation predicts a scale-invariant spectrum for the primordial density perturbations that, via the well-understood dynamics of the self-gravitating primordial plasma, evolve into the structures of the CMB. Since the COBE mission in the early 1990s, we have gathered an enormous amount of data about the temperature anisotropy and the polarisation of the cosmic microwave background, and all measurements to date have been in exquisite agreement with inflationary predictions.

In spite of the observational success of the basic framework of inflation, there remain many unsolved problems. One important unanswered question is how inflation is to be realised in particle physics. The inflationary universe can be conveniently described as one dominated by the potential energy of a scalar field,

the inflaton, that slowly rolls down along its potential-energy function. It is, however, unclear how best to embed the inflaton and its interactions in an overall particle-physics framework while still producing a sufficient amount of inflation and satisfying the observational constraints.

Warm inflation is part of this project to find a realistic microphysical model of the early universe. It is based on the generalisation that interactions of the inflaton with other fields are present throughout inflation, may change the field evolution, and lead to observably different predictions. In traditional models of inflation, such interactions are assumed to be negligible before the reheating phase that marks the transition to the radiation-dominated universe. In warm inflation, they lead to the dissipation of inflaton energy into other degrees of freedom. We will show in chapter 2 how dissipation arises from the thermal-field-theory description of the field dynamics. As we will see, dissipation can lead to the production of a thermal bath of radiation. The fluctuation–dissipation dynamics that underlie the interaction of the inflaton with the thermal bath will lead us to a Langevin-like equation of motion for the inflaton with an effective dissipation term acting as an additional friction. We will also showcase the two-stage mechanism for inflaton dissipation, where the inflaton, instead of coupling directly to the light particles of the radiation bath, produces heavy mediator fields which subsequently decay into the light particles.

In chapter 3, we will use this effective equation of motion to search the parameter space of several models of warm inflation for solutions that produce a sufficient amount of inflationary expansion and satisfy observational constraints on the tilt of the CMB power spectrum and the tensor-to-scalar ratio. We will pay particular attention to parameter regions where the dissipation is mediated by the on-shell production of the mediator particles, in contrast with the production of virtual particles, which has been the focus of most previous examinations of warm inflation.

First, however, let us spend the remainder of this chapter setting the scene. We begin by establishing the basic framework that describes the dynamics of the ΛCDM universe. We then introduce standard inflationary cosmology, describe the dynamics of an isolated inflaton whose potential energy dominates the universe, before giving a short overview of possible particle-physics realisations of such dynamics. We then discuss the observational evidence for inflation and end with

an overview of the dynamics of the reheating era.

1.2 Dynamics of the ΛCDM Universe

The Einstein equations describe the interaction between the spacetime geometry, defined by the metric $g_{\mu\nu}$ and the matter content of the universe,

$$R_{\mu\nu} - \tfrac{1}{2} g_{\mu\nu} R = -8\pi G T_{\mu\nu} \,, \tag{1.1}$$

where $R_{\mu\nu}$ is the Ricci tensor, $R = g_{\mu\nu} R^{\mu\nu}$ the Ricci scalar, $T_{\mu\nu}$ the energy-momentum tensor, and G Newton's gravitational constant. The Ricci tensor is defined as

$$R_{\mu\nu} = g^{\lambda\kappa} R_{\lambda\mu\kappa\nu} \,, \tag{1.2}$$

where $R_{\lambda\mu\kappa\nu}$ is the Riemann tensor, the unique tensor that can be constructed from the metric and its first and second derivatives while being linear in the second derivatives (Weinberg, 1972, Chapter 6.2). The Riemann tensor can be defined in terms of the Christoffel symbols

$$\Gamma^{\sigma}_{\lambda\mu} = \frac{1}{2} g^{\nu\sigma} \left\{ \frac{\partial g_{\mu\nu}}{\partial x^{\lambda}} + \frac{\partial g_{\lambda\nu}}{\partial x^{\mu}} - \frac{\partial g_{\mu\lambda}}{\partial x^{\nu}} \right\} , \tag{1.3}$$

and is then given by

$$R^{\lambda}{}_{\mu\nu\kappa} = \frac{\partial \Gamma^{\lambda}_{\mu\nu}}{\partial x^{\kappa}} - \frac{\partial \Gamma^{\lambda}_{\mu\kappa}}{\partial x^{\nu}} + \Gamma^{\eta}_{\mu\nu} \Gamma^{\lambda}_{\kappa\eta} - \Gamma^{\eta}_{\mu\kappa} \Gamma^{\lambda}_{\nu\eta} . \tag{1.4}$$

In a homogeneous, isotropic universe, the metric takes the Friedmann-Robertson-Walker (FRW) or Friedmann-Lemaître-Robertson-Walker (FLRW) form

$$\mathrm{d}s^2 = g_{\mu\nu} \mathrm{d}x^{\mu} \mathrm{d}x^{\nu} = \mathrm{d}t^2 - a^2(t) \left[\frac{\mathrm{d}r^2}{1 - kr^2} + r^2 \mathrm{d}\Omega^2 \right] , \tag{1.5}$$

where positive, negative, and vanishing values for the curvature parameter k correspond to a universe with open, closed, or flat geometry, respectively. The scale factor $a(t)$ gives the size of the universe at time t relative to its size today. It is related to the redshift z of radiation, emitted with a wavelength λ_{em} and observed at a wavelength λ_{obs}, by $1 + z = \lambda_{\mathrm{obs}} / \lambda_{\mathrm{em}} = a(t)^{-1}$.

In an FRW universe, the Einstein equations simplify to a set of two ordinary

differential equations that describe the evolution of the scale factor a and are sometimes referred to as the Friedmann equations. The $(0,0)$ component of the Einstein equation yields the acceleration equation

$$\frac{\ddot{a}}{a} = -\frac{1}{6m_{\rm P}^2}(\rho + 3p)\,, \tag{1.6}$$

while the (i,i) components yield

$$\frac{\ddot{a}}{a} + \frac{2\dot{a}^2}{a^2} + \frac{2k}{a^2} = \frac{1}{2m_{\rm P}^2}(\rho - p)\,. \tag{1.7}$$

By eliminating $\ddot{a}$ from these, we obtain the Friedmann equation

$$\left(\frac{\dot{a}}{a}\right)^2 = \frac{1}{3m_{\rm P}^2}\rho - \frac{k}{a^2}\,. \tag{1.8}$$

It is common to define the Hubble expansion rate $H = \dot{a}/a$, and the critical density $\rho_{\rm c} = 3m_{\rm P}^2 H^2$, where we have used the reduced Planck mass $m_{\rm P} = 1/\sqrt{8\pi G} \simeq 2.43 \times 10^{18}\,\text{GeV}$. The Hubble rate today is $H_0 = H(a_0) = 67.51\,\text{km/s/Mpc}$ (Ade *et al.*, 2015b), leading to a value of the critical density today equivalent to about 5.1 protons per m^3, on average. The Friedmann equation (1.8) can be expressed in terms of the density parameters $\Omega_i = \rho_i/\rho_{\rm c}$ for different components with energy densities ρ_i,

$$\Omega_{\rm tot}(t) = \sum_i \Omega_i = 1 + \frac{k}{(aH)^2}\,. \tag{1.9}$$

A flat universe, $k = 0$, hence corresponds to $\Omega_{\rm tot} = 1$ and therefore to a total energy density equal to the critical density. Observationally, Planck data, lensing reconstruction, and BAO indicate that the universe we live in is indeed very flat, with $\Omega_k = k/(aH)^2 = 0.000 \pm 0.005$ (Ade *et al.*, 2015b).

In a universe with the FRW metric, the energy-momentum tensor is that of a perfect fluid,

$$T_{\mu\nu} = (\rho + p)u_\mu u_\nu - p g_{\mu\nu}\,. \tag{1.10}$$

The velocity 4-vector u_μ is given by $u_\mu = (1,0,0,0)$, and the energy density ρ

and pressure p satisfy the continuity equation

$$T^{\mu\nu}{}_{;\nu} = \dot{\rho} + 3\left(\frac{\dot{a}}{a}\right)(\rho + p) = 0 \quad \Leftrightarrow \quad \frac{\mathrm{d}\ln\rho}{\mathrm{d}\ln a} = -3(1+w)\,, \tag{1.11}$$

where we have introduced the equation-of-state parameter $w \equiv p/\rho$. This equation tells us how the density ρ_i of an energy component with equation of state w_i evolves as a function of the scale factor,

$$\rho_i \propto \exp\left(-\int_0^a \frac{\mathrm{d}a'}{a'} 3(1+w_i)\right), \tag{1.12}$$

which, for constant w_i, implies

$$\rho_i \propto a^{-3(1+w_i)}\,. \tag{1.13}$$

Furthermore, the equation of continuity (1.11) and the time derivative of the Friedmann equation (1.8) can be combined to give the time evolution of the Hubble rate,

$$H = \frac{2}{3(1+w)t} \qquad (w \neq -1)\,, \tag{1.14}$$

and hence

$$a(t) \propto t^{\frac{2}{3(1+w)}}\,. \tag{1.15}$$

Traditionally, a few special cases for the equation of state are important for the evolution of the universe: pressureless matter, that is, dark or non-relativistic baryonic matter, has $w_\mathrm{m} = 0$, and ultra-relativistic radiation has $w_\mathrm{r} = \frac{1}{3}$. These values lead to the following evolutions,

$$\text{radiation domination:} \qquad a \propto t^{1/2}\,, \quad \rho_\mathrm{r} \propto a^{-4}\,, \tag{1.16}$$

$$\text{matter domination:} \qquad a \propto t^{2/3}\,, \quad \rho_\mathrm{m} \propto a^{-3}\,. \tag{1.17}$$

Both cases exhibit decelerated expansion, $\ddot{a} < 0$.

The special case of an energy component with $w_\Lambda = -1$ is referred to as a cosmological constant Λ. The behaviour of a matterless universe dominated by a cosmological constant was first investigated by de Sitter (1917), and we find, for such a universe,

$$\rho_\Lambda = \text{const.}, \qquad a \propto \mathrm{e}^{Ht}. \tag{1.18}$$

Hence, the expansion of a Λ-dominated universe speeds up over time. An interesting aspect of the de Sitter universe is the existence of an event horizon: objects beyond a certain distance recede from us at a speed greater than the speed of light and are hence hidden from us—their light is infinitely redshifted. As the expansion keeps accelerating, the comoving horizon shrinks until only gravitationally bound objects, decoupled from the background expansion, remain accessible to us. In the distant future, then, only our Local Group of galaxies will be visible to astronomers, any information on the history of our universe and even the very fact that it is expanding at all being obscured by the de Sitter horizon. Even though inhabitants of this island universe would be able to infer a finite age of the universe from standard stellar evolution, they would have no means of probing its origins or evolution (Krauss and Scherrer, 2007).

More generally, accelerated expansion, $\ddot{a} > 0$, occurs whenever the average equation of state of the universe is $w < -1/3$, as can be seen from equation (1.6). A generic energy component with $w < -1/3$ is referred to as dark energy, and a popular parametrisation for its equation of state is given by $w_{\mathrm{DE}} = w_0 + (1-a)w_a$ (Chevallier and Polarski, 2001; Linder, 2003). It was discovered in the late 20th century that the universe is indeed undergoing such an era of accelerated expansion at the moment (Riess *et al.*, 1998; Perlmutter *et al.*, 1999)[1]; current observations are compatible with the energy component responsible being a cosmological constant, that is, $w_0 = -1$ and $w_a = 0$ (Ade *et al.*, 2015b).

A particularly exciting possibility for the future of a universe dominated by dark energy that is not a cosmological constant is that of so-called phantom energy with $w < -1$. In this case, the scale factor diverges and reaches a singularity, the so-called big rip, at a finite time in the future (Caldwell *et al.*, 2003). All bound structures in the universe, including galaxies, planets, and eventually atoms would be ripped apart some time before the singularity. If the equation of state were as small as $w_{\mathrm{DE}} = -3/2$, for instance—a case that can be ruled out with confidence (Ade *et al.*, 2015b)—, the big rip would occur in approximately 22 billion years, with the Earth being ripped apart about 30 minutes before the singularity (Caldwell *et al.*, 2003).

Given this understanding of how the densities of various energy components evolve with the expansion of the universe, it is often convenient to rewrite the

[1]It is one of the great problems of theoretical physics why the observed dark-energy component is as small as it is; a classic review on this topic can be found in (Weinberg, 1989).

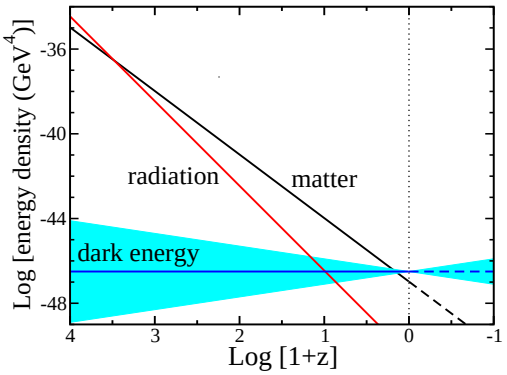

Figure 1.1: Scaling of matter, radiation, and dark energy with $w = -1.0 \pm 0.2$, represented by the blue band (Frieman et al.*, 2008).*

Friedmann equation (1.8) in terms of density parameters and their dependence on a,

$$\frac{H^2}{H_0^2} = \Omega_\mathrm{r}\, a^{-4} + \Omega_\mathrm{m}\, a^{-3} + \Omega_k\, a^{-2} + \Omega_\mathrm{DE} \exp\left(- \int_0^a \frac{\mathrm{d}a'}{a'} 3(1 + w_\mathrm{DE}) \right) . \qquad (1.19)$$

If dark energy is a cosmological constant ($w = -1$), of course, the last term simplifies to a constant Ω_Λ. These scalings and the associated changes in which component dominates are illustrated in figure (1.1) in terms of the redshift $1+z = 1/a$. The latest observations indicate that the modern universe is made up of about 4.9% baryonic matter, 26.2% cold dark matter, and 68.9% dark energy, with a radiation contribution that is negligible today.

An era of accelerated expansion in the very early universe was first suggested by Guth (1981) under the name of inflation. Around the same time, a number of related proposals for the description of the very early universe emerged (Brout *et al.*, 1978; Starobinsky, 1980; Fang, 1980; Sato, 1981). We will introduce the rationale for an early era of accelerated expansion in the following section, where we also establish the formal description of inflation as driven by the dynamics of a potential-energy-dominated scalar field.

1.3 Inflationary Cosmology

1.3.1 Cosmological Puzzles

The development of the theory of inflation was, to a large extent, prompted by a handful of cosmological and astronomical observations that lay outside the scope of the hot-big-bang model alone. The most prominent amongst these observations are the startling homogeneity and flatness of the cosmos, as well as the absence of monopoles and other topological defects produced during phase transitions in the early universe. For a more detailed discussion, consult, for example, (Linde, 2005, section 1.5) and references therein or (Baumann, 2009, chapter 4).

The Horizon Problem

The comoving particle horizon

$$\tau \equiv \int_0^t \frac{\mathrm{d}t'}{a(t')} = \int_0^a \mathrm{d}\ln a' \frac{1}{a'H(a')}\,, \tag{1.20}$$

represents the distance light travels by the time t; it is the greatest separation at which two points were in causal contact at some point in the past. The quantity $(aH)^{-1} = H_0^{-1} a^{\frac{1}{2}(1+3w)}$ in the integral is the comoving Hubble radius and can be thought of as an instantaneous comoving horizon: if H were constant and the linear Hubble law $v = H_0 d$ were an exact description of the recession velocities of distant galaxies at all times, the comoving Hubble horizon would be that comoving distance at which galaxies recede from us at the speed of light—anything further away would be unobservable to us. In a universe dominated by radiation ($w_\mathrm{r} = \frac{1}{3}$) or matter ($w_\mathrm{m} = 0$), the comoving particle horizon grows monotonically,

$$\tau \propto \begin{cases} a & \text{radiation} \\ a^{1/2} & \text{matter} \end{cases}\,. \tag{1.21}$$

This growing causal horizon implies that structures on length scales entering the horizon today have never been in causal contact before. Moreover, extrapolating the evolution of the horizon back to when the cosmic microwave background (CMB) radiation was released, around 380 000 years after the big bang, it is possible to show that the CMB is made up of a great number of regions that were

causally unconnected at the time.

Nevertheless, in the latter part of the 20th century, the COBE mission (Smoot *et al.*, 1992) and other experiments found a temperature variation in the cosmic microwave background (excluding the dipole) on the order of only 1 part in 10^5. It is extremely unlikely that a large number of causally unconnected regions in the early universe would have arrived at the same temperature to such extraordinary precision to by random chance.

The Flatness Problem

The Friedmann equation (1.9) tells us that a flat universe ($k = 0$) corresponds to $\Omega(a) = 1$ and that the quantity $|1 - \Omega|$ is proportional to the square of the comoving Hubble horizon, $(aH)^{-1} = H_0^{-1} a^{\frac{1}{2}(1+3w)}$. Since the Hubble horizon increases in both a radiation- and a matter-dominated universe, the quantity $|1 - \Omega|$ diverges with time—the universe is driven away from the unstable fixed point that represents flatness.

Finding that the universe is very nearly flat today (Ade *et al.*, 2015b), we need it to be even closer to flatness at early times, requiring that during the GUT era ($10^{16}\,\mathrm{GeV}$), for instance, $|1 - \Omega| \leq \mathcal{O}(10^{-55})$. Again, such exquisite fine tuning begs an explanation.

The Monopole Problem

It is widely assumed that during the early evolution of the cosmos, a number of fundamental symmetries (GUT symmetries, for instance) were broken when the universe cooled below the corresponding critical temperatures.

In the case of discrete symmetries, it is natural to assume that in causally unconnected regions of space the symmetry breaks to, in general, different ground states; these regions are then separated by domain walls. As it turns out, however, the energy density of such domain walls is so high that their presence in the observable universe would have a strong influence on the CMB anisotropy and can be ruled out (Zeldovich *et al.*, 1974).

Furthermore, the production of a large number of magnetic monopoles is a generic prediction of the breakdown of many GUT theories in the early universe. The large energy density associated with these monopoles would, however,

overclose the universe, that is, the universe would have recollapsed long before now if the monopoles were present in the numbers predicted by particle physics.

1.3.2 Inflation to the Rescue

To understand how inflation solves the horizon problem, consider equation (1.20). The comoving particle horizon τ is the distance beyond which particles could never have communicated; the comoving Hubble radius $(aH)^{-1}$, on the other hand, is the distance beyond which particles cannot communicate at a given time. It is quite possible for τ at any given time to be much greater than $(aH)^{-1}$, such that particles that are out of causal contact today may have been able to communicate in the past. This could be achieved if there had been a phase of decreasing Hubble radius in the history of the universe, such that $(aH)^{-1}$ was much greater in the early universe and therefore early times contributed more to the integral (1.20) than late times. The horizon problem is thus solved if thermal equilibrium across some small portion of the universe was established before the Hubble radius shrank far below the size of that domain. The entire observable universe would then be contained within one such region, explaining the overwhelming homogeneity we observe today.

Conveniently, a shrinking Hubble radius also solves the flatness problem. The Friedmann equation of a non-flat ($k = \pm 1$) universe can be written as $|1-\Omega(a)| = (aH)^{-2}$, such that decreasing $(aH)^{-1}$ drives the universe towards flatness, $\Omega = 1$. In fact, the enormous reduction of the Hubble radius that is required by the horizon problem can drive the universe so close to flatness early on that the flatness we measure today is perfectly plausible.

Using the Friedmann equation (1.6), we can rewrite the requirement for a shrinking comoving Hubble radius as

$$\frac{\mathrm{d}}{\mathrm{d}t}\left(\frac{1}{aH}\right) < 0 \quad \Rightarrow \quad \frac{\mathrm{d}^2 a}{\mathrm{d}t^2} > 0 \quad \Rightarrow \quad \rho + 3p = \rho(1+3w) < 0\,. \tag{1.22}$$

Requiring a shrinking comoving Hubble radius is therefore equivalent to accelerated expansion and dominance of fluid with negative pressure $p < -\rho/3$. This era of accelerated expansion in the early universe is what we refer to as inflation.

1.3.3 Scalar Fields and Slow Roll

In the inflationary paradigm, the conditions for accelerated expansion are realised by having the inflationary universe dominated by a scalar field ϕ, referred to as the inflaton. The Friedmann equation of a universe dominated by ϕ is

$$H^2 = \frac{1}{3m_{\mathrm{P}}^2}\left(\frac{1}{2}\dot{\phi}^2 + V(\phi)\right) , \tag{1.23}$$

where $V(\phi)$ is the potential describing the interactions and mass of ϕ. The equation of motion for a homogeneous scalar field is

$$\ddot{\phi} + 3H\dot{\phi} + V_\phi = 0 \,, \tag{1.24}$$

where $V_\phi = \partial V/\partial\phi$; its equation of a state is

$$w_\phi = \frac{p_\phi}{\rho_\phi} = \frac{\frac{1}{2}\dot{\phi}^2 - V(\phi)}{\frac{1}{2}\dot{\phi}^2 + V(\phi)}. \tag{1.25}$$

The condition $w < -\frac{1}{3}$ for accelerated expansion can be easily satisfied if the potential energy V dominates over the kinetic energy $\frac{1}{2}\dot{\phi}^2$. It is common to use the slow-roll approximation where $\frac{1}{2}\dot{\phi}^2 \ll V(\phi)$, implying $\ddot{\phi} \ll V_\phi$ and $\ddot{\phi} \ll H\dot{\phi}$. The evolution equations then simplify to

$$H^2 \simeq \frac{1}{3m_{\mathrm{P}}^2}V(\phi) \,, \qquad 3H\dot{\phi} + V_\phi \simeq 0 \,. \tag{1.26}$$

For consistency of the approximation, we have to require a very flat potential

$$\epsilon = \frac{m_{\mathrm{P}}^2}{2}\left(\frac{V_\phi}{V}\right)^2 \ll 1 \,, \qquad \eta = m_{\mathrm{P}}^2\left(\frac{V_{\phi\phi}}{V}\right) \ll 1 \,, \tag{1.27}$$

where, roughly, ϵ determines whether the slope is small enough for the energy density of the scalar field to be dominated by its potential energy, and η controls whether potential domination can be sustained for sufficiently long before the potential becomes too steep.

The amount of expansion produced by the inflationary era is measured in terms of e-foldings N_{e}, where $a_{\mathrm{end}}/a = \mathrm{e}^{N_{\mathrm{e}}}$. The number of e-folds before inflation

ends is given by

$$N_{\rm e}(\phi) = \int_t^{t_{\rm end}} H{\rm d}t = \int_\phi^{\phi_{\rm end}} \frac{H}{\dot\phi}{\rm d}\phi \approx \frac{1}{m_{\rm P}^2}\int_{\phi_{\rm end}}^{\phi} \frac{V}{V_\phi}{\rm d}\phi \approx \frac{1}{m_{\rm P}}\int_{\phi_{\rm end}}^{\phi} \frac{{\rm d}\phi}{\sqrt{2\epsilon}}\,. \quad (1.28)$$

In order to solve the horizon and flatness problems, between 40 and 60 e-foldings of observable inflation are necessary. Observable inflation refers to the amount of inflation after the point in time when the largest scales of the observable universe crossed the horizon and the fluctuations in the CMB were created. It is assumed that a (very) large amount of inflation preceded the creation of these inhomogeneities, but that era is inherently inaccessible to observation.

1.3.4 Observables

During inflation, quantum fluctuations of the inflaton field lead to perturbations of the energy density or, equivalently, the spatial curvature in the early universe. Accessible derivations of the form of these perturbations can be found in, for example, Baumann (2009) or Lyth and Riotto (1999). Here, we will focus on the main results relevant to this work, that is, the tilt $n_{\rm s}$ of the primordial perturbation spectrum and the tensor-to-scalar ratio r.

Since the dynamics of the spacetime metric are related, by the Einstein equations, to the energy content of the universe, quantum fluctuations of the inflaton induce perturbations in the metric. To first order, the most general form of the perturbed spatially flat FRW metric is

$$\begin{aligned} {\rm d}s^2 &= g_{\mu\nu}{\rm d}x^\mu{\rm d}x^\nu \\ &= -(1+2\Phi){\rm d}t^2 + 2a(t)B_i{\rm d}x^i{\rm d}t + a(t)^2[(1-2\Psi)\delta_{ij} + E_{ij}]{\rm d}x^i{\rm d}x^j\,. \end{aligned} \quad (1.29)$$

It is important to note that when we separate a given quantity into its background value and a perturbation to that background, this distinction is not unique. Instead, our choice of coordinates, our gauge choice, can introduce fictitious perturbations. When analysing perturbations, it is therefore useful to consider gauge-invariant combinations of metric and matter perturbations. Two of the most common gauge-invariant variables for connecting the theory to

observations are the curvature perturbation on uniform-density hypersurfaces

$$-\zeta \equiv \Psi + \frac{H}{\dot{\overline{\rho}}}\delta\rho, \tag{1.30}$$

and the comoving curvature perturbation

$$\mathcal{R} \equiv \Psi - \frac{H}{\overline{\rho}+\overline{p}}\delta q\,, \tag{1.31}$$

where δq is the scalar part of the 3-momentum density $T^0_i = \partial_i \delta q$. ζ and $\mathcal{R}$ are equal on super-horizon scales $k \ll aH$ and during slow-roll inflation. Furthermore, $\mathcal{R}$ is constant on super-horizon scales; perturbations with comoving wave number k are said to "freeze in" as soon as the comoving Hubble horizon shrinks so far that $k^{-1} > (aH)^{-1}$. Curvature perturbations on scales $k < aH$ stop evolving until, after inflation, the horizon grows to be larger than k^{-1} once again.

For the link between perturbation theory and cosmological observation, we can define the power spectrum of the comoving curvature perturbation in terms of its autocorrelation function,

$$\langle \mathcal{R}_{\mathbf{k}} \mathcal{R}_{\mathbf{k}'} \rangle = (2\pi)^3\, \delta(\mathbf{k}+\mathbf{k}')\, P_{\mathcal{R}}(k)\,, \qquad \Delta^2_{\mathrm{s}} \equiv \Delta^2_{\mathcal{R}} = \frac{k^3}{2\pi^2} P_{\mathcal{R}}(k)\,. \tag{1.32}$$

Here, the mode $\mathcal{R}_{\mathbf{k}}$ is given by the Fourier transform

$$\mathcal{R}_{\mathbf{k}} = \int \mathrm{d}x^3\, \mathcal{R}(x)\, \mathrm{e}^{-\mathrm{i}\mathbf{k}x}. \tag{1.33}$$

We can make an analogous definition for the two tensor polarisations $h^+, h^\times$ and find the following slow-roll expressions for the power spectra of the scalar and tensor perturbations created during inflation,

$$\Delta^2_{\mathrm{s}}(k) = \Delta^2_{\mathcal{R}}(k) = \frac{1}{8\pi^2}\frac{H^2}{m^2_{\mathrm{P}}}\frac{1}{\epsilon}\bigg|_{k=aH}\,, \quad \Delta^2_{\mathrm{t}}(k) \equiv 2\Delta^2_h(k) = \frac{2}{\pi^2}\frac{H^2}{m^2_{\mathrm{P}}}\bigg|_{k=aH}\,. \tag{1.34}$$

Different k modes leave the horizon at different times; as the inflaton rolls slowly down its potential, both H and ϵ also change slowly during inflation, and the power spectra therefore have a slight scale dependence, given by their spectral indices,

$$n_{\mathrm{s}} - 1 \equiv \frac{\mathrm{d}\ln\Delta^2_{\mathrm{s}}}{\mathrm{d}\ln k} = 2\eta - 6\epsilon\,, \quad n_{\mathrm{t}} \equiv \frac{\mathrm{d}\ln\Delta^2_{\mathrm{t}}}{\mathrm{d}\ln k} = -2\epsilon\,. \tag{1.35}$$

During slow roll, we therefore expect $n_\mathrm{s} - 1 \ll 1$ and $n_\mathrm{t} \ll 1$; scale invariance would correspond to $n_\mathrm{s} = 1$ and $n_\mathrm{t} = 0$. It is common to approximate the power spectra as power laws,

$$\Delta^2_\mathrm{s}(k) = A_\mathrm{s}(k_\star) \left(\frac{k}{k_\star}\right)^{n_\mathrm{s}(k_\star)-1+\frac{1}{2}\alpha_\mathrm{s}(k_\star)\ln(k/k_\star)} , \quad \Delta^2_\mathrm{t}(k) = A_\mathrm{t}(k_\star) \left(\frac{k}{k_\star}\right)^{n_\mathrm{t}(k_\star)} , \tag{1.36}$$

where $k_\star$ is an arbitrary reference point known as the pivot scale, and we have included a possible running of the spectral index, $\alpha_\mathrm{s} \equiv \frac{\mathrm{d}n_\mathrm{s}}{\mathrm{d}\ln k}$.

A useful quantity for discriminating between inflationary models is the ratio r of the tensor to the scalar perturbations; in the slow-roll approximation, it is given by

$$r \equiv \frac{\Delta^2_\mathrm{t}}{\Delta^2_\mathrm{s}} = 16\epsilon_\star , \tag{1.37}$$

where $(\ldots)_\star$ represents the value at horizon crossing $k = aH$. During slow-roll, it is possible to establish a relationship between the tensor-to-scalar ratio and the inflaton field excursion $\Delta\phi$ over the entire course of observable inflation (Lyth, 1997),

$$\frac{\Delta\phi}{m_\mathrm{P}} \simeq \left(\frac{r}{0.01}\right)^{1/2} . \tag{1.38}$$

Observationally detectable values $r \gtrsim 0.01$ therefore usually require changes in the inflaton field of order the Planck scale, which can be difficult to realise in particle-physics models of inflation.

1.3.5 Particle-Physics Implementations

Historical Overview

While the evidence for the existence of an era of inflation in the early universe is very compelling, there is still a great deal of uncertainty about the underlying particle physics. An overview of popular models is given by, for example, Lyth and Riotto (1999); Lyth and Liddle (2009).

The first model of inflation was proposed by Starobinsky (1980), who found deSitter solutions to the Einstein equations in the presence of massless, conformally covariant matter fields. Shortly after, Guth (1981) proposed a model of inflation that relied on a first-order phase transition of the universe: during inflation, the inflaton sits in a local minimum of its potential, where its potential

energy drives the accelerated expansion; at some point, it tunnels down to the global minimum, abruptly ending inflation via a first-order phase transition. It was quickly (even in the original paper) recognized that the ensuing process of bubble nucleation would lead to inhomogeneities grossly incompatible with observations.

Guth's model, now known as old inflation, was abandoned soon after its publication and replaced by what is called new inflation (Linde, 1982; Albrecht and Steinhardt, 1982). New inflation has a GUT Higgs field acting as the inflaton, slowly rolling away from a maximum of the potential located at the origin. Inflation ends as the field starts to oscillate about the minimum of the potential at some finite field value $\langle\phi\rangle$. The model was complicated by assuming that the initial conditions for the inflaton evolution be set by an era of thermal equilibrium. Additionally, the slow-roll conditions require the potential plateau near the origin to be extremely flat, which requires a certain amount of fine tuning.

Later on, Linde (1983) proposed a new class of models that allowed for inflation under much more generic conditions. Moving in a monomial potential $V(\phi) \propto \phi^p$, the inflaton starts out at very large values $\phi > m_\mathrm{P}$, where the lower power of ϕ in V' and V'' allows for slow-roll inflation, $\epsilon, \eta \ll 1$. Put another way, large field values lead to large energy densities, which, via the Friedmann equation, give large values of the Hubble function; this causes the Hubble friction to overdamp the motion of the inflaton, as is characteristic of slow-roll inflation. As the initial field values are expected to be randomly distributed, with inflation occurring in any patches of the universe where the field is sufficiently large and homogeneous, these models are referred to as models of chaotic inflation. Chaotic models with $p \geq 4$, have now been ruled out by observations of the cosmic microwave background (Kinney *et al.*, 2008; Finelli *et al.*, 2010).

While chaotic inflation represented a significant step forward in showing that inflation can occur under very generic conditions, it also requires large, trans-Planckian values for the inflaton field. These are, of course, perfectly permissible as long as the energy density V remains below the Planck density m_P^4, where quantum-gravitational effects are expected to become important. They do, however, make it very difficult to find a particle-physics motivation for chaotic potentials.

By contrast, hybrid models of inflation manage to keep the inflaton well below

the Planck scale by invoking additional fields that generate a sufficient amount of vacuum energy. Hybrid models are therefore small-field and multi-field models, as opposed to the single-field and the large-field models considered before.

Hybrid Inflation

In hybrid models of inflation (see, for example, the original publication by Linde (1991) and a detailed discussion by Copeland *et al.* (1994)), more than one field is responsible for generating a sufficient amount of inflation. The bulk of the potential energy is due to one or more "waterfall fields" trapping the inflaton in a false vacuum state at a large and constant energy V_0. As the inflaton field slowly evolves along its effective potential, it eventually reaches a critical value where the waterfall fields destabilize and stop confining it at high potential energy. Inflation then ends as the inflaton quickly moces down to the global minimum of its potential.

The simplest implementation of the hybrid mechanism involves one waterfall field χ and the inflaton σ moving in the potential

$$V(\chi,\sigma) = V_0 - \frac{1}{2}m_\chi^2\chi^2 + \frac{1}{4}g\chi^4 + \frac{1}{2}m^2\sigma^2 + \frac{1}{4}\lambda^2\chi^2\sigma^2 \tag{1.39}$$

$$= \kappa^2\left(M^2 - \frac{1}{4}\chi^2\right)^2 + \frac{1}{2}m^2\sigma^2 + \frac{1}{4}\lambda^2\chi^2\sigma^2\,, \tag{1.40}$$

where we have identified

$$g = \frac{\kappa^2}{4}\,, \quad m^2 = \kappa^2 M^2\,, \quad V_0 = \kappa^2 M^4 = M^2 m_\psi^2\,. \tag{1.41}$$

For inflaton values $\sigma^2 > \sigma_\mathrm{c}^2 = 2\kappa^2M^2/\lambda^2$, the minimum on constant-σ slices is located at $\chi = 0$. During inflation, the waterfall field χ sits in this false vacuum, leaving σ to move in the effective potential

$$V(\sigma) = \kappa^2 M^4 + \frac{1}{2}m^2\sigma^2\,. \tag{1.42}$$

Once the inflaton reaches $\sigma = \sigma_\mathrm{c}$, the minimum at $\chi = 0$ turns into a local maximum, χ destabilizes, and the fields quickly move to their true vacuum values, $\chi = 2M$, $\sigma = 0$. This change in the shape of the potential is illustrated in figure 1.2.

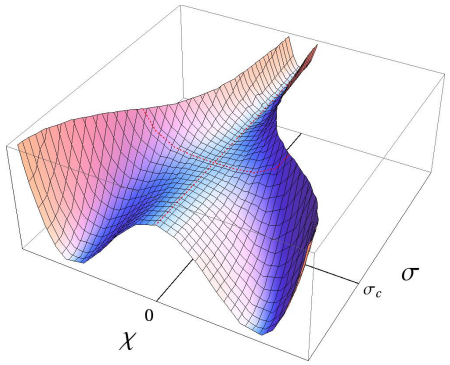

Figure 1.2: Hybrid inflation potential. The inflaton field σ moves along the minimum at $\chi = 0$ until it reaches the critical value where the waterfall field χ is destabilized and moves down to its true vacuum.

In addition to the waterfall instability, hybrid models retain, of course, the ability to end inflation via the usual break-down of the slow-roll conditions: If the potential becomes too steep along the $\chi = 0$ trajectory, inflation ends, even though the waterfall field stays trapped in the false vacuum until $\sigma < \sigma_c$.

Supersymmetric Hybrid Inflation

While there exist modifications of the Standard Model in which the Higgs field, equipped, for example, with a non-trivial coupling to the Ricci scalar (Bezrukov and Shaposhnikov, 2008), can act as the inflaton, most particle-physics models of inflation assume that new degrees of freedom dominate the inflationary dynamics. Many of these extensions invoke supersymmetry (SUSY) to solve, the problem of the radiative instability of scalar masses, thus keeping loop corrections to the inflaton potential under control. As a side effect, supersymmetric models naturally contain additional scalar fields that may act as the inflaton.

Unfortunately, we lack the space in this report to provide the reader with a comprehensive introduction to the fascinating and elegant theory of supersymmetry. The standard textbook on the subject is Wess and Bagger (1992); good reviews are given in, amongst others, Drees (1996), Martin (1997), and Aitchison (2005); the advanced reader may wish to consult Nilles (1984) or Weinberg (2000).

Particles in a supersymmetric theory can be described in terms of multi-component superfields. In a globally supersymmetric theory, the interactions of the scalar components ϕ_i of these superfields are derived from the superpotential

W, which is a holomorphic function of the ϕ_i, but not their hermitian conjugates $\overline{\phi}_i$. The scalar potential is then given in terms of the superpotential by

$$V_{\text{global}} \equiv W^i W_i + D\text{-term}\,, \tag{1.43}$$

where upper and lower indices represent differentiation with respect to ϕ_i and $\phi^{i\star}$, respectively.

For conceptual reasons, it is desirable to treat local supersymmetry, known as supergravity (SUGRA), instead. The potential is then

$$V = \mathrm{e}^{K/m_{\mathrm{P}}^2}\left(\left(K^{-1}\right)_i^{\ j} F^i F_j - 3\frac{|W|^2}{m_{\mathrm{P}}^2}\right) + D\text{-term}\,, \tag{1.44}$$

where we have defined $F^i = W^i + K^i W/m_{\mathrm{P}}^2$. The Kähler potential K is a real function of the complex scalar fields ϕ_i and $\overline{\phi}_i$ that can be expanded as $K = \sum_i |\phi_i|^2 + \cdots$, where the dots represent higher-order terms. The global-supersymmetry potential therefore receives supergravity corrections (Copeland *et al.*, 1994)

$$V = V_{\text{global}}\left(1 + \frac{1}{m_{\mathrm{P}}^2}\sum_i |\phi_i|^2 + \text{other terms}\right) + \text{other terms}\,, \tag{1.45}$$

which generically leads to a contribution $V_{\text{global}}/m_{\mathrm{P}}^2 \simeq 3H^2$ to the effective squared masses of the scalars. The slow-roll parameter η thus receives an $\mathcal{O}(1)$ contribution from SUGRA corrections, breaking the slow-roll condition $\eta \ll 1$. This effect, known as the η problem, is present in most SUGRA models of inflation and usually requires some fine-tuning in the Kähler and/or the superpotential to cancel or suppress the Hubble-scale mass contributions (Bastero-Gil *et al.*, 2007; Shafi and Wickman, 2011).

For a specific implementation of SUSY hybrid inflation, consider the superpotential (Linde and Riotto, 1997; Lazarides, 2002)

$$W = \kappa S(\overline{\phi}\phi - M^2)\,, \tag{1.46}$$

where the conjugate superfields ϕ, $\overline{\phi}$ transform under non-trivial representations of some gauge group G while the superfield S is a gauge singlet whose scalar component acts as the inflaton. W possesses a $U(1)_R$ R-symmetry under which

$\overline{\phi}\phi \to \overline{\phi}\phi$, $S \to \mathrm{e}^{\mathrm{i}\alpha}S$, $W \to \mathrm{e}^{\mathrm{i}\alpha}W$; it is the most general renormalisable superpotential consistent with G and $U(1)_R$.

To begin with, consider the global-SUSY scalar potential derived from W,

$$V_{\mathrm{global}}(\overline{\phi},\phi,S) = \kappa^2\left|M^2-\overline{\phi}\phi\right|^2 + \kappa^2|S|^2\left(\left|\overline{\phi}\right|^2+|\phi|^2\right) + D\text{-term}\,. \tag{1.47}$$

Since a non-zero vacuum energy breaks supersymmetry, the supersymmetric vacuum states lie at $\langle\overline{\phi}\rangle^\star = \langle\phi\rangle = \pm M$ and $\langle S\rangle = 0$, where $|\langle\overline{\phi}\rangle| = |\langle\phi\rangle|$ ensures that the D-term vanishes. Using G and $U(1)_R$ transformations, we can rotate $\overline{\phi}$, ϕ, S onto the real axis and write (Lazarides, 2002) $\overline{\phi} = \phi \equiv \chi/2$, $S \equiv \sigma/\sqrt{2}$, where χ and σ are normalized real scalar fields. This transformation turns V into the same form as the non-SUSY hybrid potential (1.40) with $\kappa = \lambda$ and $m = 0$.

Without an inflaton mass term, of course, the trajectory $\overline{\phi} = \phi = 0$, $|S| > S_{\mathrm{c}} \equiv M$ is an exactly flat direction of the potential (1.42); we need some mechanism for lifting this direction in order to drive the fields towards the true vacuum.

There are several effects that can lift the inflaton potential. First, take one-loop radiative corrections (Dvali *et al.*, 1994): the vacuum energy density κ^2M^4 along the inflationary valley breaks supersymmetry and introduces a mass splitting in the $\overline{\phi}$, ϕ supermultiplets that causes non-zero radiative corrections to the potential (Coleman and Weinberg, 1973)

$$\Delta V = \sum_i \frac{(-1)^{F_i}}{64\pi^2} M_i^4 \ln\left(\frac{M_i^2}{\Lambda^2}\right)\,, \tag{1.48}$$

where the sum extends over all helicity states i with fermion numbers F_i and masses M_i, and the factor $(-1)^{F_i}$ leads to opposite-sign contributions from bosons and fermions; Λ is the renormalisation scale. Far above the waterfall instability S_{c}, the effective potential along the inflationary valley can then be expanded as

$$V_{\mathrm{eff}}(S \gg S_{\mathrm{c}}) \approx \kappa^2M^4\left[1+\frac{\kappa^2\mathcal{N}}{16\pi^2}\left(\ln\frac{\kappa^2|S|^2}{\Lambda^2}+\frac{3}{2}\right)\right]\,, \tag{1.49}$$

where $\mathcal{N}$ is the dimensionality of the representations under which $\overline{\phi},\phi$ transform.

A second source of curvature along the inflaton direction are supergravity corrections arising from the additional terms in the local-SUSY potential (1.44).

A common choice of Kähler potential is the minimal form

$$K = |S|^2 + |\overline{\phi}|^2 + |\phi|^2 \,. \tag{1.50}$$

Note that this is a somewhat fine-tuned choice as there are no symmetries protecting the Kähler potential against higher-order contributions. With a minimal Kähler potential and the superpotential (1.46), the $|S|^2$ contribution from the expansion of the exponential factor in (1.44) exactly cancels a mass term coming from the superpotential: choosing a minimal Kähler potential solves the η problem. Along the D-flat direction $|\phi| = |\overline{\phi}|$ and to leading order in the SUGRA expansion, the scalar potential is thus (Bastero-Gil *et al.*, 2007)

$$V(\overline{\phi}, \phi, S) = 2\kappa^2 |S|^2 |\phi|^2 + \kappa^2 (|\phi|^2 - M^2)^2 \left(1 + 2\frac{|\phi|^2}{m_{\rm P}^2} + \frac{|S|^4}{2m_{\rm P}^4} + \frac{|\phi|^4}{m_{\rm P}^4}\right) + \cdots \,, \tag{1.51}$$

where the $|S|^2$ terms have indeed cancelled.

As a third source of curvature along the inflaton trajectory, consider terms arising from soft supersymmetry breaking. To leading order in the SUGRA corrections and including radiative and soft SUSY-breaking terms, the potential for the rescaled inflaton field $x = |S|/M$ along the inflationary trajectory $|\phi| = |\overline{\phi}| = 0$ is (Rehman *et al.*, 2010),

$$V(x) \approx \kappa^2 M^4 \left(1 + \left(\frac{M}{m_{\rm P}}\right)^4 \frac{x^4}{2} + \frac{\kappa^2 \mathcal{N}}{8\pi^2} F(x) + a\left(\frac{m_{3/2} x}{\kappa M}\right) + \left(\frac{m_{3/2} x}{\kappa M}\right)^2\right) \,, \tag{1.52}$$

where $m_{3/2}$ is the gravitino mass,

$$a = 2|2 - A| \cos[\arg S + \arg(2 - A)] \,, \tag{1.53}$$

and the 1-loop corrections are contained in

$$F(x) = \frac{1}{4}\left(\left(x^4 + 1\right) \ln \frac{(x^4 - 1)}{x^4} + 2x^2 \ln \frac{x^2 + 1}{x^2 - 1} + 2 \ln \frac{\kappa^2 M^2 x^2}{\Lambda^2} - 3\right) \,. \tag{1.54}$$

The last two terms in (1.52) are the soft SUSY-breaking linear and mass-squared terms coming from gravity-mediated SUSY breaking (Nilles, 1984). Rehman *et al.* (2010) showed that including the soft-breaking terms leads to a lower spectral

index n_s than the SUGRA and radiative corrections alone. With just SUGRA and radiative corrections, they obtain a lower limit $n_\mathrm{s} \geq 0.985$, outside of the Planck range $n_\mathrm{s} = 0.9645 \pm 0.0049$. Including the soft terms, however, lowers the predicted value for the spectral index, bringing the model into better agreement with observations.

Finally, the flat inflaton potential can be lifted by corrections from a non-minimal Kähler potential (Bastero-Gil *et al.*, 2007). Consider the expansion

$$K = |S|^2 + |\phi|^2 + |\overline{\phi}|^2 + \kappa_S \frac{|S|^4}{4m_\mathrm{P}^2} + \kappa_{S\phi} \frac{|S|^2|\phi|^2}{m_\mathrm{P}^2} + \kappa_{S\overline{\phi}} \frac{|S|^2|\overline{\phi}|^2}{m_\mathrm{P}^2} + \kappa_{SS} \frac{|S|^6}{6m_\mathrm{P}^4} + \cdots . \quad (1.55)$$

The factor $\left(\partial^2 K / \partial S \partial S^\star\right)^{-1} = 1 - \kappa_S |S|^2 / m_\mathrm{P}^2 + \cdots$ in equation (1.44) now generates a mass-squared for S that is not cancelled. In order to avoid re-introducing the η problem, we have to require $\kappa_S < 1$. Bastero-Gil *et al.* (2007) show that the inclusion of the non-minimal Kähler terms lowers the prediction for the spectral index, improving compatibility with WMAP observations compared to SUGRA and radiative corrections alone. The authors find that generating a sufficient amount of inflation and observationally allowed n_s imposes the rather stringent constraint $\kappa_S \lesssim 0.02$. While they voice some concern about the naturalness of suppressed coefficients in the Kähler potential, they cite the model of Watari and Yanagida (2001) as an example of how these might emerge naturally in an $N = 2$ global SUSY model.

1.3.6 Observational Status of Inflation

Our main source of observational evidence for inflation is the cosmic microwave background. In the inflationary paradigm, the temperature fluctuations we observe in the CMB were seeded by the density perturbations created during inflation; their properties, therefore, are an invaluable tool for probing the distant physics of inflation. Historically, CMB observations have focussed on the power spectrum of the temperature anisotropy; more recently, constraints from primordial CMB polarisation have also become relevant for models of inflation.

The CMB power spectrum is shown in figure (1.3). The oscillatory structures are due to the coherent oscillation of overdensities in the universe before recombination, and they encode great amounts of information about the dynamics and composition of the early universe.

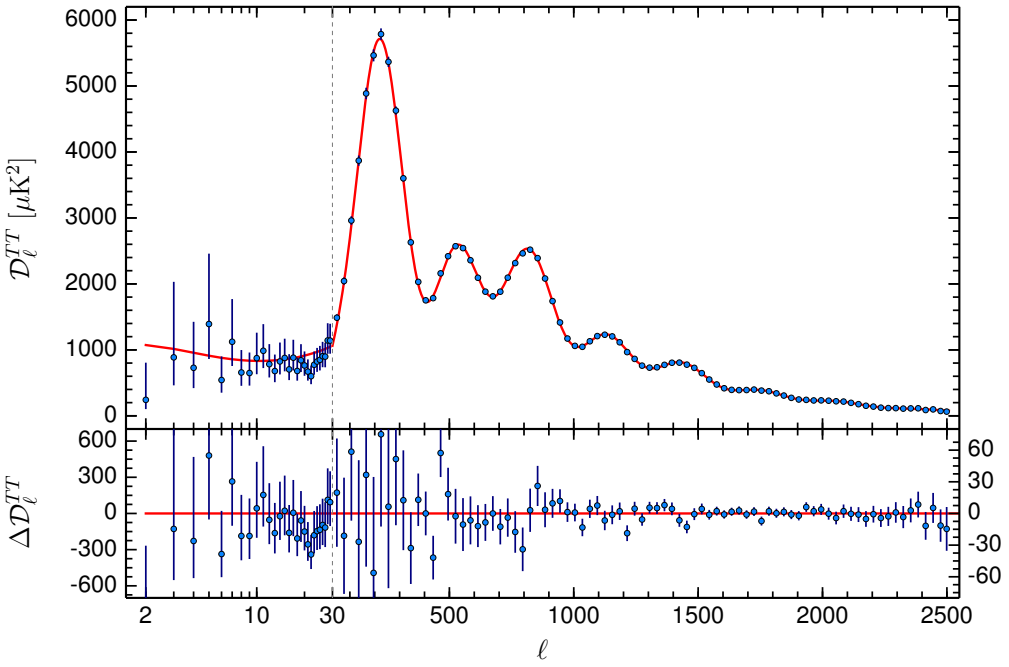

Figure 1.3: CMB power spectrum as measured by the Planck satellite (Ade et al.*, 2015c).*

One of the strongest arguments for inflation as the mechanism that generated the primordial density perturbations is the fact that we see coherent structures in the CMB power spectrum at all. These structures come about because all modes of a given wavenumber k undergo the same number of oscillations between entering the horizon and the time of recombination, when oscillations stop. Consider, for example, the modes that add up to the first peak in the power spectrum. From the start of their oscillation until recombination, they all undergo one full cycle, arriving at maximum amplitude just when their oscillation gets cut short, as seen in the first panel of figure (1.4). Similarly, in the second panel, modes corresponding to the first trough in the power spectrum all go to zero at recombination. This is why the power-spectrum amplitudes for perturbations of these wavenumbers are clearly different. Compare, however, panels three and four of that figure; if the same modes are allowed to begin their oscillation at random phases, they are each in different phases at recombination. In this situation, the average amplitude of the power spectrum would be equal at these, and all other,

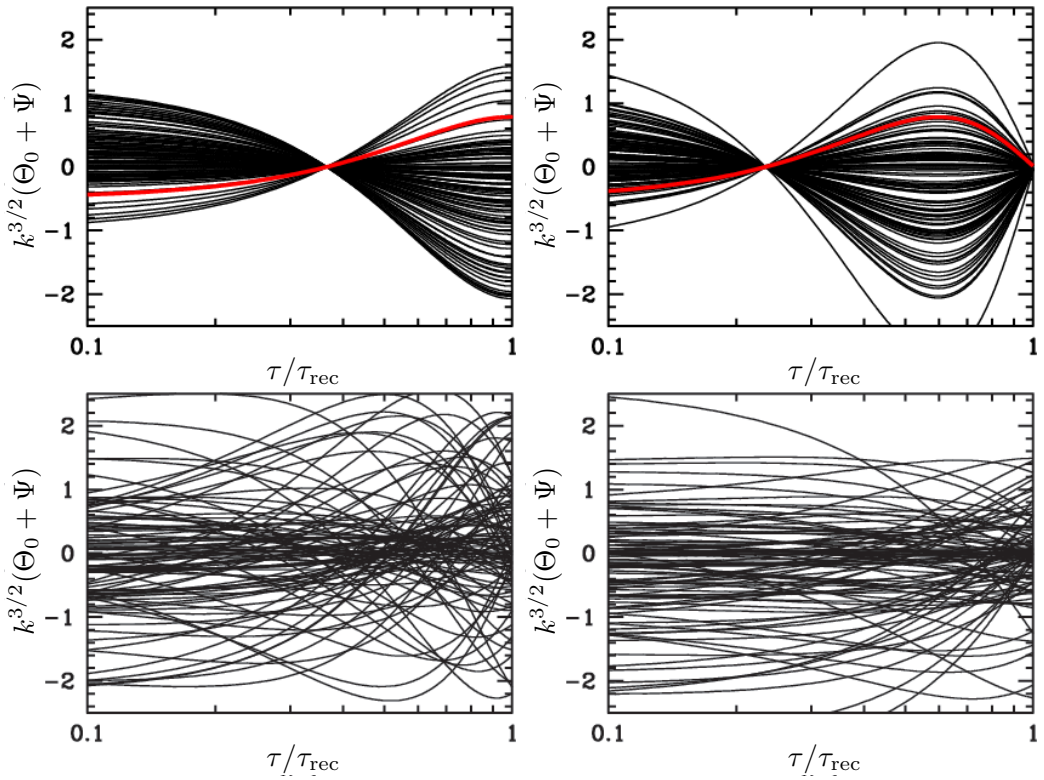

Figure 1.4: Simulated evolution of many modes of the same wavelength. Left column: modes that would contribute to the first peak in the CMB power spectrum; right column: modes that would contribute to the first trough. Top row: all modes start out in the same phase, at constant amplitude; bottom row: modes start with random phases. Without coherent phases, the rms amplitudes at both wavelengths would be indistinguishable at recombination. (Dodelson, 2003)

wavenumbers: the power spectrum would be flat.

If, therefore, the oscillatory structure of the CMB power spectrum relies on all modes of a given wavenumber being in the same phase when they begin oscillating, and those oscillations begin as soon as the modes enter the horizon, the temperature perturbations must have been set up before they entered the horizon. Inflation accomplishes this by causally creating density fluctuations from quantum (and, possibly, thermal) fluctuations before shrinking the comoving Hubble length. Once outside the Hubble horizon, the fluctuations are frozen in until they re-enter after inflation. Essentially, the empirical requirement of coherent phases means that the modes that lead to the oscillatory structure of the CMB must have been inside the horizon at an earlier time, if we assume

they were generated by a causal mechanism. In fact, it has been shown that a phase of decreasing the Hubble length, $\mathrm{d}(1/(aH))/\mathrm{d}t < 0$, is the only causal mechanism for generating super-Hubble density perturbations (Liddle, 1995). It is worth mentioning that models have been proposed that postulate topological defects, such as cosmic strings, as the source of the CMB temperature anisotropy (Vilenkin, 1985; Vilenkin and Shellard, 2000; Hindmarsh and Kibble, 1995). Such models produce very different signatures in the power spectrum, notably because the sub-horizon production of density fluctuations in defect models tends to destroy the phase coherence necessary for the peak structure seen in figure (1.3) (Albrecht *et al.*, 1996). Defect models are now ruled out as the main source of the temperature anisotropy (Ade *et al.*, 2015b).

Inflation predicts that the curvature density parameter Ω_k is driven rapidly towards zero by the exponential expansion and should therefore be small in the post-inflationary universe. One can use the sound horizon at recombination, the distance to which acoustic oscillations can propagate in the primordial plasma before recombination, as a standard ruler to measure the spatial curvature of the universe. The sound horizon manifests itself not only in the first peak of the CMB power spectrum, but also appears as the baryon-acoustic-oscillation (BAO) peak in the galaxy-galaxy correlation function (Eisenstein *et al.*, 2005). Using these observations and adding lensing data, Planck can constrain the curvature density parameter to $\Omega_k = 0.000 \pm 0.005$ at 95% confidence (Ade *et al.*, 2015b), which is compatible with the simplest models of inflation.

The primordial density perturbations generated by inflation should have almost the same amplitude at all scales. A perfectly scale-invariant spectrum corresponds to spectral index $n_\mathrm{s} = 1$, the Harrison–Zel'dovich spectrum (Harrison, 1970; Zeldovich, 1972; Peebles and Yu, 1970), but if inflation is to end, we have to allow for small changes in the Hubble rate and the slow-roll parameters, which will cause the spectrum to deviate from scale invariance. Spectra with $n_\mathrm{s} > 1$ are referred to as blue-tilted, while $n_\mathrm{s} < 1$ is called red tilt. The most accurate observation to date is $n_\mathrm{s} = 0.9645 \pm 0.0049$ at 68% confidence (Ade *et al.*, 2015b, tensor-to-scalar ratio fixed at 0), so that the Harrison–Zel'dovich is now disfavoured at 5.6σ significance if we assume standard ΛCDM cosmology.

Besides scalar perturbations, inflation typically produces a tensor contribution to the power spectrum that can be estimated by the Lyth bound (1.38). Tensors

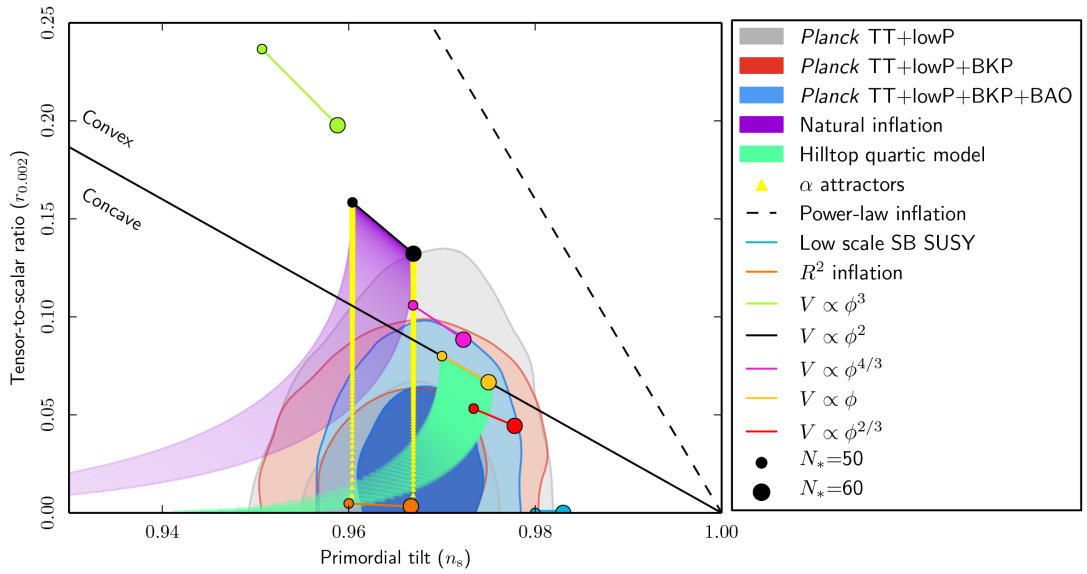

Figure 1.5: Marginalised joint 68% and 95% confidence limits for n_s and r ($k_\star = 0.002\,\mathrm{Mpc}^{-1}$). (Ade et al.*, 2015c)*

have, so far, eluded detection, but improved measurements of CMB polarisation have helped tighten the constraints to a level where some previously appealing models can now be ruled out. The current best upper limit on the detection of tensor modes is $r < 0.08$ at 95% confidence (at pivot scale $k_\star = 0.002\,\mathrm{Mpc}^{-1}$), which is obtained from the Planck temperature anisotropy and polarisation data combined with a BICEP2/Keck–Planck joint analysis (Ade *et al.*, 2015a). Perhaps the most prominent of the models to be ruled out on the basis of too large a tensor contribution is the classic $\lambda\phi^4$ potential, which, in the cold inflationary framework, predicts $r \simeq 0.26$. It is clear from figure (1.5) that low tensor fractions favour concave potentials and that, amongst the models examined by Planck, the R^2 model of Starobinsky (1980) is currently the best fit to the n_s–r data.

As we will demonstrate in section 3.5, this picture changes when inflaton dissipation is included. In warm inflation, scalar perturbations are predominantly produced by thermal, not quantum fluctuations, and their spectrum can be measurably different, as we will describe in section 2.5. Thermal fluctuations generically increase the amplitude of scalar perturbations compared to quantum fluctuations alone, whereas the tensor contribution remains unchanged. Consequently, the tensor-to-scalar ratio is suppressed in warm inflation. This suppression can bring some of the models that are ruled out by n_s–r measurements

in the standard inflationary paradigm back into agreement with the data. Notably, the quartic chaotic inflation model is in good agreement with Planck data if one includes inflaton dissipation and non-zero inflaton occupation numbers at horizon crossing (Bartrum *et al.*, 2014).

1.4 Reheating

During inflation, the energy density of the universe is by definition dominated by the inflaton potential—the inflationary universe is cold and empty. In order to recover the hot big bang and radiation domination after the end of inflation, the energy stored in the inflaton field has to be transferred into other fields and ultimately into the standard-model particles that make up the structures we see today. Any successful model of inflation needs to explain this transition from the vacuum- to the radiation-dominated universe.

Traditionally, the transition from inflation to radiation domination is accomplished during a distinct reheating period during which the inflaton field oscillates about the minimum of its potential and its couplings to other fields lead to rapid particle production (Albrecht *et al.*, 1982; Dolgov and Linde, 1982; Abbott *et al.*, 1982).

The first models of reheating implemented this transition by treating the inflaton field as a collection of particles undergoing single-body decay into other scalar (χ) or fermion (ψ) fields through interactions like $\nu\sigma\phi\chi^2$ and $h\phi\overline{\psi}\psi$, where σ has dimensions of mass and ν and h are dimensionless couplings. If the χ and ψ masses are negligible compared to the inflaton mass, the decay rates are given by (Bassett *et al.*, 2006)

$$\Gamma_{\phi\to\chi\chi} = \frac{\nu^2\sigma^2}{8\pi m_\phi}\,, \qquad \Gamma_{\phi\to\bar{\psi}\psi} = \frac{h^2 m_\phi}{8\pi}\,. \tag{1.56}$$

The expansion of the universe only allows the decay products from these processes to reach thermal equilibrium once $\Gamma_{\rm tot} = \Gamma_{\phi\to\chi\chi} + \Gamma_{\phi\to\bar{\psi}\psi} \simeq H$. Assuming that the energy density is, at this point, dominated by relativistic particles, $\rho \simeq g_\star \pi^2 T^4/30$, where $g_\star$ is the effective number of relativistic degrees of freedom, we can estimate the reheating temperature at the end of the thermalisation

process to be

$$T_{\rm reh} = 0.2 \left(\frac{100}{g_\star}\right)^{1/4} \sqrt{\Gamma_{\rm tot} m_{\rm P}}\,. \tag{1.57}$$

We can then impose the constraint $m_\phi \sim 10^{-6}\, m_{\rm P}$ from the normalisation of the CMB on large scales and require that the coupling constants be small so that radiative corrections don't spoil the flatness of the potential; we thus find that the reheat temperature is constrained to be $T_{\rm reh} < 10^{16}\,{\rm GeV}$. Fortunately, then, reheating does not lead to restoration of the GUT symmetry, which would cause a new phase of GUT breaking and the associated production of monopoles—reheating does not spoil the solution to the monopole problem that inflation was introduced to provide. That being said, reheating can cause problems with the observationally well-supported results of big-bang nucleosynthesis (BBN). In supergravity models, there is a risk of transferring a large amount of energy into gravitinos, which may not decay until after BBN, potentially spoiling the primordial element abundances. In order to avoid this for a large range of gravitino masses, the reheat temperature needs to lie below at most $10^9\,{\rm GeV}$.

Since the original models of reheating were first established, it has been realised that the transition from inflation to radiation domination can be drastically different when considering the influence of effective masses. At the end of inflation, the occupation number of the homogeneous $k = 0$ mode, which contains most of the inflaton energy, is very large large, so that the inflaton essentially behaves as a classical field. When slow-roll ends, the field begins coherent oscillations about the minimum of its potential. The effective masses of any matter fields coupled to the inflaton then change rapidly, which allows for the excitation of field fluctuations by parametric resonance. Particle production via this mechanism leads to what is called preheating and can easily dominate over the older picture of single-particle decay of a large collection of independent particles (Dolgov and Kirilova, 1990; Traschen and Brandenberger, 1990; Kofman *et al.*, 1994; Shtanov *et al.*, 1995).

For definiteness, we will focus here on an inflaton ϕ with quadratic potential, coupled to a massless scalar χ,

$$V_{\rm eff} = \frac{1}{2} m_\phi^2 \phi^2 + \frac{1}{2} g^2 \phi^2 \chi^2\,, \tag{1.58}$$

leading to an effective mass for χ given by

$$m_{\chi,\mathrm{eff}} \equiv \frac{\partial^2 V_{\mathrm{eff}}}{\partial \chi^2} = g^2\phi^2(t)\,. \tag{1.59}$$

Note that it would be straightforward to accommodate a bare mass for χ; we will make use of that possibility shortly.

As usual, the modes χ_k follow a Klein-Gordon equation

$$\ddot{\chi}_k + 3H\dot{\chi}_k + \left[\frac{k^2}{a^2} + g^2\phi^2\right]\chi_k = 0\,. \tag{1.60}$$

If the frequencies $\omega_k \equiv [k^2/a^2 + g^2\phi^2]^{1/2}$ are constant or vary only slowly, the modes $\chi_k(t)$ do not grow: no particles are produced. Varying frequencies, on the other hand, open up the possibility of parametric resonance in the system. We can measure the deviation from constant frequencies in terms of the ratio

$$R_a \equiv \frac{\dot{\omega}_k}{\omega_k^2}\,. \tag{1.61}$$

In the regime $|R_a| \gg 1$, we expect a significant amount of particle production. For small wave numbers, $k/(aH) \ll 1$, we find

$$R_a \simeq \frac{\dot{\phi}}{g\phi^2} \sim \frac{m_\phi}{g\phi}\,, \tag{1.62}$$

where we have used that $\dot{\phi} \sim m_\phi\phi$ is a suitable approximation for most periodic inflaton oscillations after inflation (Bassett *et al.*, 2006). As this expression diverges whenever $\phi \to 0$, we expect bouts of dramatic particle production during every inflaton oscillation.

Using the rescaled variable $X_k = a^{3/2}\chi_k$, we can transform the Klein-Gordon equation into the Mathieu equation

$$\frac{\mathrm{d}^2 X_k}{\mathrm{d}z^2} + (A_k - 2q\cos 2z)\,X_k = 0\,, \tag{1.63}$$

where we have introduced

$$z = m_\phi t \tag{1.64}$$

$$A_k = 2q + \frac{k^2}{m_\phi^2 a^2} \tag{1.65}$$

$$q = \frac{g^2 \overline{\phi}^2(t)}{4m_\phi^2} \tag{1.66}$$

$$\overline{\phi} = \frac{m_\mathrm{P}}{\sqrt{3}\pi m_\phi t}\,. \tag{1.67}$$

The strength of the resonance is then determined by A_k and q, which are confined to the region $A_k \geq 2q$ and can be investigated using the stability–instability chart of the Mathieu equation. For $q < 1$, the instability band is small, and the effect of the resonance is washed out by expansion; with $q \gg 1$, however, broad resonance is possible in large parts of parameter space and for a wide range of momentum modes. Assuming the COBE constraint $m_\phi \sim 10^{-6} m_\mathrm{P}$ and an initial amplitude of the inflaton oscillation of $\phi_0 \sim 0.2 m_\mathrm{P}$, we can obtain $q \gg 1$ if $g \gtrsim 10^{-4}$.

If the system finds itself in an instability band of the Mathieu equation, the perturbations X_k grow exponentially with Floquet index $\mu_k > 0$,

$$X_k \propto \mathrm{e}^{\mu_k z}\,. \tag{1.68}$$

For $q \gg 1$, particle production only occurs in the vicinity of the point $\phi = 0$, so we can Taylor expand the potential and the effective mass of the χ fields around that point. The problem can then be rephrased as that of a particle scattering in a parabolic potential, and the Floquet index for the j-th 0-crossing of the oscillating inflaton is given by (Kofman *et al.*, 1997)

$$\mu_k^j = \frac{1}{2\pi} \ln\left[1 + 2E - 2\sin\theta_\mathrm{tot}^j \sqrt{E(1+E)}\right] \tag{1.69}$$

with $E = \exp(-\pi\kappa^2)$, $\kappa^2 = k^2/(a^2 k_\star^2)$, $k_\star = g m_\phi \overline{\phi}$. Since the frequencies ω_k change dramatically between successive instances of $\phi = 0$, the phases of the field χ_k are practically uncorrelated (Kofman *et al.*, 1997). It turns out that this regime of stochastic resonance is much more robust than the usual broad resonances of the Mathieu equation would be.

An interesting scenario arises when the χ bosons are coupled to a fermion

field via the term $h\chi\overline{\psi}\psi$. The boson decay rate is then given by

$$\Gamma_{\chi\to\overline{\psi}\psi} = \frac{h^2 g|\phi|}{8\pi}\,. \tag{1.70}$$

There are thus no χ decays during the bursts of χ production around $\phi = 0$. However, as ϕ reaches the maximum of its oscillation, so do the decay rate and mass of the χ bosons. The χ bosons are kinematically permitted to decay into fermion pairs with mass up to $g|\phi|$; with initial oscillation amplitudes $|\phi| \sim 0.1 m_{\rm P}$, this process, also known as instant reheating, can therefore produce particles near the Planck mass (if we permit $g \sim 1$) and transfer large amounts of energy into massive bosons in just a few oscillations.

It is interesting to note that preheating differs from the original reheating models based on individual inflaton decays in the kinds of particles that it can produce. If we include in the above treatment a bare mass for the χ bosons, we find

$$R_a \simeq \frac{m_\phi g^2 \phi^2}{\left(m_\chi^2 + g^2\phi^2\right)^{3/2}}\,. \tag{1.71}$$

For $g^2 > 0$, this ratio now remains finite even for $k \to 0$ and $\phi = 0$, but for $g^2 < 0$, it can still diverge when the effective mass $m_{\chi,\rm eff}^2 = m_\chi^2 + g^2\phi^2$ vanishes. Unlike inflaton decays, for which decay products with $m_\chi > m_\phi$ are kinematically forbidden, preheating can hence resonantly produce extremely massive particles (Bassett *et al.*, 2006). In a distributed-mass model, for instance, where many possible decay channels with different masses exist, the effective masses of different states vanish as the inflaton roles down its potential, leading to successive bursts of production of the corresponding particles. It is interesting to note that a similar mechanism has been implemented as a way for the inflaton to slow down its own motion by dumping some of its kinetic energy into the production of particles that become light at specific points in field space (Kofman *et al.*, 2004; Green *et al.*, 2009). Called trapped inflation, this model is similar to warm inflation in that it allows for relaxed slow-roll conditions on the inflaton potential. An important difference, however, is that, following each production event in trapped inflation, the Hubble expansion quickly dilutes the particles produced, while warm inflation results in a thermal bath that persists and affects inflaton evolution throughout.

In an attempt to discriminate between various single-field models of inflation,

a recent study used CMB data in a Bayesian model selection approach to assessing the evidence for these models (Martin *et al.*, 2014). The authors found that the evidence for a given inflationary model depends on the assumptions made on the era of reheating, summarised by them in the value of the mean equation-of-state parameter during that era. They conclude that in our era of precision cosmology, where CMB observations can help constrain reheating, any model of inflation has to include the details of how the universe is to be reheated before we can try to estimate its performance compared to other models.

Given the importance of reheating predictions for the discrimination between models of inflation, it may be beneficial to consider models that make reheating a natural part of the inflationary expansion itself instead of treating it as a distinct epoch. If the inflaton field is suitably coupled to other degrees of freedom, and if those degrees of freedom thermalise quickly, the universe can be reheated continuously during inflation and transition smoothly into the subsequent radiation-dominated era (Berera, 1997). Dissipation of even a modest amount of inflaton energy into other fields can have a significant influence on inflaton evolution and on density perturbations produced during inflation. We will provide a detailed overview of the warm-inflation paradigm in the next chapter.

Chapter 2

Warm Inflation

2.1 Introduction

Now that we have established the basics of conventional inflationary cosmology, let us consider a generalisation. Traditional models of inflation (we will refer to them as cold inflation) assume the inflaton field's couplings to other field are only relevant during reheating; it is assumed that, even if those couplings lead to the production of other particles, these are quickly diluted away by the exponential expansion and have no impact on the dynamics or outcomes of inflation. However, if we consider inflation happening at the grand-unification scale $10^{15} - 10^{16}\,\mathrm{GeV}$, for example, and imagine that as little as one part in 10^{20} of the inflaton's potential energy density is transferred into radiation, the resulting temperature is on the order of $10^{11}\,\mathrm{GeV}$. Given that the success of big-bang nucleosynthesis relies on a reheat temperature after inflation below $10^{9}\,\mathrm{GeV}$, it is not obvious that a possible radiation bath at such high temperature can be neglected. Warm inflation, therefore, includes inflaton interactions throughout and attempts to better understand how these interactions, and the particle production they allow, affect the course of inflation and the transition to the post-inflationary, radiation-dominated universe. The idea of particle production alongside inflation was first proposed by Fang (1980); Moss (1985), and Yokoyama and Maeda (1988) subsequently introduced a dissipative term in the equations of motion that is associated with the radiation production. Berera and Fang (1995) independently rediscovered this idea and elaborated on the fluctuation–dissipation dynamics underlying the dissipation term; Berera (1995) and Berera (1996), finally, began

the process of developing specific particle-physics implementations of the new framework of warm inflation.

As is clear from the reasoning above, the production of thermal radiation concurrent with slow-roll inflation can eliminate the need for a separate period of reheating (Berera, 1997). As the inflaton rolls further and further down its potential, all the while creating and sustaining a radiation bath, its energy slowly decreases. The universe may thus experience a smooth transition from inflation to radiation domination as the radiation density simply comes to be greater than the potential energy remaining in the inflaton field. Of course, much like in traditional reheating, there is a risk of overproducing gravitinos and potentially spoiling big-bang nucleosynthesis. This problem has been examined, for instance, by Bueno Sanchez *et al.* (2011) and Bartrum *et al.* (2012), and we will not consider it further here.

In addition to these theoretical advantages, warm inflation also presents a great phenomenological opportunity. The dissipation of inflaton energy effectively acts as extra friction, adding to what is provided by Hubble expansion alone. This increased friction relaxes the flatness constraints on the inflaton potential, making it easier to satisfy the slow-roll conditions and to sustain a large number of e-folds of expansion using steeper potentials than would be possible in cold inflation. As a consequence, warm inflation opens up the possibility for chaotic inflation, which traditionally requires field values greater than the Planck mass, to occur at sub-Planckian field values. Moreover, warm inflation modifies the primordial perturbation spectrum. Whilst primordial density perturbations in cold inflation are generated by the quantum fluctuations of the inflaton field alone, the radiation fluid present during warm inflation adds thermal fluctuations, which can have a measurable impact on the power spectrum of the cosmic microwave background.

Early implementations of warm inflation struggled to find a regime where dissipation was strong enough to have a significant effect without spoiling inflation completely (Berera *et al.*, 1998, 1999; Yokoyama and Linde, 1999). Initially, the search for suitable regions of parameter space concentrated on the high-temperature regime. Unfortunately, high temperatures led to significant thermal corrections to the inflaton potential while the dissipation term appeared as only a small correction. Such models therefore struggled to maintain slow roll for a sufficient number of e-foldings.

More recent implementations operate at low temperatures and suppress corrections to the inflaton potential using, for instance, supersymmetry. Berera and Ramos (2001) introduced a low-temperature model that achieves significant dissipation without spoiling the flatness of the inflaton potential. There, the inflaton decays by coupling to a heavy mediator field, which in turn couples to light fields that ultimately form a thermalised radiation bath. As long as the mass of the mediators is greater than the temperature of the thermal bath, they will remain effectively in their ground state. Supersymmetry can then cancel the zero-temperature corrections to the effective potential arising from the mediator fields. On the other hand, supersymmetry does not affect the time-non-local effects that lead to dissipation.

This two-stage mechanism for inflaton dissipation has been very successful. A thermal-field-theory derivation of the dissipation coefficient in such models was first accomplished by Moss and Xiong (2006). Graham and Moss (2009) found that the thermal fluctuations resulting from the presence of the radiation bath can lead to a primordial perturbation spectrum significantly different from the cold-inflation expectation for a given inflationary model. They also realised, however, that the strong dissipative regime can produce a growing mode in the primordial spectrum that would make it difficult to bring predictions into agreement with cosmological observations. This obstacle can be avoided in the weak-dissipation regime.

Since the two-stage mechanism leads to production of light fields slightly out of equilibrium, Bastero-Gil *et al.* (2011b) considered the effects of shear viscosity in the radiation fluid. They found that viscous effects will tend to inhibit the growth of perturbations and that, in the presence of sufficiently strong shear-viscous damping, the growing mode is absent from the primordial spectrum.

As a further generalisation, the primordial spectrum has since been derived in the presence of both shear and bulk viscosity and including a non-zero occupation number of the inflaton field at horizon crossing (Bastero-Gil *et al.*, 2014a; Bartrum *et al.*, 2014).

Since the on-shell production of heavy mediator particles is Boltzmann suppressed in the low-temperature regime, it was originally believed that inflaton dissipation occurred predominantly via virtual mediator particles. Nevertheless, the study by Bastero-Gil *et al.* (2013) revealed that on-shell production can

contribute significantly in certain parameter ranges. Specifically, the strength of on-shell dissipation depends on the inverse square of the coupling $\hat{h}$ of mediator fields to the light fields. Thus, when the mediator mass is greater than the temperature of the radiation fluid by only a factor of $\mathcal{O}(10)$, the exponential suppression can be compensated by a reasonably small coupling $\hat{h}$. It has to be noted, however, that even though dissipation is inherently an out-of-equilibrium process, the derivation of the dissipation coefficients (see, for example, Berera *et al.* (2009) for an overview), requires the system to remain close to equilibrium at all times. This puts important constraints on the parameter ranges accessible to warm inflation. Notably, this means that the coupling $\hat{h}$ between the mediators and the radiation bath must be big enough to keep relaxation times small compared to the other dynamical timescales, thus preventing the system from ever straying too far from equilibrium.

Given an out-of-equilibrium process in the early universe, as provided by inflaton dissipation, a natural line of enquiry is the search for a warm-inflationary origin of the baryon asymmetry in the universe. It would seem that all that is required to satisfy the Sakharov criteria for the generation of such an asymmetry is a model that incorporates, in addition to inflaton dissipation, interactions that violate B and CP symmetry (Sakharov, 1967). Bastero-Gil *et al.* (2012) have attempted the construction of just such a model. They implement warm inflation with two-stage dissipation embedded in a supersymmetric GUT theory. Their model allows for the B-violating decay of the mediator fields and includes complex couplings between the mediators and the light sector, which allows for C and CP violation. At the same time, they operate in the low-temperature regime $T \ll M_{\mathrm{GUT}}$, which ensures that thermal corrections to the inflaton potential are under control. Additionally, the low temperatures avoid restoring the GUT symmetry and subsequently producing undesirable relics such as magnetic monopoles, which might otherwise over-close the universe. The authors find that, for natural parameter choices, their model can produce a value of the baryon asymmetry that is indeed compatible with current estimates from big-bang nucleosynthesis. This illustrates that the application of fluctuation–dissipation dynamics to the very early universe is a promising endeavour that may lead to interesting new connections between the physics of inflation and the post-inflationary universe.

In this chapter, we are going to introduce the physics underlying all of these findings. In section 2.2, we will start out with a quick overview of the effective dynamics of the inflaton field during warm inflation in order to set the scene and establish some basic notation. In the process, we will summarise all the constraints that need to be imposed on the dynamics in order for the derivations and approximations in the rest of this chapter to be valid. Next, section 2.3 will outline the derivation of the effective dynamics, primarily the effective dissipation coefficient, from thermal field theory. We will show that the inflaton field equation during warm inflation is a Langevin-like equation of motion that emerges from a local, Markovian approximation to a fluctuation–dissipation relation. In section 2.4, we will introduce the specific particle-physics model used in our work; we will apply the findings of the preceding sections to an implementation of the two-stage dissipation mechanism based on a widely-used superpotential containing the interactions of the inflaton, the mediator fields, and the light fields. Section 2.5 will establish that the spectral index and tensor-to-scalar ratio obtained from the power spectrum of the cosmic microwave background may be measureably different in warm inflation. Section 3.2, finally, derives a set of models for which the ratio between mediator mass and radiation temperature remains approximately constant during warm inflation.

2.2 Overview of Warm-Inflation Dynamics

Under certain assumptions that we will elaborate on later in this chapter, the influence of dissipation on inflaton dynamics can be summarised by a time-local effective dissipation term in the field equation. This is represented, quite simply, as an extra friction term in the inflaton equation of motion (1.24) (Berera and Fang, 1995; Berera, 1995),

$$\ddot{\phi} + (3H + \Upsilon)\dot{\phi} + V_\phi = 0\,, \tag{2.1}$$

where we will call Υ the dissipative coefficient. We can re-write this in terms of the energy density in the inflaton field,

$$\dot{\rho}_\phi + 3H(\rho_\phi + p_\phi) = -\Upsilon(\rho_\phi + p_\phi)\,, \tag{2.2}$$

where the energy density and pressure of the scalar field are given by $\rho_\phi = \frac{1}{2}\dot{\phi}^2 + V(\phi)$ and $p_\phi = \frac{1}{2}\dot{\phi}^2 - V(\phi)$, respectively. The dissipated inflaton energy serves as a source for the energy density ρ_α of the fluid component that represents the dissipation products,

$$\dot{\rho}_\alpha + 3H(\rho_\alpha + p_\alpha) = \Upsilon(\rho_\phi + p_\phi)\,. \tag{2.3}$$

If the end product of dissipation is light particles that thermalise quickly, we can treat this as radiation with $\rho_\alpha = \rho_\mathrm{R}$ and $p_\mathrm{R} = \frac{1}{3}\rho_\mathrm{R}$,

$$\dot{\rho_\mathrm{R}} + 4H\rho_\mathrm{R} = \Upsilon\dot{\phi}^2\,. \tag{2.4}$$

It is convenient to characterise the strength of dissipation in comparison to the Hubble friction. In terms of the dissipative ratio

$$Q \equiv \frac{\Upsilon}{3H}\,, \tag{2.5}$$

we distinguish between the weak dissipative regime, $Q \ll 1$, and the strong dissipative regime, $Q \gg 1$. In the weak regime, the effect of dissipation on inflaton evolution is small, and we arrive at the same slow-roll field equation as we would in cold inflation; nevertheless, the presence of thermal fluctuations in the radiation bath will modify the spectrum of primordial density fluctuations even in this regime. Strong dissipation, on the other hand, has a significant impact on the behaviour of the inflaton. Potentials that would not be flat enough to sustain a sufficient amount of inflationary expansion in cold inflation, may be perfectly viable for slow-roll warm inflation, thanks to the added friction due to dissipation.

The added friction modifies the slow-roll conditions (1.27). The constraints on the flatness parameters ϵ, η are relaxed by the factor $1 + Q$—a formal expression of the intuitive expectation that relatively steep potentials can be viable given a sufficient amount of dissipation. In addition, in order to keep the quantities in the slow-roll field equation from varying too quickly, we have to ensure that the new parameter

$$\beta = m_\mathrm{P}^2 \left(\frac{\Upsilon' V'}{\Upsilon V}\right) \tag{2.6}$$

remains small. The full set of warm-inflation slow-roll conditions then reads (Hall

et al., 2004; Moss and Xiong, 2008)

$$\epsilon < 1 + Q\,, \quad \eta < 1 + Q\,, \quad \beta < 1 + Q\,. \tag{2.7}$$

If these conditions hold, the slow-roll equations governing the evolution of the warm inflationary universe are

$$\dot{\phi} = -\frac{V_\phi}{3H(1+Q)}\,, \tag{2.8a}$$

$$4\rho_{\mathrm{R}} = 3Q\dot{\phi}^2\,, \tag{2.8b}$$

$$3H^2 = 8\pi G V\,. \tag{2.8c}$$

If the inflaton potential receives thermal corrections, it is essential for the viability of warm inflation that there be a mechanism in place to prevent these corrections from spoiling the flatness requirements. This can be quantified in the additional slow-roll condition

$$\delta = \frac{TV_{\phi T}}{V_\phi} < 1\,. \tag{2.9}$$

In the models explored in this work, thermal corrections to the potential are suppressed by supersymmetry.

We will see in section 2.3.5 that the derivation of a dissipation coefficient that is local in time requires that the system remain close to equilibrium at all times. In order to accomplish this, we will have to ensure that the relaxation time of the mediator particles, characterised by their decay width Γ_χ, is short compared to the other dynamical time scales in the system. For this purpose, we enforce, in addition to the slow-roll conditions, the adiabaticity condition

$$\Gamma_\chi > H\,. \tag{2.10}$$

Assuming that the light particles produced by dissipation thermalise quickly, we can assign to the resultant radiation bath a temperature $T \propto \rho_{\mathrm{R}}^{1/4}$. If thermally-induced density perturbations are to compete with quantum mechanical ones as the dominant contribution to the primordial power spectrum, we have to require

that the temperature be sufficiently high,

$$T > H\,. \tag{2.11}$$

Since the production of thermal density perturbations is one of the hallmarks and the primary observable effect of warm inflation, we will impose this condition as a necessary requirement on all models examined in this work.

Conversely, it was realised early on that at too high a temperature, it is very difficult to obtain successful warm inflation due to the competing requirements of keeping finite-temperature thermal corrections to the inflaton potential small and of producing a relevant amount of dissipation, all the while satisfying the adiabaticity requirements (Berera *et al.*, 1998, 1999; Yokoyama and Linde, 1999). More recent implementations of warm inflation use a two-stage mechanism for inflaton dissipation to help satisfy these constraints. In the low-temperature regime

$$m_\chi > T\,, \tag{2.12}$$

such models use supersymmetry to cancel the zero-temperature corrections to the inflaton potential. At the same time, supersymmetry leaves the time-non-local effects that lead to dissipation intact; it becomes possible to produce significant dissipation without spoiling the flatness of the inflaton potential.

2.3 Langevin Equation and Fluctuation–Dissipation Dynamics

In warm inflation, the interactions between the inflaton and other fields modify the field evolution and lead to the production of a thermal bath in the inflationary universe. In this section, we will show how such interactions introduce a stochastic source and a non-local dissipation-like term in the inflaton field equation, turning it into a Langevin-type stochastic equation. It is an important finding in statistical physics that the response of a system to a perturbation can be related to the correlation spectra of fluctuations in the system in thermal equilibrium. Here, we will begin by briefly illustrating these concepts in the simple case of Brownian motion. The motion of a Brownian particle suspended in a fluid is governed by a Langevin equation, and we will give an outline of how a fluctuation–

dissipation theorem relates the strength of the stochastic forces in the medium to the hydrodynamic drag acting on the particle. Similar notions about a system in interaction with its environment will, when applied to a scalar field subject to thermal fluctuations, lead us to the equation of motion for the scalar field that governs the warm-inflation universe.

2.3.1 Brownian Motion

The archetypal example of a Langevin equation is that describing the motion of a particle immersed in a fluid. The collisions of the particle with the molecules in the fluid can be separated into a systematic part and a random part. The systematic part constitutes the hydrodynamic drag that inhibits motion; the random part is a fluctuating, stochastic force on the particle. The velocity $u(t)$ of a particle subject to these forces is evolves according to

$$m\dot{u}(t) = -m\gamma u(t) + R(t), \tag{2.13}$$

where γ characterises the hydrodynamic drag whilst $R(t)$ represents the fluctuating force. The fluctuation–dissipation theorem for this system states that, given their shared microscopic origin, the strength of the systematic drag force is related to the strength of the fluctuations. More generally, the admittance of a given system, that is, its response to an external perturbation, is determined by the internal fluctuations of the system in equilibrium (Kubo, 1966).

Formally, the solution of equation (2.13) is given by

$$u(t) = u(0)\exp(-\gamma t) + \int_0^t \mathrm{d}\tau \exp[-\gamma(t-\tau)]R(\tau). \tag{2.14}$$

In order to obtain useful information from this solution, let us consider averages over the possible realisations of the stochastic force $R(t)$. $R(t)$ is usually assumed to be drawn from a Gaussian distribution with mean zero and to satisfy the white-noise assumption

$$\langle R(t)\rangle = 0, \tag{2.15}$$

$$\langle R(t)R(t')\rangle = 2\pi\Gamma\delta(t-t'), \tag{2.16}$$

where Γ determines the strength of the correlations. Microscopically, the Gaussian assumption is justified because the force $R(t)$ results from many collisions of the Brownian particle with the molecules in the medium; under these conditions, the central limit theorem ensures the Gaussianity of the resulting distribution. In this setting, the assumption (2.16) of an infinitely short correlation time is also reasonable since individual impacts happen on a timescale much shorter than that of the Brownian motion.

By taking the average of equation (2.14), we obtain

$$\langle u(t) \rangle = u(0) \exp(-\gamma t), \tag{2.17}$$

indicating that, in spite of the random force acting on our particle, its average velocity evolves deterministically. In order to constrain the noise strength Γ, we can calculate the average of $\langle u^2 \rangle$,

$$\begin{aligned} \left\langle u(t)^2 \right\rangle = u(0)^2 \exp(-2\gamma t) + 2 \int_0^t \mathrm{d}\tau \exp[-\gamma(2t-\tau)] u(0) \left\langle R(t) \right\rangle \\ + \int_0^t \mathrm{d}\tau \int_0^t \mathrm{d}\tau' \exp[-\gamma(2t-\tau-\tau')] \left\langle R(\tau) R(\tau') \right\rangle . \end{aligned} \tag{2.18}$$

Using the white-noise assumptions (2.16), we find

$$\left\langle u(t)^2 \right\rangle = u(0)^2 \exp(-2\gamma t) + \frac{\Gamma}{2\gamma} [1 - \exp(-2\gamma t)]. \tag{2.19}$$

For large times t, we know from the equipartition theorem that $\frac{1}{2} m \langle u^2 \rangle = \frac{1}{2} kT$, which now allows us to relate the strength of the fluctuations to the hydrodynamic drag,

$$\Gamma = \frac{kT\gamma}{\pi m}. \tag{2.20}$$

This connection between the stochastic and the dissipative forces is an example of the more general fluctuation–dissipation theorem.

An alternative approach to describing the behaviour of the velocity $u(t)$ uses the fact that, owing to the assumptions (2.16), $u(t)$ is both Gaussian and Markovian, that is, the probability of a change in velocity at any given moment only depends on the state of the system in that instant. All information about the behaviour of $u(t)$ is then contained in the transition probability

$W(u_0, t_0; u, t)$, which is governed by a Fokker-Planck equation that can be derived from equation (2.13),

$$\frac{\partial}{\partial t}W = \frac{\partial}{\partial u}\left(D_u\frac{\partial}{\partial u} + \gamma u\right)W \tag{2.21}$$

with $W(u_0, t_0; u, t_0) = \delta(u - u_0)$. It is found that the velocity-space diffusion constant D_u is given by (Kubo, 1966)

$$D_u = \frac{1}{m^2}\int_0^\infty \langle R(t_0)R(t_0 + t)\rangle \,\mathrm{d}t. \tag{2.22}$$

In thermal equilibrium, where the transition probability W coincides with the Maxwell-Boltzmann distribution, D_u is given by

$$D_u = \frac{\gamma}{m}kT, \tag{2.23}$$

which implies

$$m\gamma = \frac{1}{kT}\int_0^\infty \langle R(t_0)R(t_0 + t)\rangle \,\mathrm{d}t. \tag{2.24}$$

This illustrates once more the close connection between these two forces that share a microscopic origin: the systematic part of the force, the friction, is determined by the fluctuations in the random part. This has been our first encounter with the fluctuation–dissipation theorem, and we shall see further manifestations of it in the following sections. An illustrative derivation of the fluctuation–dissipation dynamics in a simple quantum mechanical model that leads to warm inflation is given, for example, by Berera (1996).

2.3.2 The Closed-Time-Path Formalism

If we wish to understand the origin of the dissipative term in the inflaton field equation (2.1) and its connection to stochastic noise in the coupled inflaton–radiation system, we must first give a brief review of the underlying formalism of thermal field theory.

We will be interested, here, in ensemble averages of operator expectation values, which can be expressed in terms of derivatives of a generating functional. It will prove convenient for our purposes, which involve the calculation of the two-point correlation functions of various fields, to conduct our treatment in the

closed-time-path (CTP) or Schwinger-Keldysh formalism. In the CTP formalism, the generating function of correlation functions, expressed in terms of sources J_1 and J_2 and of the complete sets of (initial and final) states $|\psi_\mathrm{i}\rangle$ and $|\psi_\mathrm{f}\rangle$ and density matrix ρ is

$$Z[J_1, J_2] = \sum_{\mathrm{i,f}} \langle\psi_\mathrm{i}|\, \rho\, T^\star \exp\left(-i\int J_2\, \hat{\phi}\right) |\psi_\mathrm{f}\rangle\, \langle\psi_\mathrm{f}|\, T \exp\left(i\int J_1\, \hat{\phi}\right) |\psi_\mathrm{i}\rangle\ . \quad (2.25)$$

Here, $T^\star$ represents the time-ordering operator with the smallest time on the left. In order to obtain, say, the ensemble average of a product of the operators $\hat{\phi}$, such as, $\langle T^\star \hat{\phi}(x_1) \ldots \hat{\phi}(x_r)\, T \hat{\phi}(x_{r+1}) \ldots \hat{\phi}(x_n)\rangle$, we simply differentiate the generating functional r times with respect to J_2 and $n-r$ times with respect to J_1. For convenience, we shall remove the minus sign in front of J_2 by defining $J^1 = J_1$ and $J^2 = -J_2$.

The two-point correlation functions will be of particular interest to us. We can construct, from the derivatives of Z, four different connected two-point functions,

$$G_{ab}(x, x') = -i \frac{\delta \ln Z}{\delta J^a(x) \delta J^b(x')}. \quad (2.26)$$

We obtain

$$G_{ab}(x, x') = \begin{pmatrix} \langle T\hat{\phi}(x)\hat{\phi}(x')\rangle_\mathrm{c} & \langle \hat{\phi}(x')\hat{\phi}(x)\rangle_\mathrm{c} \\ \langle \hat{\phi}(x)\hat{\phi}(x')\rangle_\mathrm{c} & \langle T^\star \hat{\phi}(x')\hat{\phi}(x)\rangle_\mathrm{c} \end{pmatrix} \quad (2.27)$$

and can identify G_{11} as the usual Feynman propagator. G_{21} is known as the thermal Wightman function, and G_{12} is its transpose; G_{22} is the thermal Dyson function. We can split the propagator into its real and imaginary parts by introducing the real spectral function ρ and the real anticommutator function F, defined as

$$\rho(x, x') = i \left\langle \left[\hat{\phi}(x), \hat{\phi}(x')\right] \right\rangle_\mathrm{c}\ , \quad (2.28)$$

$$F(x, x') = \frac{1}{2} \left\langle \left\{\hat{\phi}(x), \hat{\phi}(x')\right\} \right\rangle_\mathrm{c}\ . \quad (2.29)$$

The propagator matrix can then be written as

$$G_{ab}(x, x') = F(x, x') + \frac{i}{2}\rho(x, x') \begin{pmatrix} -\operatorname{sgn}(t-t') & +1 \\ -1 & \operatorname{sgn}(t-t') \end{pmatrix}\ . \quad (2.30)$$

In thermal equilibrium, the system is invariant under space-time translations and satisfies certain periodicity relations in imaginary time; propagators can then only depend on the difference $x - x'$. The imaginary-time periodicity implies a relation between the Fourier transforms of the spectral function and the anticommutator function (Bellac, 1996),

$$F(\mathbf{p},\omega) = -\frac{i}{2}\left[1 + 2n(\omega)\right]\rho(\mathbf{p},\omega)\,, \tag{2.31}$$

where $n(\omega)$ is the thermal distribution function at inverse temperature β

$$n(\omega) = \frac{1}{\mathrm{e}^{\beta\omega} - 1}\,. \tag{2.32}$$

It turns out, therefore, that in thermal equilibrium, the full thermal propagator is determined by the spectral function alone.

We can obtain the spectral function perturbatively by solving the Schwinger-Dyson equation

$$\left(\omega^2 - \mathbf{k}^2 - m^2\right) G_{ab} - \Sigma_a^{\,c} G_{cb} = i c_{ab}\,, \tag{2.33}$$

where Σ_{ab} is the self-energy matrix and c_{ab} is a diagonal matrix with entries ± 1 that is used to raise and lower indices a, b and keeps track of the sign changes due to inverse time ordering. Much like the propagator matrix, the Σ_{ab} can be expressed as

$$i\Sigma_\rho = i\left(\Sigma_{21} - \Sigma_{12}\right) \tag{2.34}$$

$$i\Sigma_F = \frac{1}{2}\left(\Sigma_{21} + \Sigma_{12}\right)\,, \tag{2.35}$$

and satisfies the thermal-equilibrium relation

$$\Sigma_F(\mathbf{p},\omega) = -\frac{i}{2}\left(1 + 2n(\omega)\right)\Sigma_\rho(\mathbf{p},\omega)\,. \tag{2.36}$$

The connection between Σ_ρ and the decay processes in the model introduces the relaxation timescale

$$\tau(\mathbf{p},\omega) = \frac{4\omega}{i\Sigma_\rho(\mathbf{p},\omega)}\,, \tag{2.37}$$

which will be important in obtaining the dissipation coefficient Υ that enters the inflaton field equation (2.1) in warm-inflation models.

2.3.3 Interactions and the Effective Equations of Motion

In order to introduce interactions into the CTP description of field dynamics, let us take a look at the effective equations of motion that result from the generating functional.

In the path-integral formalism, the generating functional (2.25) takes the form

$$Z[J_1, J_2] = \int \mathrm{d}\mu[\phi_1]\mathrm{d}\mu[\phi_2]\, \rho[\phi_1(t_\mathrm{i}), \phi_2(t_\mathrm{i})] \exp\left(iS[\phi_1] + i\int J_1\phi_1 - iS[\phi_2] - i\int J_2\phi_2 \right), \tag{2.38}$$

where the paths cross asymptotically at $t \to \infty$. It is worth noting that the density matrix ρ only enters at the initial time, which is why this approach is also referred to as the in-in formalism. This path integral is equivalent to integrating a single field along a closed contour in the complex time plane from $t = t_\mathrm{i}$ to ∞ (forward branch) and back to t_i (backward branch). Here, keeping the fields and branches distinct will enable us to make a convenient field re-definition known as the Keldysh rotation.

We see from equation (2.27) that the elements of the propagator matrix G_{ab} in the CTP formalism are not all independent of each other; an appropriate transformation can make some of them vanish. Instead of using the fields ϕ_1 and ϕ_2, signifying the inflaton on the forward and backward branch of the contour integration, respectively, we define the fields

$$\phi_\mathrm{c} = \frac{1}{2}(\phi_1 + \phi_2)\,, \tag{2.39}$$

$$\phi_\Delta = \phi_1 - \phi_2\,. \tag{2.40}$$

This transformation is know as the Keldysh rotation. It leads to the new propagator matrix

$$G_{a'b'}(x, x') = \begin{pmatrix} F(x, x') & G_\mathrm{R}(x, x') \\ G_\mathrm{A}(x, x') & 0 \end{pmatrix}, \tag{2.41}$$

where

$$G_{\mathrm{R}}(x,x') = -i\rho(x,x')\Theta(t-t')\,, \tag{2.42}$$

$$G_{\mathrm{A}}(x,x') = i\rho(x,x')\Theta(t'-t)\,, \tag{2.43}$$

$$F(x,x') = \frac{1}{2}\left\langle \left\{ \hat{\phi}(x), \hat{\phi}(x') \right\} \right\rangle_{\mathrm{c}}\,. \tag{2.44}$$

The self-energy matrix takes the form

$$\Sigma^{a'b'}(x,x') = \begin{pmatrix} 0 & \Sigma_{\mathrm{A}}(x,x') \\ \Sigma_{\mathrm{R}}(x,x') & -i\Sigma_{\mathrm{F}}(x,x') \end{pmatrix} \tag{2.45}$$

with

$$\Sigma_{\mathrm{R}}(x,x') = \Sigma_{\rho}(x,x')\Theta(t-t')\,, \tag{2.46}$$

$$\Sigma_{\mathrm{A}}(x,x') = -\Sigma_{\rho}(x,x')\Theta(t'-t)\,. \tag{2.47}$$

To illustrate the usefulness of the Keldysh representation, let us consider the example of $\lambda\phi^4$ theory. In the CTP formalism, the classical action is

$$S[\phi_1,\phi_2] = \int \mathrm{d}^4x \left[\frac{1}{2}\phi_1\left(-\partial^2 - m^2\right)\phi_1 - \frac{\lambda}{4!}\phi_1^4\right] - \int \mathrm{d}^4x \left[\frac{1}{2}\phi_2\left(-\partial^2 - m^2\right)\phi_2 - \frac{\lambda}{4!}\phi_2^4\right]\,. \tag{2.48}$$

After Keldysh rotation, we have

$$S[\phi_{\mathrm{c}},\phi_{\Delta}] = \int \mathrm{d}^4x \left[\phi_{\Delta}\left(-\partial^2 - m^2\right)\phi_{\mathrm{c}} - \frac{\lambda}{4!}\left(4\phi_{\Delta}\phi_{\mathrm{c}}^3 + \phi_{\Delta}^3\phi_{\mathrm{c}}\right)\right]\,, \tag{2.49}$$

which vanishes if the field configurations on the forward and the backward branch are identical, that is, $\phi_{\Delta} = 0$. Conveniently, this remains true for the effective action, restricting the possibilities for vertex and self-energy corrections. For instance, any c–c terms in the self energy have to vanish, since $\Sigma^{\mathrm{cc}} = 0$. The action (2.49) returns the classical equation of motion, which is given by

$$\left.\frac{\delta S[\phi_{\mathrm{c}},\phi_{\Delta}]}{\delta\phi_{\Delta}}\right|_{\phi_{\Delta}=0} = 0\,, \tag{2.50}$$

which reproduces the usual equation

$$\left(\partial^2 + m^2\right)\phi_{\rm c} + \frac{\lambda}{3!}\phi_{\rm c}^3 = 0\,. \tag{2.51}$$

In the Keldysh representation, quantum corrections to the classical action can be expressed in the form

$$\Gamma[\phi_{\rm c},\phi_\Delta] = -\int {\rm d}^4x \mathcal{F}(x)\phi_\Delta(x) + \frac{1}{2}\int {\rm d}^4x\,{\rm d}^4x'\phi_\Delta(x)\,i\Sigma_{\rm F}(x,x')\,\phi_\Delta(x') + \mathcal{O}(\phi_\Delta^3)\,, \tag{2.52}$$

where, in absence of the second term, the first term yields the effective field equation

$$\mathcal{F}(x) = -\left.\frac{\delta\Gamma[\phi_{\rm c},\phi_\Delta]}{\delta\phi_\Delta}\right|_{\phi_\Delta=0} = 0\,. \tag{2.53}$$

For now, neglecting the vertex corrections but keeping the full self-energy, leads to the field equation

$$\mathcal{F} = \left(\partial^2 + m^2 + \frac{\lambda}{3!}\phi_{\rm c}(x)^2\right)\phi_{\rm c}(x) + \int {\rm d}^4x'\,\Sigma_{\rm R}(x,x')\,\phi_{\rm c}(x') = 0\,. \tag{2.54}$$

We can now introduce a random field $\xi(x)$ to decouple the quadratic term in the effective action and recover the information contained therein about the fluctuations of the system about the solutions of the effective field equations. The Hubbard-Stratonovich transform (Stratonovich, 1957; Hubbard, 1959) allows us to transform the partition function in the following way,

$$\begin{aligned}&\exp\left(-\frac{1}{2}\int {\rm d}^4x\,{\rm d}^4x'\phi_\Delta(x)\,i\Sigma_{\rm F}(x,x')\,\phi_\Delta(x')\right)\\ &= |\det\Sigma_{\rm F}|^{1/2}\int D\xi\exp\left\{-\frac{1}{2}\int {\rm d}^4x\,{\rm d}^4x'\xi(x)\Sigma_{\rm F}(x,x')^{-1}\xi(x') + i\int\xi(x)\phi_\Delta(x)\right\}.\end{aligned} \tag{2.55}$$

This leaves the action with a quadratic term in the random field ξ and a term linear in ϕ_Δ and leads to an effective field equation with a stochastic source,

$$\left(\partial^2 + m^2 + \frac{\lambda}{3!}\phi_{\rm c}(x)^2\right)\phi_{\rm c}(x) + \int {\rm d}^4x'\,\Sigma_{\rm R}(x,x')\,\phi_{\rm c}(x') = \xi(x)\,. \tag{2.56}$$

The field $\xi(x)$ can be interpreted as Gaussian stochastic noise with

$$\langle \xi(x) \rangle = 0\,, \quad \langle \xi(x)\xi(x') \rangle = \Sigma_{\mathrm{F}}(x, x')\,. \tag{2.57}$$

As we can see, the dynamics of our background scalar field coupled to the quantum fields that constitute its environment can be described in terms of a Langevin-type equation. Of course, that is exactly what we would expect for the equations of motion of a system interacting with its environment.

It is now possible to define a dissipation kernel $\mathcal{D}(x, x')$ as

$$\Sigma_\rho(x, x') = -\frac{\partial}{\partial t'}\mathcal{D}(x, x')\,, \tag{2.58}$$

such that the field equation explicitly contains a dissipation-like term,

$$\left(\partial^2 + m^2 + \frac{\lambda}{3!}\phi_{\mathrm{c}}(x)^2\right)\phi_{\mathrm{c}}(x) + \int \mathrm{d}^4x'\,\mathcal{D}(x, x')\,\dot{\phi}_{\mathrm{c}}(x') = \xi(x)\,. \tag{2.59}$$

Under Fourier transformation, the noise and dissipation kernels are related by the equation (2.36),

$$\Sigma_F(\mathbf{p}, \omega) = 2\omega\left(n(\omega) + \frac{1}{2}\right)\mathcal{D}(\mathbf{p}, \omega)\,, \tag{2.60}$$

which is an instance of a fluctuation–dissipation relation. With the noise kernel defined above, we also find that, in the Rayleigh-Jeans regime, where $\omega \ll T$, we can simplify $2\omega\left(n(\omega) + \frac{1}{2}\right) \to 2T$ and find for the auto-correlation of the noise,

$$\langle \xi((p), t)\xi((p), t') \rangle = 2T\int \frac{\mathrm{d}\omega}{2\pi}\mathcal{D}(\mathbf{p}, \omega)\mathrm{e}^{-i\omega(t-t')}\,, \tag{2.61}$$

which is an important ingredient in the analysis of the scalar-field fluctuations that, in the inflationary context, will lead to density fluctuations.

2.3.4 Markovian Approximation

The field equation (2.59) is a non-linear, non-local stochastic equation, which makes it very difficult to solve analytically or numerically. The problem would be greatly simplified if it could be approximated by a Markovian version, which would not require knowledge (and storage) of the entire history of the scalar

field. It has been shown (Moss and Xiong, 2006; Berera *et al.*, 2007) that a local approximation for the dissipation and fluctuation kernels is indeed possible in the two-stage decay mechanism (Berera and Ramos, 2001), which underlies the models of warm inflation considered in this work.

The dissipative term Υ takes on a local form if the variation of the spatially homogeneous background field ϕ_c about its equilibrium value $\phi(t)$ is slow compared to the relaxation time of the system. Defining $\delta\phi_\mathrm{c} = \phi_\mathrm{c} - \phi(t)$, we can expand the CTP effective field equation for ϕ (Moss and Xiong, 2006),

$$\mathcal{F}(x) = \sum_{n=0}^{\infty} \mathcal{F}_n(x)\,, \tag{2.62}$$

$$\mathcal{F}_n(x) = -\frac{1}{n!}\int \mathrm{d}^4x_1 \ldots \mathrm{d}^4x_n \left.\frac{\delta^{n+1}\Gamma}{\delta\phi_\Delta(x)\delta\phi_\mathrm{c}(x_1)\ldots\delta\phi_\mathrm{c}(x_n)}\right|_{\phi_\mathrm{c}=\phi(t)} \delta\phi_\mathrm{c}(x_1)\ldots\delta\phi_\mathrm{c}(x_n)\,. \tag{2.63}$$

The first term, $\mathcal{F}_0$, contains those terms in the field equation that are free from derivatives; they can be expressed as the derivative of an effective potential $V(\phi)$,

$$-\left.\frac{\delta\Gamma}{\delta\phi_\Delta(x)}\right|_{\phi_\mathrm{c}=\phi(t)} = \frac{\partial V}{\partial\phi}\,. \tag{2.64}$$

The second term, $\mathcal{F}_1$, contains the derivative terms and the equilibrium self-energy of the background scalar field,

$$-\left.\frac{\delta^2\Gamma}{\delta\phi_\Delta(x)\delta\phi_\mathrm{c}(x')}\right|_{\phi_\Delta=\phi(t)} = \left(\partial^2 + m^2\right)\delta(x-x') + \Sigma_\mathrm{R}(x,x')\,. \tag{2.65}$$

To first order in $\delta\phi$, the field equation then takes the form

$$\ddot{\phi} + \int \mathrm{d}^4x_1 \Sigma_\mathrm{R}(x-x_1)\delta\phi(t_1) + \frac{\partial V}{\partial\phi} = 0\,, \tag{2.66}$$

which again contains a non-local dissipation term. The system remains always close to equilibrium if the inflaton field varies slowly with respect to the response time (2.37) of the heavy catalyst fields. This separation of timescales allows us to use the Taylor expansion

$$\phi(t_1) = \phi(t) + (t_1 - t)\dot{\phi}(t) + \ldots\,, \tag{2.67}$$

which leads to a linear dissipative term in the field equation for ϕ,

$$\ddot{\phi} + \Upsilon\dot{\phi} + \frac{\partial V}{\partial \phi} = 0 \tag{2.68}$$

with dissipation coefficient

$$\Upsilon = -\int \mathrm{d}^4x' \Sigma_{\mathrm{R}}(x')t' = \frac{i}{2}\frac{\partial \Sigma_\rho(0,\omega)}{\partial \omega}\bigg|_{\omega=0} . \tag{2.69}$$

2.3.5 Indirect Decay

We saw in equation (2.69) that the Markovian dissipation coefficient can be obtained from the equilibrium self energy, harkening back to the fluctuation–dissipation relations that underlie the dynamics of this theory. Using the expressions (2.30) and (2.31), the field propagators contained in the self energy can be written in terms of the spectral function.

An important application of these results is the decay of inflaton particles during warm inflation (Moss and Xiong, 2006). Here, we focus on the so-called two-stage mechanism for indirect decay of the inflaton (Berera and Ramos, 2001). The inflaton is taken to couple to the radiation fields σ only through heavy mediator fields χ. This allows us to separate the thermalisation process of the heat bath from the dissipation of inflaton energy.

As a simple example, consider the two interaction Lagrangians coupling the inflaton to the mediator fields,

$$\mathcal{L}_{\mathrm{I}} = g\, m \left(\delta\phi + \delta\phi^\star\right) |\chi|^2 + 2g^2 |\delta\phi|^2 |\chi|^2 , \tag{2.70}$$

and the mediators to the radiation field,

$$\mathcal{L}'_{\mathrm{I}} = \frac{1}{\sqrt{2}} h\, m \left(\sigma^2\chi^\star + \sigma^{\star 2}\chi\right) . \tag{2.71}$$

Here m is a mass that, in supersymmetric models, is often given by the mediator mass m_χ. The use of complex fields will make it easier to embed these interactions in a supersymmetric theory.

At order g^2, the contribution to the inflaton self energy is given by the diagram in figure (2.1). When the self energy is expressed in terms of the χ spectral

function, the dissipation coefficient (2.69) is given by (Moss and Xiong, 2006)

$$\Upsilon = 4g^2m^2 \int \frac{\mathrm{d}^3k}{(2\pi)^3} \int_0^\infty \frac{\mathrm{d}\omega}{2\pi} \rho_\chi^2 n' \,, \tag{2.72}$$

where n' is the derivative of the thermal distribution function, $n' = \mathrm{d}n(\omega)/\mathrm{d}\omega$. There are two regimes where this expression for Υ simplifies significantly. Firstly, for small h and fixed T, the energy integral is dominated by the point $\omega = \omega_k \equiv (k^2 + m^2)^{1/2}$. This point lies close to the poles of the spectral function at $\omega = \omega_k \pm i\tau_\chi^{-1}$, where the relaxation time τ_χ for the χ boson is given by equation (2.37). The dissipation coefficient in this weak-coupling regime is then given by

$$\Upsilon \approx g^2m^2\beta \int \frac{\mathrm{d}^3k}{(2\pi)^3} \frac{\tau_\chi}{\omega_k^2} n(n+1) \,. \tag{2.73}$$

The relaxation time changes with the strength of the coupling between mediators and radiation field, $\tau_\chi \propto h^{-2}$. Therefore, as we decrease h, the relaxation time increases, which increases the dissipation coefficient. It is worth noting that we cannot allow h to shrink to zero within our approximations: we require the system to be close to equilibrium at all times, which sets an upper limit on the relaxation time.

The second interesting limit of the dissipation coefficient (2.72) is that of low temperatures, $T \ll m_\chi$ with fixed coupling h. There, the integrals are dominated by the low-momentum and low-energy regime, where $\omega, k \ll m_\chi$, and we obtain (Berera *et al.*, 2009)

$$\Upsilon \approx Cg^2h^4 \left(\frac{m}{m_\chi}\right)^6 \frac{T^3}{m_\chi^2} \,. \tag{2.74}$$

For the interaction Lagrangian considered here, the constant C takes on the value $C \approx 0.006$.

The low-temperature approximation to the full dissipation coefficient will also be the focus of the following section. There, we will consider a different interaction Lagrangian based on a supersymmetric model of inflaton dissipation. It is important to note that results obtained here do not take into account the finite decay width of the χ fields. In the following, in section 2.4.2, we will see that finite-width effects change the dependence of the low-momentum

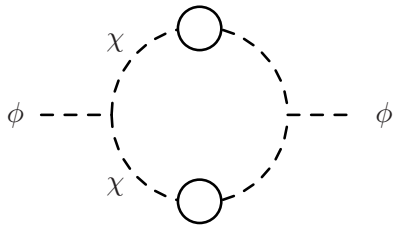

Figure 2.1: Contribution to the self energy of ϕ at order g^2.

dissipation coefficient on the effective coupling to be $\Upsilon \propto h^2 N_Y$ for N_Y light fields; nevertheless, we will recover the same temperature dependence $\Upsilon \propto T^3/m_\chi^2$.

2.4 A Particle-Physics Implementation

Let us now apply the analysis of the previous section to the interactions that form the basis for this work. These interactions implement the two-stage decay mechanism we encountered above and reproduce many of the same results for the dissipation coefficient. Additionally, we will make use of supersymmetry as a convenient mechanism for suppressing radiative corrections to the inflaton potential; such corrections might otherwise prevent a sufficiently long period of slow-roll inflation.

The relevant fields are contained in the chiral superfields Φ, X, and Y_i with $i = 1, \ldots N_Y$. Their interactions are described by the superpotential

$$W = \frac{g}{2}\Phi X^2 + \frac{h_i}{2} X Y_i^2 + f(\Phi)\,, \tag{2.75}$$

where we sum over the index i. Self-interaction in the inflaton sector is described by the holomorphic function $f(\Phi)$. We will denote the scalar component of Φ by ϕ. The background value φ of the inflaton field is then given by the expectation value $\langle|\phi|\rangle = \varphi/\sqrt{2}$, which we assume to be real. Superpotentials like this can be obtained, for example, in D-brane inflation (Bastero-Gil *et al.*, 2011c).

The scalar components of X and Y_i are denoted by χ and σ_i, respectively, and we can write their interactions with the vacuum expectation value of the inflaton

as

$$\mathcal{L}_{\text{scalar}} = V(\varphi) + \frac{1}{2}g^2\varphi^2|\chi|^2 + \frac{g}{2}\sqrt{V(\varphi)}\left(\chi^2 + \chi^{\dagger 2}\right) + \frac{g^2}{4}|\chi|^4 + \\ + \frac{h_i}{2}\frac{g\varphi}{\sqrt{2}}\left(\chi\sigma_i^{\dagger 2} + \chi^\dagger\sigma_i^2\right) + \frac{h_i h_j}{4}\sigma_i^2\sigma_j^{\dagger 2} + h_i^2|\chi|^2|\sigma_i|^2\,, \tag{2.76}$$

where we have introduced the inflaton potential $V(\varphi) = |f'(\phi)|^2$. The interactions between the fermionic components ψ_χ and ψ_{σ_i} and the inflaton are given by

$$\mathcal{L}_{\text{fermion}} = \frac{g\varphi}{\sqrt{2}}\overline{\psi}_\chi P_{\text{L}}\psi_\chi + h_i\chi\overline{\psi}_{\sigma_i}P_{\text{L}}\psi_{\sigma_i} + \frac{h_i}{2}\sigma_i\overline{\psi}_{\sigma_i}P_{\text{L}}\psi_\chi + \text{h.c.}\,, \tag{2.77}$$

where $P_{\text{L}} = (1-\gamma_5)/2$ is the left-handed chiral projector.

We can see that the X fields, coupling to the inflaton directly, acquire a tree-level mass that is expected to be large for large inflaton vevs. The Y_i fields, on the other hand, remain massless at tree level. Furthermore, the non-zero potential energy of the inflaton breaks supersymmetry and induces a mass splitting in the χ sector,

$$m^2_{\chi_{\text{R,I}}} = \frac{g^2\varphi^2}{2}\left(1 \pm \frac{\sqrt{V(\varphi)}}{g\varphi^2}\right)\,, \tag{2.78}$$

$$m^2_{\psi_\chi} = \frac{g^2\varphi^2}{2}\,, \tag{2.79}$$

where $\chi = (\chi_{\text{R}} + i\chi_{\text{I}})/\sqrt{2}$. However, we expect the inflaton self-interactions to be small during inflation to allow for sufficiently long slow roll and for a sufficiently small amplitude of primordial density perturbations. For a typical $\lambda\varphi^4$ potential, for example, the splitting in equation (2.78) would be given by $\sqrt{\lambda}/g$; using a typical value $\lambda \simeq \mathcal{O}(10^{-14})$ and values for g seen in figure (3.8), we find $g \gg \sqrt{\lambda}$. Therefore, the mass splitting can generally be neglected during inflation, and we will consider the common mass for all χ fields to be

$$m_\chi = \frac{g\varphi}{\sqrt{2}}\,. \tag{2.80}$$

As long as the inflaton mass exceeds the temperature of the radiation bath during warm inflation, that is, as long as the inflaton vev is sufficiently large, thermal corrections to the mass from X-field loops are Boltzmann suppressed

with $\exp(-m_\chi/T) \ll 1$. The flatness of the tree-level inflaton potential therefore remains intact in spite of such corrections.

Even though the mass splitting in the scalar sector is small during inflation, the breakdown of supersymmetry means that loop corrections to the inflaton potential no longer vanish. The Coleman-Weinberg correction to the inflaton potential is then given by (Coleman and Weinberg, 1973; Hall and Moss, 2005; Bastero-Gil *et al.*, 2014b)

$$V_{\mathrm{CW}} = \frac{1}{32\pi^2}\,\mathrm{Str}\left[\mathcal{M}_X^4\left(\ln\left(\frac{\mathcal{M}_X^2}{\mu^2}\right) - \frac{3}{2}\right)\right] \simeq \frac{g^2}{32\pi^2}V(\varphi)\ln\left(\frac{m_\chi^2}{\mu^2}\right)\,, \qquad (2.81)$$

where μ is the renormalisation scale, $\mathrm{Str}(\dots)$ is the supertrace and $\mathcal{M}_X$ is the mass matrix of the X fields. If one considers, as we will, N_χ multiplets of mediator fields coupled to the inflaton as in equation (2.75), the radiative corrections are proportional to $g^2 N_\chi$. For sufficiently small couplings g between the inflaton and the X fields, we may therefore be able to accommodate many X multiplets without spoiling the flatness of the inflaton potential.

It is interesting to note that the mass splitting (2.79) can induce a phase transition like those typical of hybrid inflation. If, for example, $f(\Phi) = gM^2\Phi$, we find $V(\varphi) \simeq g^2M^4$ and $m^2_{\chi\mathrm{R,I}} = m_\chi^2 \pm M^2/\varphi^2$, such that the imaginary component of χ becomes tachyonic for $\varphi < \varphi_{\mathrm{c}} = M$. In the absence of a radiation bath, inflation would then end via the usual hybrid mechanism. The effects of non-zero temperature can delay the phase transition by modifying this critical field value (Bastero-Gil *et al.*, 2014b). If we allow for a thermal correction $+\alpha^2T^2$ to each of the masses (2.79), the critical field value is $\varphi_{\mathrm{c}} = \sqrt{M^2 - \alpha^2T^2/2g^2}$, and the hybrid transition may be delayed. We will neglect such corrections in this work.

The couplings described by the superpotential (2.75) also allow the χ fields to decay in the processes $\chi \to \sigma\sigma, \psi_\sigma\psi_\sigma$ and $\psi_\chi \to \sigma\psi_\sigma$. When (real or virtual) χ and ψ_χ pairs are produced by the rolling inflaton, they can therefore decay into Y_i fields—an implementation of the two-stage decay mechanism of dissipative particle production (cf. section 2.3.5). Additionally, the decay of X fields into Y_i fields may be needed to help reheat the universe if hybrid inflation ends via the delayed waterfall transition discussed above (Bastero-Gil *et al.*, 2014b).

It is also clear from the interactions (2.76) and (2.77) that the light Y_i fields

may scatter off each other. These scatterings help keep the radiation bath near thermal equilibrium and significantly simplify the derivation of the dissipative dynamics, as we saw in section 2.3.5.

2.4.1 Finite-temperature effects

A brief word on finite-temperature effects. Owing to their coupling to the inflaton vev, the X fields have large tree-level masses during inflation. Since we focus on the low-temperature regime $T < m_\chi$, the X-field contribution to thermal-loop corrections is Boltzmann suppressed and can be ignored.

The X fields themselves, however, receive thermal corrections from their interaction with the light Y_i fields, given by the first three diagrams in figure (2.2). The fermionic and bosonic components receive identical corrections, leading to the effective mass (Hall and Moss, 2005; Bastero-Gil *et al.*, 2013)

$$\tilde{m}_\chi^2 = m_\chi^2 + \frac{h^2 N_Y}{8} T^2 \,. \tag{2.82}$$

The leading-order thermal correction to the inflaton potential is then given by replacing m_χ by $\tilde{m}_\chi$ in the Coleman-Weinberg correction (2.81). We see that they are logarithmic and, in the low-temperature regime, smaller than the zero-temperature radiative corrections; nevertheless, we will include them in the calculation of the dissipation coefficient.

The fourth diagram in figure (2.2) modifies the χ two-point function in a way that requires a perturbative resummation of higher-order diagrams of that form (Bastero-Gil *et al.*, 2013). This resummation is only valid when $h^2 N_Y \lesssim 1$, and therefore we impose that constraint on all the work done here.

Finally, thermal corrections to the σ_i masses are, at leading order, given by

$$m_\sigma^2 = m_0^2 + \frac{h^2}{12} T^2 + \mathcal{O}(h^4 N_Y) \,. \tag{2.83}$$

Here, m_0 is a tree-level mass that could arise from SUSY breaking effects. If the light fields include the MSSM fields, we expect $m_0 \sim 1\,\mathrm{TeV} \ll T$ (Bastero-Gil *et al.*, 2013); and since $h^2 N_Y \lesssim 1$ requires $h < 1$, we will assume that $m_\sigma \ll T$, such that thermal production is efficient.

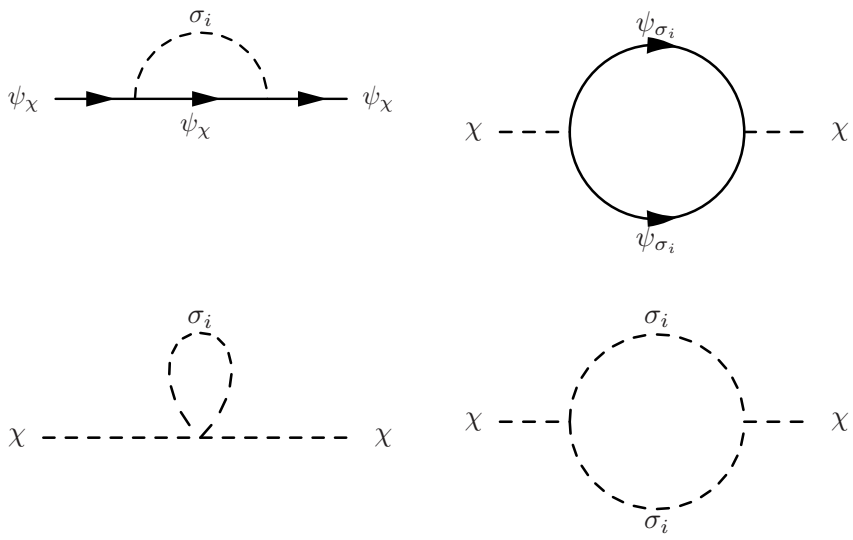

Figure 2.2: Leading contributions to the self-energy of the ψ_χ and χ fields (Bastero-Gil et al.*, 2013).*

2.4.2 The Dissipation Coefficient

Let us now return to some of our earlier results for the dissipation coefficient and apply them to the model (2.75). The interactions specified by this superpotential implement the two-stage decay mechanism for the dissipation of inflaton energy. The inflaton φ is coupled to the fields in the X multiplet, which in turn decay into the light fields of the Y_i multiplet. This leads, in the adiabatic regime $\dot{\varphi}/\varphi, H \ll \Gamma_\chi$, to the effective friction term $\Upsilon\dot{\varphi}^2$ in the inflaton field equation. The dissipation coefficient (2.69) is then given by (Berera *et al.*, 2009; Bastero-Gil *et al.*, 2011a)

$$\Upsilon = \frac{4}{T}\left(\frac{g^2}{2}\right)^2 \varphi^2 \int \frac{\mathrm{d}^4 p}{(2\pi)^4} \rho_\chi^2 n_\mathrm{B}\left(1 + n_\mathrm{B}\right) , \tag{2.84}$$

where $n_\mathrm{B}(p_0) = \left(\mathrm{e}^{p_0/T} - 1\right)^{-1}$ is the Bose–Einstein distribution. The spectral function for the χ fields is given by

$$\rho_\chi(p_0, p) = \frac{4\omega_p \Gamma_\chi}{\left(p_0^2 - \omega_p^2\right)^2 + 4\omega_p^2 \Gamma_\chi^2} , \tag{2.85}$$

where $\omega_p = \sqrt{\tilde{m}_\chi^2 + p^2}$ for modes with 3-momentum $|\mathbf{p}| = p$ and energy p_0, and $\tilde{m}_\chi$ is the thermally-corrected χ mass (2.82).

The shape of ρ_χ determines the two dissipation regimes we are interested in. We will consider contributions from virtual, low-momentum modes and from on-shell modes near the pole of ρ_χ at $p_0^2 = \omega_p^2$. Bosonic and fermionic decays have equal branching ratios in the pole regime, but fermionic decays turn out to be negligible in the low-momentum regime (Bastero-Gil *et al.*, 2011a). We will therefore focus on the bosonic channels $\chi \to \sigma_i \sigma_i$. Their decay width is given by

$$\Gamma_\chi = \frac{h^2 N_Y}{64\pi} \frac{m_\chi^2}{\omega_p} F_T(p, p_0)\,, \tag{2.86}$$

where

$$\begin{aligned} F_T(p,p_0) = &\left[\frac{\omega_+ - \omega_-}{p} + \frac{T}{p}\log\left(\frac{1-\mathrm{e}^{-\frac{\omega_+}{T}}}{1-\mathrm{e}^{-\frac{\omega_-}{T}}}\frac{1-\mathrm{e}^{-\frac{p_0-\omega_-}{T}}}{1-\mathrm{e}^{-\frac{p_0-\omega_+}{T}}}\right)\right]\theta\big(p_0^2 - p^2 - 4m_\sigma^2\big) + \\ &+ \left[\frac{T}{p}\log\left(\frac{1-\mathrm{e}^{-\frac{\omega_+}{T}}}{1-\mathrm{e}^{-\frac{\omega_-}{T}}}\frac{1-\mathrm{e}^{-\frac{p_0+\omega_-}{T}}}{1-\mathrm{e}^{-\frac{p_0+\omega_+}{T}}}\right)\right]\theta\big(-p_0^2 + p^2 - 4m_\sigma^2\big) \end{aligned} \tag{2.87}$$

with the Heaviside function $\theta(x)$ and with

$$\omega_\pm = \sqrt{k_\pm^2 + m_\sigma^2}\,, \qquad k_\pm = \frac{1}{2}\left|p \pm p_0\left(1 - \frac{4m_\sigma^2}{p_0^2 - p^2}\right)^{\frac{1}{2}}\right|\,, \tag{2.88}$$

where m_σ is the mass of the bosons σ_i. Below, we will take a closer look at the behaviour of the dissipation coefficient (2.84) as a function of the effective coupling $\hat{h} = h\sqrt{N_Y}$, the mass of the χ fields, and the ratio m_χ/T.

Low-Momentum-Dominated Dissipation

Dissipation via low-momentum, virtual χ modes with $p,\, p_0 \ll m_\chi$ is dominant for large m_χ and $h\sqrt{N_Y}$. If these modes have a narrow width, $\Gamma_\chi \ll m_\chi$, and we can neglect the thermal mass correction, the spectral function takes the simple form $\rho_\chi \simeq 4\Gamma_\chi/m_\chi^3$. The dissipation coefficient is then given by

$$\Upsilon^{\mathrm{LM}} = A g^2 \hat{h}^4 \frac{T^3}{m_\chi^2}\,, \tag{2.89}$$

where the constant A is determined from numerical data to be $A \simeq 1.63 \times 10^{-3}$ for $m_\sigma/T = 0.01$ (Bastero-Gil *et al.*, 2013).

For larger couplings $\hat{h} \lesssim 1$, the thermal mass correction and the finite width of the χ fields become relevant, and the dissipation coefficient is described by

$$\Upsilon^{\mathrm{LM}} = \frac{A g^2 \hat{h}^4}{1 + \alpha \hat{h}^2} \frac{T^3}{m_\chi^2}, \tag{2.90}$$

where $\alpha = 0.16$ for $m_\sigma/T = 0.01$. Numerically, the coefficients are given by

$$A \simeq -4.3 \times 10^{-4} \ln\left(1 - \mathrm{e}^{-\frac{5}{2}\frac{m_\sigma}{T}}\right), \tag{2.91}$$

$$\alpha \simeq -0.05 \ln\left(1 - \mathrm{e}^{-4\frac{m_\sigma}{T}}\right). \tag{2.92}$$

In the limit $m_\sigma \ll T$, where the large negative logarithm makes α large, the low-momentum-dominated dissipation coefficient can then be written as (Bastero-Gil *et al.*, 2013)

$$\Upsilon^{\mathrm{LM}} \simeq C_\phi \frac{T^3}{m_\chi^2}, \quad C_\phi \simeq 0.01 g^2 h^2 N_Y \tag{2.93}$$

with $m_\chi = g\varphi/\sqrt{2}$. Comparing to the earlier result (2.74) (Moss and Xiong, 2006), we see that finite-width effects change the dependence of the low-momentum dissipation coefficient on the effective coupling to $\Upsilon \propto h^2 N_Y$.

Pole-Dominated Dissipation

Let us now consider the contribution of real χ modes. Their production is Boltzmann suppressed as $\mathrm{e}^{-m_\chi/T}$ but can, even in the low-temperature regime, be enhanced by sufficiently small values of the effective coupling $\hat{h}$.

Real, on-shell χ modes are produced when $p_0 \simeq \omega_p$, which corresponds to the pole of the spectral function (2.85). By expanding the spectral function about this pole, the dissipation coefficient (2.84) turns into

$$\Upsilon^{\mathrm{pole}} = \frac{2}{T}\left(\frac{g^2}{2}\right)^2 \varphi^2 \int \frac{\mathrm{d}^3 p}{(2\pi)^3} \frac{1}{\Gamma_\chi \omega_p^2} n_{\mathrm{B}} \left(1 + n_{\mathrm{B}}\right) \tag{2.94}$$

with $n_{\mathrm{B}} = n_{\mathrm{B}}(\omega_p)$.

It is worth noting that the branching ratios for the decay of φ to the on-shell scalars and fermions of the X multiplet are the same. For simplicity, we will focus on decay into scalars alone, but it should be noted that the inclusion of the fermionic channels would halve the dissipation coefficient.

Thermal corrections to the decay width (2.86) are given by the function F_T (2.87). At low temperatures $T \lesssim m_\chi$ and momenta $p \lesssim T$, the $m_\sigma \ll T$ limit of F_T can be expanded as

$$F_T(p, \omega_p) \simeq 1 + 2\mathrm{e}^{-\frac{1}{2}\frac{m_\chi}{T}} + \mathcal{O}\left(\frac{p}{T}\right)^2 . \tag{2.95}$$

Thermal corrections to Γ_χ can therefore be neglected in this regime and remain sub-leading even for $p \gtrsim T$; we proceed using the zero-temperature decay width $\Gamma_\chi \simeq (h^2/64\pi)(m_\chi^2/\omega_p)$. The dissipation coefficient is then given by

$$\Upsilon^{\mathrm{pole}} = \frac{32}{\pi}\frac{g^2}{\hat{h}^2}\frac{1}{T}\int \frac{p^2\,\mathrm{d}p}{\omega_p} n_{\mathrm{B}}\left(1 + n_{\mathrm{B}}\right) . \tag{2.96}$$

For $m_\chi \gg T$, we can simplify this further by recognising that the integral is dominated by small momenta. Defining $x = p/T$, we can write

$$n_{\mathrm{B}}(1 + n_{\mathrm{B}}) \simeq \mathrm{e}^{-\sqrt{x^2 + (m_\chi/T)^2}} \simeq \mathrm{e}^{-m_\chi/T}\mathrm{e}^{\frac{1}{2}\frac{x^2}{m_\chi/T}} . \tag{2.97}$$

Using the integral

$$\int_0^\infty \mathrm{d}x \frac{x^2}{\sqrt{x^2 + \left(\frac{m_\chi}{T}\right)^2}} \mathrm{e}^{-\frac{x^2}{2m_\chi/T}} \simeq \sqrt{\frac{\pi m_\chi}{2\,T}} , \tag{2.98}$$

we then obtain the dissipation coefficient in the pole-dominated regime,

$$\Upsilon^{\mathrm{pole}} \simeq \frac{32}{\sqrt{2\pi}}\frac{g^2}{\hat{h}^2}\sqrt{m_\chi T}\mathrm{e}^{-m_\chi/T} . \tag{2.99}$$

As we can see from this expression, this pole term increases towards small effective couplings $\hat{h}$, so that the exponential suppression may be overcome by the χ resonance in this regime. Furthermore, in the small-$\hat{h}$ regime, the low-momentum term (2.93), proportional to $\hat{h}^2$, tends to be small, so the pole contribution to inflaton dissipation can be significant and can even come to dominate.

Full Dissipation Coefficient

Combining the results for the low-momentum (2.93) and the pole regions (2.99) of inflaton dissipation via intermediate χ fields, we can write the full dissipation coefficient as

$$\Upsilon = \Upsilon_{\rm LM} + \Upsilon_{\rm pole} \equiv C_\phi \frac{T^3}{\varphi^2}, \tag{2.100}$$

with

$$\Upsilon_{\rm LM} = C_\phi^{\rm LM} \frac{T^3}{m_\chi^2}, \tag{2.101}$$

$$\Upsilon_{\rm pole} = C_\phi^{\rm pole} \sqrt{m_\chi T}\, \mathrm{e}^{-m_\chi/T}, \tag{2.102}$$

where $m_\chi = g\varphi/\sqrt{2}$. The various coefficients are given by

$$C_\phi^{\rm pole} = \frac{32}{\sqrt{2\pi}} \frac{g^2 N_\chi}{h^2 N_Y}\,, \tag{2.103}$$

$$C_\phi^{\rm LM} = 0.01\, h^2 N_Y\, g^2 N_\chi\,, \tag{2.104}$$

$$C_\phi = \frac{2}{g^2}\left(C_\phi^{\rm pole} \left(\frac{m_\chi}{T}\right)^{5/2} \mathrm{e}^{-m_\chi/T} + C_\phi^{\rm LM} \right)\,, \tag{2.105}$$

The expression (2.100) holds for $m_\sigma \ll T$ and $\hat{h} = h\sqrt{N_Y} \lesssim 1$ and forms the basis for the numerical analysis in this work. As the pole contribution decreases with $\hat{h}$ and the low-momentum contribution grows, the two terms become comparable at

$$\hat{h} \simeq 6 \left(\frac{m_\chi}{T}\right)^{5/8} \mathrm{e}^{-\frac{1}{4}\frac{m_\chi}{T}}\,. \tag{2.106}$$

For a given value of $\hat{h}$, this crossover point allows us to determine the ratio m_χ/T above (below) which dissipation is dominated by virtual (real) modes.

To summarise, the difference between the $\hat{h}$ dependences in the two regimes originates in the different approximations used for the spectral function ρ_χ. These approximations result in different dependences of Υ on the decay width $\Gamma_\chi \propto h^2$, which is inversely proportional to the relaxation time of the system. In the low-momentum regime, Υ is proportional to Γ_χ^2 and hence increases with growing $\hat{h}$. In the pole regime, on the other hand, $\Upsilon \propto \Gamma_\chi^{-1}$. Here, an increased relaxation time, that is, a reduced effective coupling $\hat{h}$ leads to an increase in dissipation.

We should note, however, that $\hat{h}$ cannot be lowered arbitrarily. The derivation

of the dissipation coefficient assumes that the system remains close to thermal equilibrium, which puts a limit on how large we can make the relaxation time, that is, how small we can make $\hat{h}$. Specifically, we have to satisfy the adiabaticity condition $\Gamma_\chi/H > 1$. Using $\Gamma_\chi = \hat{h}^2 m_\chi/(64\pi)$, we can write this as

$$\frac{\Gamma_\chi}{H} = \frac{\hat{h}^2}{64\pi}\left(\frac{m_\chi}{T}\right)\left(\frac{T}{H}\right) > 1. \tag{2.107}$$

In the pole regime, we find typical values $m_\chi/T \sim \mathcal{O}(5)$ and $T/H \sim \mathcal{O}(200)$, leading to a lower bound of $\hat{h} > 0.3$.

2.5 Density Perturbations and Observables

One of the most important effects of a thermalised radiation bath during inflation is the contribution of thermal fluctuations to the spectrum of primordial density perturbations, which can significantly alter the inflationary predictions for the parameters of the CMB power spectrum. It was Berera and Fang (1995) who first examined the impact of thermal fluctuations on the primordial density perturbation; detailed calculations of fluctuation–dissipation effects on inflaton fluctuations were then done by Berera (2000). In this section, we will give the warm-inflation expression for the primordial perturbation in the weak dissipative regime. We will also give expressions for the spectral index and the tensor-to-scalar ratio, which will allow us, in the following chapter, to assess the viability of our theoretical and numerical results by comparison to observation.

It was first realised by Graham and Moss (2009) that the coupling between quantum fluctuations in the scalar field and thermal fluctuations in the radiation bath can lead to an excessive increase of the perturbation amplitude if Υ grows with temperature. They found that in low-momentum dissipation with $\Upsilon \propto T^c$, the radiation fluctuations backreact on the inflaton fluctuations, leading to an enhancement $P_\mathcal{R}(k) \propto (Q/Q_c)^{3c}$, where Q_c depends on c, and $Q_3 \approx 7.27$. Consistency of warm inflation requires that $|c| < 4$, such that radiation is produced at a higher rate than it is diluted by the expansion of the universe (Moss and Xiong, 2008); the growing mode appears for $c > 0$. Warm-inflation predictions in the strong dissipative regime would therefore be difficult to reconcile with observations of the primordial power spectrum.

There have been attempts to mitigate the growing mode by considering non-equilibrium effects in the radiation fluid. Since dissipation is an inherently out-of-equilibrium process, and the radiation fluid has a small but non-zero relaxation time to reach equilibrium, viscosity may become important (Zimdahl, 1996; Maartens, 1996). In particular, it has been shown by Bastero-Gil *et al.* (2011b) that a sufficiently big shear viscosity may be able to suppress the growing mode. In this work, we will avoid the growing mode by focusing on the weak dissipative regime.

For $Q \lesssim 0.1$, quantum and thermal perturbations lead to a perturbation amplitude given by (Bastero-Gil *et al.*, 2014a; Bartrum *et al.*, 2014)

$$P_{\mathcal{R}} \simeq \left(\frac{H_\star}{2\pi}\right)^2 \left(\frac{H_\star}{\dot{\phi}_\star}\right)^2 \left(1 + 2\mathcal{N}_\star + \frac{T_\star}{H_\star}\frac{2\pi Q_\star}{\sqrt{1+\frac{4\pi}{3}Q_\star}}\right) , \tag{2.108}$$

where the subscript "$\star$" denotes quantities evaluated at horizon crossing. The first two terms are due to inflaton fluctuation in the vacuum state and with occupation number $\mathcal{N}_\star$, respectively; the third term is the contribution from dissipation. In the following, we will assume that the inflaton occupation number at horizon crossing is negligible. The spectral index is given by

$$n_{\rm s} - 1 = \frac{\mathrm{d}\ln P_{\mathcal{R}}}{\mathrm{d}\ln k} \simeq \frac{\mathrm{d}\ln P_{\mathcal{R}}}{\mathrm{d}N_{\rm e}} , \tag{2.109}$$

where $N_{\rm e}$ is the number of e-folds. This leads to the following expression,

$$\begin{aligned} n_{\rm s} - 1 = {} & \frac{\epsilon_\phi}{1+Q_\star}\left(-6 + \frac{3}{2}\frac{\Delta_\star}{1+\Delta_\star} + \left(2Q_\star + A\frac{\Delta_\star}{1+\Delta_\star}\right)\frac{2+c_{\rm eff}}{4-c_{\rm eff}+Q_\star(4+c_{\rm eff})}\right) \\ & + \frac{\eta_\phi}{1+Q_\star}\left(2 - \frac{1}{2}\frac{\Delta_\star}{1+\Delta_\star} - \left(2Q_\star + A\frac{\Delta_\star}{1+\Delta_\star}\right)\frac{2c_{\rm eff}}{4-c_{\rm eff}+Q_\star(4+c_{\rm eff})}\right) \\ & - \frac{\sigma_\phi}{1+Q_\star}\left(2Q_\star + A\frac{\Delta_\star}{1+\Delta_\star}\right)\frac{4(1-c_{\rm eff})}{4-c_{\rm eff}+Q_\star(4+c_{\rm eff})} . \end{aligned} \tag{2.110}$$

We have used the slow-roll parameters

$$\epsilon_\phi = \frac{m_{\rm P}^2}{2}\left(\frac{V_\phi}{V}\right)^2 , \qquad \eta_\phi = m_{\rm P}^2\frac{V_{\phi\phi}}{V} , \qquad \sigma_\phi = m_{\rm P}^2\frac{V_\phi}{\phi V} , \tag{2.111}$$

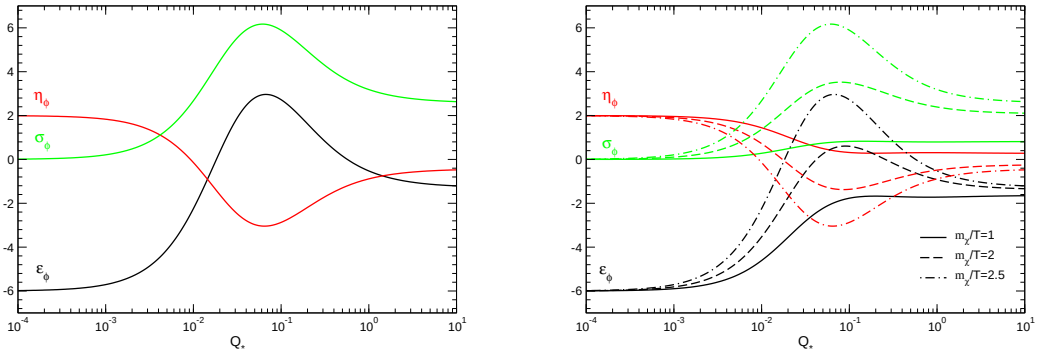

Figure 2.3: Left: Coefficients of the slow-roll parameters ϵ, η, and σ in the low-momentum limit of equation (2.110) *for the spectral index, that is, $c_{\rm eff} = 3$. Right: Same in the pole-dominated regime, $\Upsilon \simeq \Upsilon_{\rm pole}$, for different values of m_χ/T. For small Q, the coefficients take their cold-inflation values $\{-6, 2, 0\}$. Figure extracted from Bastero-Gil* et al. *(2015).*

and defined

$$c_{\rm eff} = \frac{3\Upsilon_{\rm LM}}{\Upsilon} + \frac{\Upsilon_{\rm pole}}{\Upsilon}\left(\frac{1}{2} + \frac{m_\chi}{T}\right), \tag{2.112}$$

$$\Delta_\star = \frac{T_\star}{H_\star}\frac{2\pi Q_\star}{\sqrt{1+\frac{4\pi}{3}Q_\star}}, \tag{2.113}$$

$$A = \frac{15 + Q_\star(9 + 12\pi + 4\pi Q_\star)}{4(3 + 4\pi Q_\star)}. \tag{2.114}$$

In the limit that dissipation at horizon crossing is dominated by the low-momentum modes, with $c_{\rm eff} \simeq 3$, we recover previous expressions for the spectral index given in the literature (Bartrum *et al.*, 2014; Bastero-Gil *et al.*, 2014a). In the limit of very weak dissipation $Q_\star \ll 1$ and $\Delta_\star \ll 1$, we recover the standard cold-inflation expression

$$n_{\rm s} - 1 \simeq -6\epsilon_\phi + 2\eta_\phi\,. \tag{2.115}$$

However, this does not mean that predictions are the same as in cold inflation. Even if inflation starts with a small amount of dissipation, Q can increase, changing inflaton evolution and therefore the values of the slow-roll parameters. Typically, when Q increases, smaller inflaton field values are required in order to get $N_{\rm e} \sim \mathcal{O}(50-60)$.

For $Q \gtrsim 10^{-3}$, the form of the spectral index (2.110) changes, with the coefficients now functions of Q, as illustrated in figure (2.3). In the left panel we have plotted the coefficients for low-momentum-dominated dissipation, while the right panel shows the pole-dominated case for different values of $m_\chi/T = \{1, 2, 2.5\}$, that is, different values of $c_{\rm eff} = \{1.5, 2.5, 3\}$. At large Q, the coefficients decrease as $1/Q$.

The coefficients depend also on the combination $Q_\star(T_\star/H_\star)$. During slow roll, this quantity can be derived from the radiation equation (2.4) and the perturbation spectrum (2.108)

$$\frac{T_\star}{H_\star} = \left[\frac{45}{8\pi^4}\frac{Q_\star}{g_\star P_\mathcal{R}}\left(1+\frac{T_\star}{H_\star}\frac{2\pi Q_\star}{\sqrt{1+\frac{4\pi}{3}Q_\star}}\right)\right]^{1/4}, \tag{2.116}$$

Indeed, we can use the Planck observation $P_\mathcal{R} = 2.2\times10^{-9}$ to put a first constraint on the amount of dissipation required for warm inflation from equation (2.116). We conclude that for $g_\star = 2$ the warm-inflation condition $T > H$ can be satisfied as long as $Q_\star > 8\times10^{-8}$, showing that even a very small amount of dissipation can be enough to produce an era of warm inflation. Of course, both Q and T/H change over the course of inflation; their slow-roll evolution equations can be written as

$$\frac{{\rm d}\ln Q}{{\rm d}N_{\rm e}} \simeq \frac{1}{4-c_{\rm eff}+Q(4+c_{\rm eff})}\left((4+2c_{\rm eff})\epsilon_\phi - 2c_{\rm eff}\eta_\phi - 4(1-c_{\rm eff})\sigma_\phi\right), \tag{2.117}$$

$$\frac{{\rm d}\ln T/H}{{\rm d}N_{\rm e}} \simeq \frac{1}{4-c_{\rm eff}+Q(4+c_{\rm eff})}\left(\frac{7-c_{\rm eff}+Q(5+c_{\rm eff})}{1+Q}\epsilon_\phi - 2\eta_\phi - (1-c_{\rm eff})\frac{1-Q}{1+Q}\sigma_\phi\right). \tag{2.118}$$

The primordial tensor perturbation in warm inflation is given by its standard vacuum form

$$P_T = 8\left(\frac{H_\star}{2\pi m_{\rm P}}\right)^2, \tag{2.119}$$

but since the thermal contribution enhances the scalar spectrum, the tensor-to-scalar ratio is suppressed in warm inflation,

$$r = \frac{16\epsilon_\star}{(1+Q_\star)(1+2\mathcal{N}_\star+\Delta_\star)}. \tag{2.120}$$

Since models of chaotic inflation, for example, typically involve large (super-Planckian) field excursions, they are expected to produce tensor-to-scalar ratios that far exceed observational bounds (Lyth, 1997). Those models in particular can benefit from the suppression of tensors in warm inflation, as has been shown, for instance, for the $\lambda\phi^4$ model (Bartrum *et al.*, 2014).

2.6 Summary

We have, in this chapter, introduced the effective dynamics of warm inflation and saw that the closed-time-path formalism can be used to derive these dynamics from a thermal-field-theory description of an inflaton field interacting with its environment. In the case of warm inflation, this environment is provided by a thermal bath of light particles produced by inflaton dissipation. We saw that a fluctuation–dissipation relation links the auto-correlation function of the noise in the thermal bath to the dissipation experienced by the inflaton field.

With equation (2.69), we found that it is possible to derive a local effective dissipation coefficient if there is a clear separation of timescales in the system, that is, if the microscopic dynamics of dissipation and relaxation are much faster than the evolution of the background inflaton field and the expansion of the universe. We then used that expression to obtain the dissipation coefficient first for a historically important toy model in section 2.3.5. In section 2.4, we introduced the well-established set of interactions that form the basis for the rest of our work. The model based on the superpotential (2.75) implements a two-stage dissipation mechanism, wherein the inflaton is directly coupled only to some heavy mediator fields X. As it rolls along its potential, the inflaton produces real or virtual X particles, which can then decay into the light fields that form the Y multiplet in the superpotential (2.75). It is this separation of the inflaton from light fields that enables the two-stage decay mechanism to produce significant amounts of dissipation while keeping thermal corrections to the inflaton potential under control.

It then turned out that the distinction between producing real and virtual mediator particles is of tremendous importance for the form of the effective dissipation coefficient. Virtual, low-momentum mediators lead to a dissipation coefficient $\Upsilon \propto T^3/m_\chi^2$, whereas real mediators, produced on shell, near the pole

of the spectral function, result in $\Upsilon \propto \sqrt{m_\chi T}\exp(-m_\chi/T)$. Whilst the low-momentum contribution has been subject to detailed examination for a long time, it was, until recently, assumed that the pole term would be doomed to irrelevance by the exponential Boltzmann suppression in the low-temperature regime $m_\chi > T$. And yet, it has been shown that, in some regions of parameter space, the exponential suppression can be overcome, and the pole term can contribute significantly. Specifically, if the coupling between mediators and light fields is sufficiently small and the ratio m_χ/T is not too large, the pole contribution can easily come to dominate over the more traditional low-momentum dissipation.

It is the main purpose of the present work to uncover new regions of parameter space that allow for successful warm inflation. To this end, we will, in the following chapter, present a numerical code that searches the parameter space of the model (2.75) for regions where the spectral index (2.110) and the tensor-to-scalar ratio (2.120) are compatible with Planck observations. We shall indeed find that the as-yet poorly examined pole regime is host to some of the most interesting points in our data sets.

Chapter 3

Exploring the Parameter Space of Warm Inflation

3.1 Introduction

With the framework of warm inflation established, let us move on to this work's original contributions. We have developed a numerical code that searches the parameter space of models derived from the superpotential (2.75) for regions where warm inflation produces a universe that is compatible with CMB observations. The parameter space in question contains the parameters of the superpotential itself, that is, the couplings between inflaton and mediator fields and between mediators and light fields; further parameters are the initial values of the inflaton field and the ratio between radiation density and inflaton potential; the number of mediator fields; and the parameters that describe the inflaton potential. Whilst previous codes were able to integrate the equations of motion for specific sets of initial conditions and parameter values, ours actively scans the entire parameter space (within given ranges) for solutions, integrates the equations of motion, and evaluates the spectral index and tensor-to-scalar ratio in order to assess observational viability.

We have also derived a set of inflaton potentials for which the ratio m_χ/T remains constant during warm inflation. These potentials, along with more common monomial, hybrid, and hilltop potentials are the basis for the parameter scans in this section.

3.2 Potentials with constant $\mathbf{m_\chi/T}$

We are mainly interested in exploring the possibility of warm inflation in the pole-dominated regime. Although there is clearly an enhancement of the dissipative coefficient compared to the low-momentum regime for $m_\chi/T \simeq \mathcal{O}(1-10)$, as seen in figure (3.4), the dissipative coefficient is suppressed by the Boltzmann factor $\mathrm{e}^{-m_\chi/T}$. Therefore, whenever the ratio m_χ/T increases during inflation, the pole contribution may quickly vanish, so we first explore which kind of potentials may render this ratio approximately constant during slow-roll inflation.

We derive an equation of motion for $x := \phi/T$ in warm inflation, starting from

$$\frac{x'}{x} = \frac{\phi'}{\phi} - \frac{T'}{T} = \frac{\phi'}{\phi} - \frac{1}{4}\frac{\rho_{\mathrm{R}}'}{\rho_{\mathrm{R}}}\,, \tag{3.1}$$

where primes denote derivatives with respect to the number of e-folds. During slow roll, the energy density in radiation is given by

$$\rho_{\mathrm{R}} = \frac{3}{4}\frac{Q}{(1+Q)^2}\frac{V_\phi^2}{3H^2}\,, \tag{3.2}$$

from which we obtain

$$\frac{\rho_{\mathrm{R}}'}{\rho_{\mathrm{R}}} = \frac{1-Q}{1+Q}\frac{Q'}{Q} + 2\frac{V_\phi'}{V_\phi} - 2\frac{H'}{H}\,. \tag{3.3}$$

From the definition of the dissipative ratio, $Q = \Upsilon/(3H)$, with Υ given in equation (2.100), we find

$$\frac{Q'}{Q} = -\frac{H'}{H} + \frac{\phi'}{\phi} - c_{\mathrm{eff}}\frac{x'}{x}\,. \tag{3.4}$$

This yields the equation of motion for x,

$$\frac{x'}{x} = \frac{1}{4 - c_{\mathrm{eff}} + Q(4+c_{\mathrm{eff}})}\left(-\frac{3+Q}{1+Q}\,\epsilon_\phi + 2\eta_\phi - \frac{3+5Q}{1+Q}\,\sigma_\phi\right)\,. \tag{3.5}$$

Hence, we determine potentials that exhibit constant ϕ/T by setting $x' = 0$ and integrating twice the resulting relation between the potential and its derivatives,

$$\frac{V_{\phi\phi}}{V_\phi} - \frac{3+Q}{4(1+Q)}\,\frac{V_\phi}{V} = \frac{3+5Q}{1+Q}\,\frac{1}{2\phi}\,. \tag{3.6}$$

For $Q \gg 1$, this yields a potential

$$V^{Q\gg1} \propto \mathrm{e}^{C_1}\left(C_2+\phi^{7/2}\right)^{4/3}\,, \tag{3.7}$$

where C_1 and C_2 are integration constants. For $Q \ll 1$, we get

$$V^{Q\ll1} \propto \mathrm{e}^{C_1}\left(C_2+\phi^{5/2}\right)^{4}\,. \tag{3.8}$$

Depending on the whether ϕ is super- or sub-Planckian, we can write these as either chaotic or hybrid potentials: for $\phi > m_\mathrm{P}$,

$$V^{Q\gg1} \approx V_0\left(\frac{\phi}{m_\mathrm{P}}\right)^{14/3}\,, \qquad V^{Q\ll1} \approx V_0\left(\frac{\phi}{m_\mathrm{P}}\right)^{10}\,, \tag{3.9}$$

and for $\phi < m_\mathrm{P}$,

$$V^{Q\gg1} \approx V_0\left(1+\tilde{\gamma}\left(\frac{\phi}{m_\mathrm{P}}\right)^{7/2}\right)\,, \qquad V^{Q\ll1} \approx V_0\left(1+\tilde{\gamma}\left(\frac{\phi}{m_\mathrm{P}}\right)^{5/2}\right)\,, \tag{3.10}$$

where we have defined $V_0 = \lambda m_\mathrm{P}^4$ for monomial and $V_0 = \lambda\phi_\mathrm{c}^4$ for hybrid potentials, ϕ_c being the critical field value at which we expect inflation to end via the waterfall transition.

In addition to chaotic and hybrid potentials, we will also study hilltop potentials, for different powers of the field.[1] The potentials are then:

$$\begin{aligned}
\text{Chaotic: } V &= V_0\left(\frac{\phi}{m_\mathrm{P}}\right)^p\,,\\
\text{Hybrid: } V &= V_0\left(1+\frac{\gamma}{p}\left(\frac{\phi}{m_\mathrm{P}}\right)^p\right)\,,\\
\text{Hilltop: } V &= V_0\left(1-\frac{\gamma}{p}\left(\frac{\phi}{m_\mathrm{P}}\right)^p\right)\,.
\end{aligned} \tag{3.11}$$

[1] Owing to anx algebra error, our simulation covered hybrid and hilltop potentials with exponents $p = 14/3, 10$ instead of the exponents $p = 7/2, 5/2$. The corresponding hilltop models did not produce a sufficient amount of data, so they were never represented in our plots. Amongst the hybrid models, we have have removed plots relating to $p = 14/3$ from this study but retain $p = 10$ as an example of hybrid potentials with integer exponents, adding to the more conventional potentials with $p = 2, 4$. Let us be clear, however, that we do not expect hybrid models with $p = 10$ to exhibit constant m_χ/T.

3.3 Description of the Code

To search the parameter space of our models for points that allow for a significant amount of warm inflation, we first find initial conditions near a slow-roll trajectory using the method described in the following paragraph. Once we have identified suitable initial conditions, we check whether they satisfy the necessary constraints for warm inflation. If they do, we let the system evolve until either the slow-roll or the warm-inflation conditions break down or until radiation dominates over the inflaton's potential energy.

We begin by generating random values for the coupling constants g and h, the initial values of ϕ and ρ_{R}/V, the number of mediator fields N_χ, and in the case of hybrid and hilltop potentials, the coupling constant γ. To avoid any prejudice for what the order of magnitude of these quantities should be, we generate their values from a distribution flat in the logarithm (bounded from above and below); this ensures that we sample values of different orders of magnitude equally. We then obtain slow-roll initial conditions by simultaneously solving the equation for the Hubble parameter and the slow-roll versions of the equations (2.4) and (2.1) for V_0, $\dot{\phi}$, and H. Hence, the relevant equations are,[2]

$$V_0 = -\frac{\dot{\phi}}{v_\phi}(3H + \Upsilon)\,, \tag{3.12}$$

$$-\dot{\phi} = \sqrt{\frac{4H\rho_{\mathrm{R}}}{\Upsilon}}\,, \tag{3.13}$$

$$H = \sqrt{\frac{V_0 v + \rho_{\mathrm{R}} + \frac{1}{2}\dot{\phi}^2}{3m_{\mathrm{P}}^2}}\,, \tag{3.14}$$

where we have defined $v = V/V_0$.

Given these initial conditions, the system should find itself close to a slow-roll trajectory. We solve the full equations of motion for the inflaton, the radiation density, and the scale factor. In order to convert the second-order ordinary differential equation (ODE) for the inflaton field into a set of two first-order ODEs, let us introduce the variables

$$u = \phi\,, \quad v = \frac{\mathrm{d}\phi}{\mathrm{d}t} = \dot{\phi}\,. \tag{3.15}$$

[2] In order to ensure non-negativity of V_0 and H and to avoid some of the possible numerical problems, we work with the logarithms of these equation.

We then solve the set of equations given by,

$$\frac{\mathrm{d}u}{\mathrm{d}t} = v\,, \tag{3.16a}$$

$$\frac{\mathrm{d}v}{\mathrm{d}t} = -\frac{\mathrm{d}V}{\mathrm{d}u} - (\Upsilon + 3H)\,v\,, \tag{3.16b}$$

$$\frac{\mathrm{d}\ln\rho_{\mathrm{R}}}{\mathrm{d}t} = \frac{\Upsilon}{\rho_{\mathrm{R}}}v^2 - 4H\,, \tag{3.16c}$$

$$\frac{\mathrm{d}\ln a}{\mathrm{d}t} = H\,. \tag{3.16d}$$

We solve the initial-value problem using the `CVODE` solvers from version v.2.5.0 of the `SUNDIALS` suite (Hindmarsh *et al.*, 2005; Serban and Hindmarsh, 2005). To describe the solver we use, let us write a generic initial-value problem in the form

$$\dot{y} = f(t, y)\,, \quad y(t_0) = y_0\,, \tag{3.17}$$

where $\dot{y} = \mathrm{d}y/\mathrm{d}t$ and $y \in \mathbb{R}^N$. For the problem we are interested in, given by the set of equations (3.16), we have $N = 4$, and the vector y is given by

$$y = (u, v, \ln\rho_{\mathrm{R}}, \ln a) \tag{3.18}$$

with $u = \phi\,, v = \mathrm{d}\phi/\mathrm{d}t$.

Using `CVODE`, we can solve such problems using variable-order, variable-step multistep methods based on backwards differentiation formulas (BDF). Let us briefly summarise BDF methods for the simplified case of a fixed step size h. We can write the k-th-degree Newton polynomial interpolating points $(t_n, y_n), (t_{n+1}, y_{n+1}), \ldots, (t_{n+k}, y_{n+k})$ as

$$y(t) \approx y_n + \frac{1}{h}(t-t_n)\nabla y_n + \frac{1}{2h^2}(t-t_n)(t-t_{n-1})\nabla^2 y_n + \cdots + \frac{1}{h^k k!}(t-t_n)\cdots(t-t_{n-k+1})\nabla^k y_n\,, \tag{3.19}$$

where ∇ is the backward difference operator $\nabla y_n = y_n - y_{n-1}$ and $\nabla^p y_n = \nabla^{p-1} y_n - \nabla^{p-1} y_{n-1}$. By differentiating with respect to t and setting $t = t_n$, we obtain the backward differentiation formula of degree k,

$$h\beta_k f(t_{n+k}, y_{n+k}) = \sum_{i=0}^{k} \alpha_{k,i} y_{n+i}\,, \tag{3.20}$$

where the coefficients $\alpha_{k,i}, \beta_k$ are chosen such that the method achieves order k. For example, the expressions up to order $k = 3$ are given by

$$\begin{aligned}
k = 1: &\quad y_{n+1} = y_n + hf(t_{n+1}, y_{n+1})\,, \\
k = 2: &\quad y_{n+2} = \tfrac{4}{3}y_{n+1} - \tfrac{1}{3}y_n + \tfrac{2}{3}hf(t_{n+2}, y_{n+2})\,, \\
k = 3: &\quad y_{n+3} = \tfrac{18}{11}y_{n+2} - \tfrac{9}{11}y_{n+1} + \tfrac{2}{11}y_n + \tfrac{6}{11}hf(t_{n+3}, y_{n+3})\,,
\end{aligned}$$

where the method for $k = 1$ represents the familiar backward Euler method. The `CVODE` implementation of BDF is allowed to vary the step size h_n and the order of the method used; the order k may vary between 1 and 5. Both changes are made such that the local truncation error of the method remains safely below a set threshold.

Alongside solving ODEs, `CVODE` can find the roots of a set of user-defined functions $g_i(t, y)$ that depend on t and the solution vector $y = y(t)$. This is accomplished by checking for a change of the sign of $g_i(t)$ at every time step; if a sign change is detected, `CVODE` uses a modified secant method to home in on the root (Hiebert and Shampine, 1980). In our code, we use these root-finding capabilities to check for breakdown of the slow-roll conditions and the consistency conditions required by warm inflation, and for radiation taking over as the dominant energy density in the universe,

$$\begin{aligned}
\frac{|\epsilon|}{1+Q} < 1\,, \qquad \frac{|\eta|}{1+Q} < 1\,, \qquad \frac{\rho_{\mathrm{R}}}{V} < 1\,, \\
\frac{T}{H} > 1\,, \qquad \frac{m_\chi}{T} > 1\,, \qquad \frac{\Gamma_\chi}{H} > 1\,.
\end{aligned} \tag{3.21}$$

When any of these conditions is violated, we consider warm inflation to be over, and we end evolution.

If evolution lasted for at least 5 e-folds, we store the corresponding set of parameter values and initial conditions. It is worth noting that we sometimes see strong oscillations of the dynamical quantities at the start of evolution. These oscillations can make it difficult to classify the corresponding data point as, for example, pole or low-momentum dominated. We have, however, found that, within a few e-folds, these oscillations die down and the system converges onto a nearby slow-roll trajectory. To avoid any confusion due to these initial oscillations, we disregard the first 4 e-folds of evolution and consider the conditions at $N_{\mathrm{e}} = 4$

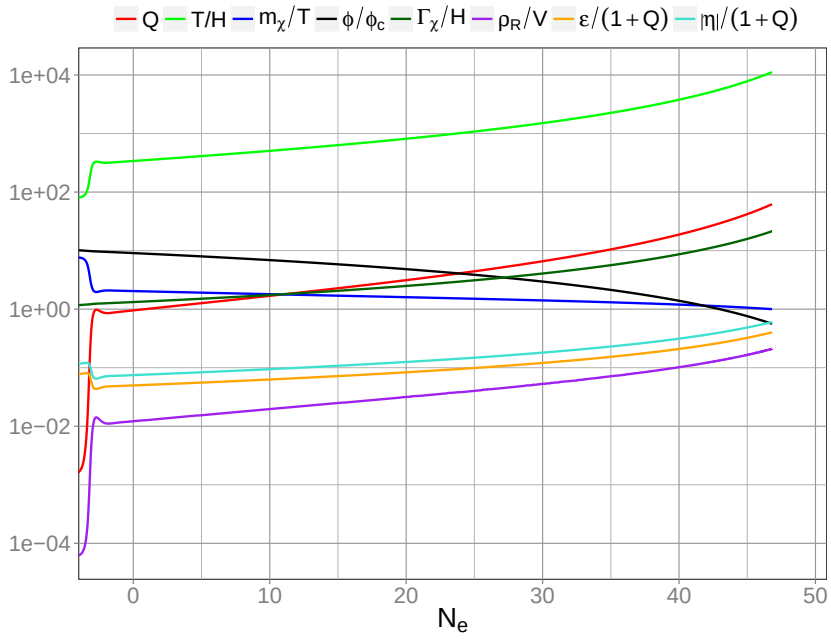

Figure 3.1: Example of warm-inflation evolution in the $\lambda\phi^4$ potential. Initial oscillations die down quickly.

to be the initial conditions of warm inflation in all subsequent analysis. Therefore, ignoring the unreliable initial phase, we effectively retain all data points that reach at least 1 e-fold of inflation. For illustration, we show a typical example of such a case for the $\lambda\phi^4$ potential in figure (3.1), which plots the evolution of various dynamical quantities as a function of the number of e-foldings.

3.4 Validation

Before we proceed to discuss the new results we produced using our code, let us ensure that we can reproduce the theoretical expectations described in section 2.4.2.

First of all, let us examine the behaviour of Υ as a function of the effective coupling $\hat{h}$ and the transition between pole- and low-momentum-dominated dissipation. Figure (3.2) shows the transition from the pole-dominated to the low-momentum regime as the effective coupling $\hat{h} = h\sqrt{N_Y}$ varies for different values of m_χ/T. As we saw in equation (2.100), dissipation decreases as $\Upsilon \propto 1/\hat{h}^2$ in the pole regime and grows as $\Upsilon \propto \hat{h}^2$ in the low-momentum regime. The minimum

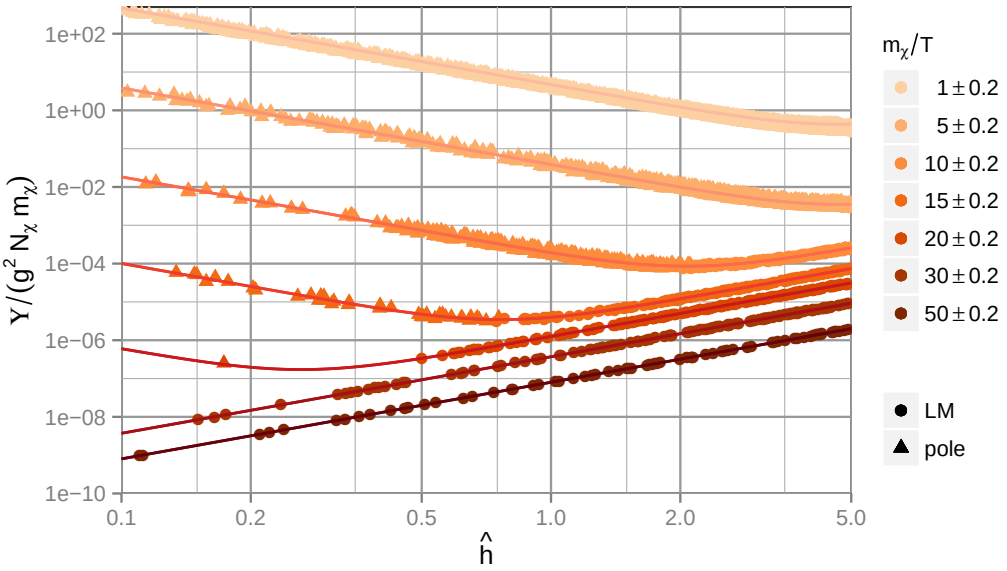

Figure 3.2: Dissipation coefficient as a function of the effective coupling $\hat{h}$ for different values of m_χ/T for $m_\sigma/T = 0.01$. The change in trend signifies the transition from the low-momentum regime at large $\hat{h}$ to the pole regime at small $\hat{h}$. Numerical data agrees with the theoretical predictions given by the solid lines (Bastero-Gil et al.*, 2013).*

in each curve indicates the transition from pole to low-momentum domination, and the corresponding value of $\hat{h}$ is given by the expression (2.106).

The transition from the pole to the low-momentum regime in the $(m_\chi/T, \hat{h})$ plane is shown in figure (3.3). The dashed line indicates the transition from the pole-dominated regime below to the low-momentum regime above; it is given by equation (2.106) and lines up perfectly with the transition in the numerical data between points with pole-dominated and points with low-momentum-dominated dissipation.

Finally, figure (3.4) demonstrates the advantage of including the pole contribution in spite of the Boltzmann suppression at low temperature. For $m_\chi/T \sim \mathcal{O}(1)$ and especially for small values of $\hat{h}$, the pole contribution dramatically enhances the dissipation, opening up a parameter range that was previously thought inaccessible to warm inflation.

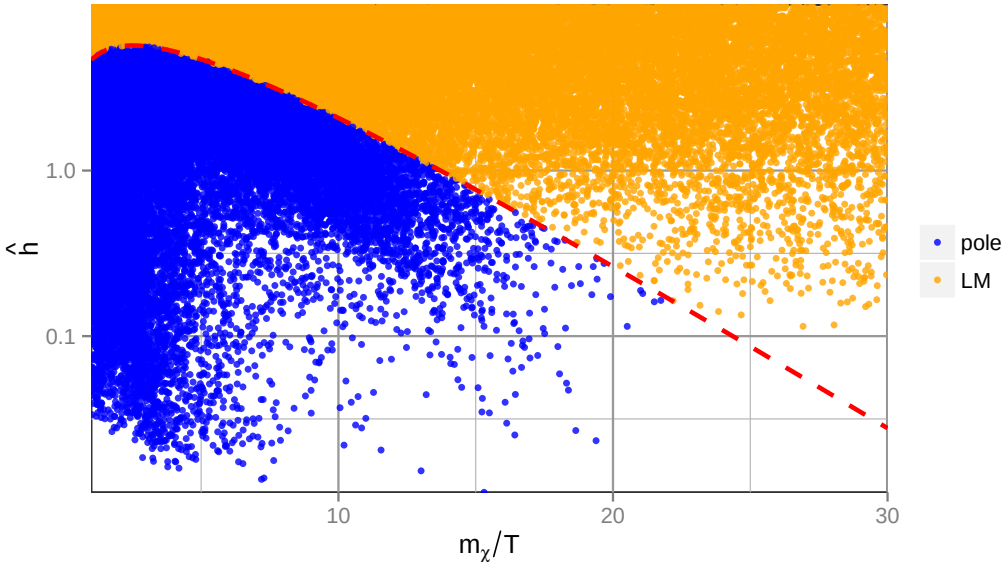

Figure 3.3: Regions of the $(m_\chi/T, \hat{h})$ plane dominated by either the pole or the low-momentum contribution to the dissipation coefficient. Numerical data agrees with the theoretical predictions given by the dashed line (Bastero-Gil et al.*, 2013).*

3.5 Results of Parameter Scans

In order to assess the viability of our models, we compare our predictions for the spectral index and the tensor-to-scalar ratio to observations by the Planck satellite (Ade *et al.*, 2015b) in figure (3.5). We show the results for monomial (phi$p$), hilltop (hill$p$), and hybrid (hyb$p$) potentials, for different powers of the field p as indicated in the figure (the label "4667" refers to $p = 14/3$). Our potentials are given by

$$\begin{aligned} \text{Chaotic: } V &= V_0 \left(\frac{\phi}{m_\text{P}}\right)^p , \\ \text{Hybrid: } V &= V_0 \left(1 + \frac{\gamma}{p}\left(\frac{\phi}{m_\text{P}}\right)^p\right) , \\ \text{Hilltop: } V &= V_0 \left(1 - \frac{\gamma}{p}\left(\frac{\phi}{m_\text{P}}\right)^p\right) . \end{aligned} \tag{3.22}$$

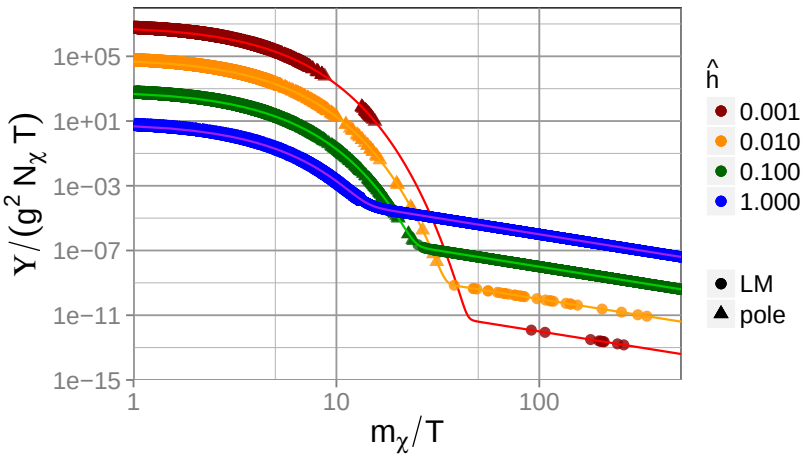

Figure 3.4: Full dissipation coefficient as a function of m_χ/T for different values of the effective coupling $\hat{h}$. Numerical data agrees with the theoretical predictions given by the solid lines (Bastero-Gil et al.*, 2013)*

For hilltop and hybrid, $p = 0$ refers to a logarithmic potential

$$V = V_0 \left(1 \pm \gamma \ln\left(\frac{\phi}{m_\mathrm{P}}\right)\right) . \tag{3.23}$$

It is worth pointing out that we find solutions with very small tensor-to-scalar ratios for all our models. This is especially noteworthy for the monomial potentials, which, in their cold-inflation implementations, produce large r and are therefore strongly disfavoured by the data. Warm inflation will be able to keep such models consistent with CMB observation even in the face of future experiments' promise of stricter bounds on the order of $r \lesssim 10^{-3}$.

For monomial potentials, figure (3.6) shows the n_s–r plane separately with a linear r axis to emphasize the large-r region. We can see that, for increasing Q, the trajectory in that plane follows an arc similar to the one seen in refs Bartrum *et al.* (2014); Bastero-Gil *et al.* (2014c). We find low-momentum-dominated points at low Q that allow for a spectral index compatible with Planck results for the ϕ^4 and $\phi^{14/3}$ models; these points do, however, have tensor-to-scalar ratios much bigger than the Planck constraint $r < 0.08$ (Ade *et al.*, 2015c, combination with BICEP2/Keck Array-Planck cross-correlation, no spectral running). At larger Q and smaller r, the trajectory for these two potentials returns to the Planck range for the spectral index; those points tend to be pole-dominated and have $r < 10^{-3}$

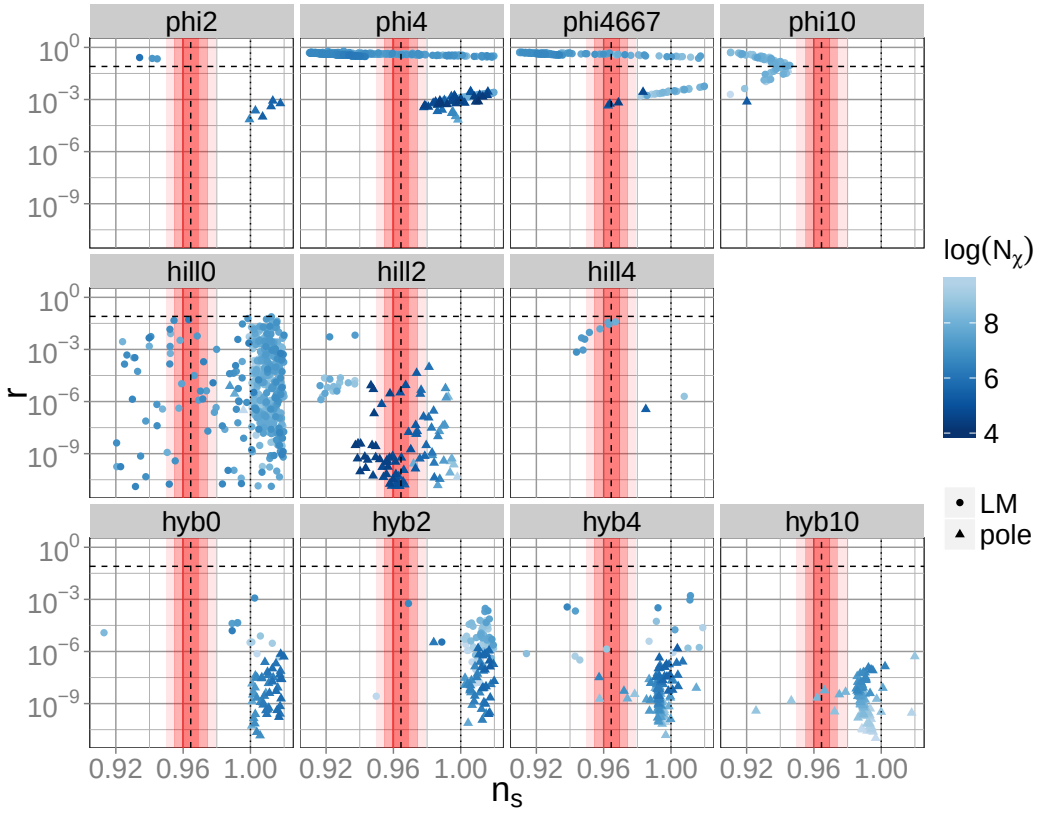

Figure 3.5: Tensor-to-scalar ratio r vs spectral index n_s for monomial, hilltop, and hybrid potentials. Triangles represent pole-dominated, disks low-momentum-dominated points; colour represents the number of mediator fields, N_χ. All points lie between 45 and 55 e-folds. The dashed black line and shaded intervals indicate, respectively, the central value and 1σ, 2σ, and 3σ confidence intervals of n_s based on the Planck data; the dashed line for r represents the upper limit $r < 0.08$ (Ade et al., 2015c).

(compare figure (3.5)). For $p = 4$ and especially $p = 14/3$, these pole points come closest to the n_s–r region favoured by Planck and also show the lowest values of N_χ, reaching as low as $N_\chi \approx 2.3 \times 10^4$ for $p = 14/3$. Such numbers could be achieved, for example, in brane-antibrane models of inflation (Burgess *et al.*, 2001).

We observe further that the maximum n_s for each of these models is reached around $Q \approx 5 \times 10^{-2}$ and $T/H \approx 50$; this large-n_s cusp of the trajectory moves to smaller and smaller n_s as the exponent of the potential increases until, by $p = 10$, all points lie below the Planck constraint. At its largest values, n_s is dominated

by the (positive) contributions from the η and σ terms in expression (2.110); the low-momentum points below $Q \approx 5 \times 10^{-3}$ and $T/H \approx 20$, where the coefficients of ϵ and η go through zero, are dominated by the (negative) contribution of the ϵ term.

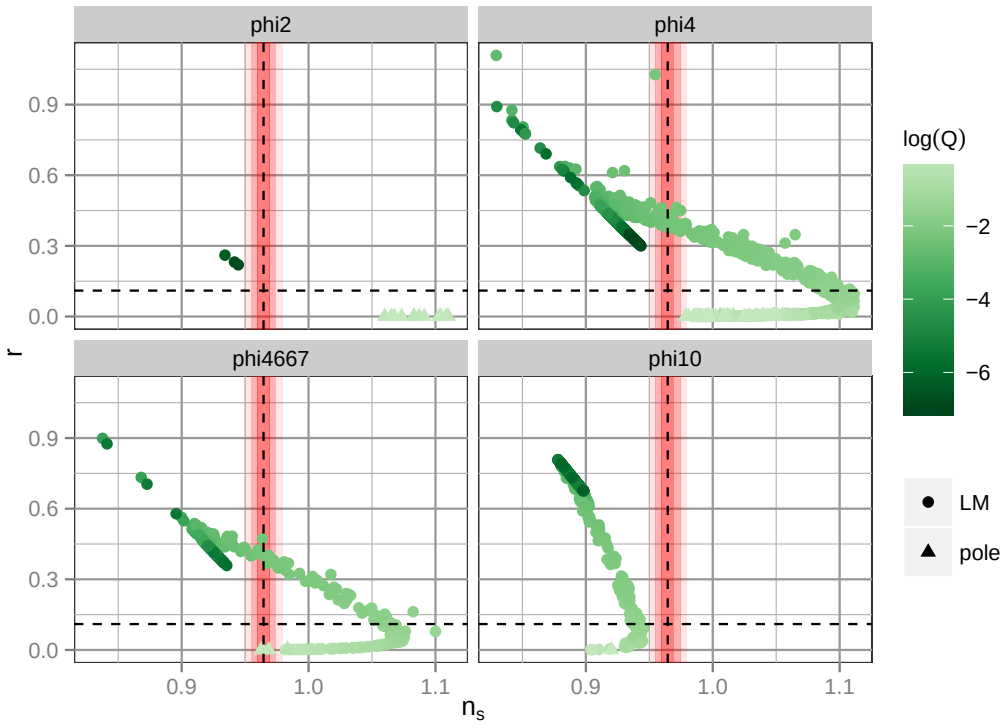

Figure 3.6: Tensor-to-scalar ratio r vs spectral index n_s for monomial potentials with exponents $p = 2, 4, \frac{14}{3}, 10$. Triangles represent pole-dominated, disks low-momentum-dominated points; colour represents the dissipative ratio, Q. All points lie between 45 and 55 e-folds. The dashed black line and shaded intervals indicate, respectively, the central value and 1σ, 2σ, and 3σ confidence intervals of n_s based on the Planck data; the dashed line for r represents the upper limit $r < 0.08$ (Ade et al., 2015c).

The full shape of the dependence of the spectral index on Q and the number of e-folds achieved is plotted in figure (3.7), where we show data for the deviation of n_s from the Planck value for the quartic monomial potential; analytically, the shape of the data is given by (2.110). Focusing on points with $N_e \approx 50$, we recognise the arc followed by the data in figures (3.5) and (3.6).

Hybrid potentials do not fare well in our analysis; in figure (3.5), our hybrid data in both the LM and pole regimes tend to cluster around $n_s = 1$, with

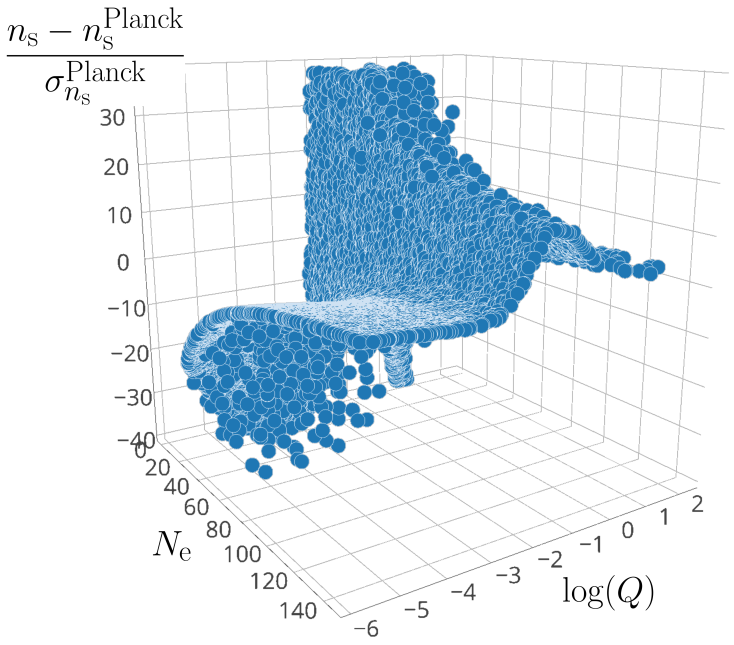

Figure 3.7: Full shape of the dependence of n_s on N_e and Q in the low-momentum regime of the quartic monomial potential.

only the quartic hybrid potential producing points compatible with Planck. The contribution of the ϵ term to the spectral index (2.110) tends to be negligible for our hybrid data; instead, n_s is set by the (negative) η and the (positive) σ term. On the whole, all the hybrid models we consider here struggle to produce a sufficiently red-tilted spectrum.

The hilltop potentials, on the other hand, are promising. Especially for the quadratic hilltop potential, we find many pole-dominated points compatible with Planck data. As in the hybrid model, ϵ at horizon crossing is negligible with respect to η and σ, and therefore the tensor-to-scalar ratio is suppressed below $r < 10^{-3}$. It is worth mentioning that the rate at which our code produced data varied significantly between potentials. Hilltop potentials were generally the slowest to make progress, and the absence of $p = \{14/3, 10\}$ from the set of hilltop potentials is due to our code's inability to generate viable solutions for these potentials within a reasonable amount of time.

Figure (3.8) illustrates a main advantage of allowing the pole term to contribute to dissipation. Pole-dominated dissipation allows for a significant amount of warm inflation with noticeably smaller couplings, typically around $g \sim \mathcal{O}(10^{-6} \dots 10^{-4})$ compared to $g \sim \mathcal{O}(10^{-3} \dots 1)$ in the low-momentum

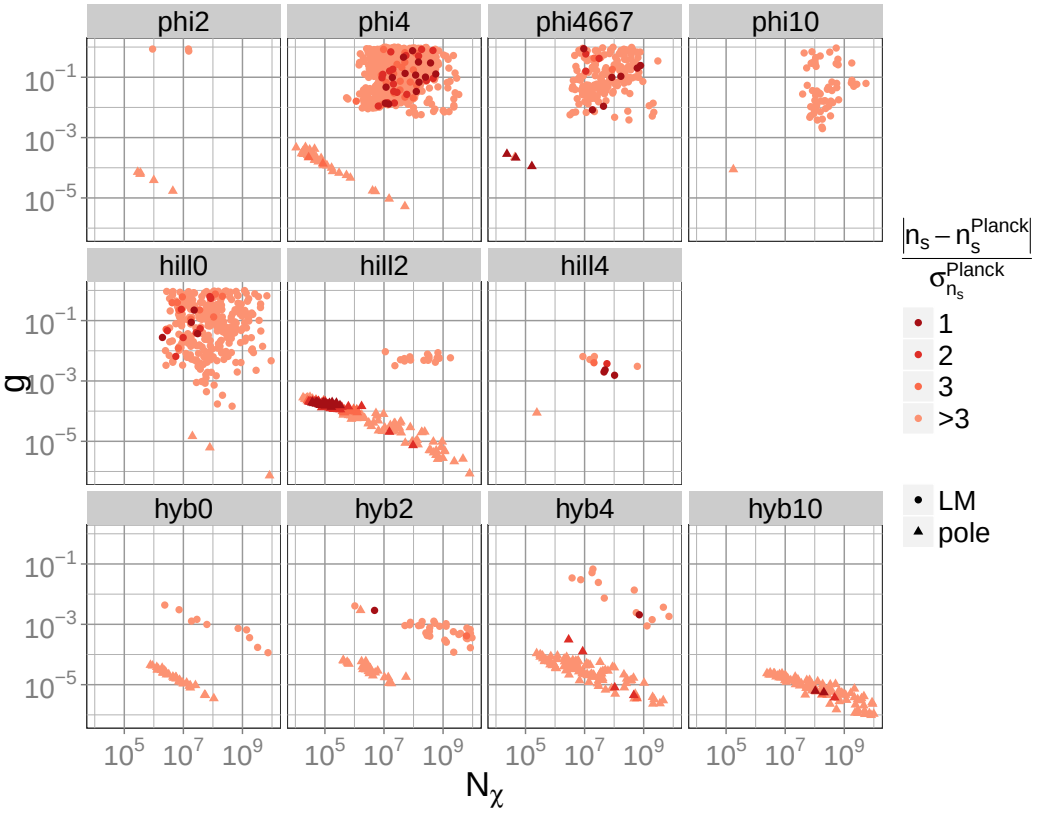

Figure 3.8: Points in the g–N_χ plane that allow for 45–55 e-folds of inflation. Colour indicates the deviation from the central value of n_s as measured by Planck data (Ade et al., 2015c). Circles indicate low-momentum-dominated dissipation, triangles indicate pole-dominated dissipation.

regime. N_χ can also be lower in the pole than in the low-momentum regime, reaching values as low as $N_\chi \sim \mathcal{O}(10^4)$ for the quadratic hilltop potential. For all potentials, the pole and low-momentum regions are cleanly separated, corresponding to the different ranges of m_χ/T inhabited by the two regimes. The same effect appears in figure (3.9), where we compare $N_\chi g^2$ for low-momentum and pole domination—pole values are consistently smaller. Once we have picked a value for the coupling g that is small enough to keep radiative corrections under control, figure (3.9) can provide a rough estimate of the number of mediator fields that need to be introduced to obtain warm inflation.

It is interesting to look at the way warm inflation ends; as shown in figure (3.10), the condition (3.21) that ends evolution depends strongly on the potential under consideration. In monomial potentials, we mostly see a breakdown

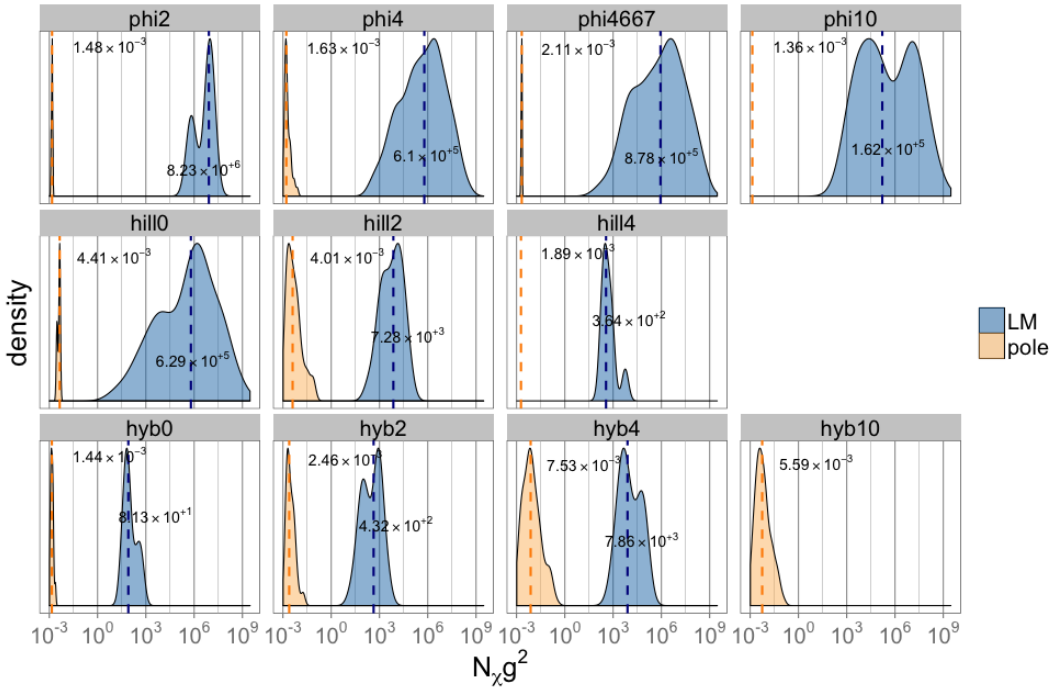

Figure 3.9: Distributions and median values of $N_\chi g^2$ for low-momentum- and pole-dominated points between 45 and 55 e-folds in monomial, hilltop, and hybrid potentials.

of slow-roll when $\eta = 1 + Q$; we will take a closer look at these points in section 3.5.1. For most of our pole points in ϕ^2 and some in ϕ^4 and $\phi^{14/3}$, warm inflation ends with $\Gamma_\chi/H = 1$.

In the hybrid potentials, $\Gamma_\chi/H = 1$ is the dominant mode for ending warm inflation, but there remain pole points in the logarithmic and quadratic potentials that end via $m_\chi/T = 1$; for $p \geq 4$, many points end in $T/H = 1$.

Hilltop models, both logarithmic in the LM regime and quadratic in the pole one, have the parameter T/H decreasing by the end of inflation and reaching the lower limit $T/H = 1$. For the quadratic model, we have $\eta_\phi = \sigma_\phi < 0$, and therefore from equations (2.118) and (3.5) in the weak dissipative regime $Q \ll 1$:

$$\begin{aligned} \frac{\mathrm{d}\ln T/H}{\mathrm{d}N_\mathrm{e}} &\simeq -\frac{3 - c_\mathrm{eff}}{4 - c_\mathrm{eff}}\sigma_\phi\,, \\ \frac{\mathrm{d}\ln \phi/T}{\mathrm{d}N_\mathrm{e}} &\simeq -\frac{1}{4 - c_\mathrm{eff}}\sigma_\phi\,. \end{aligned} \tag{3.24}$$

It is worth noting that the end of warm inflation does not imply the end of

inflation per se. If the temperature drops below the Hubble rate ($T/H < 1$) and dissipation is weak ($Q \ll 1$) but slow-roll persists, warm inflation may be followed by an additional phase of cold inflation. If the amount of cold inflation, $N_{\rm e}^{\rm cold}$, following the end of warm inflation were large enough, the remaining radiation bath could be diluted away, which might threaten the ability of warm inflation to fully replace reheating. Furthermore, the values of $n_{\rm s}$ and r are set 50–60 e-folds before the end of inflation, which would in fact be $N_{\rm e}^{\rm cold}$ later than the point during warm inflation at which we calculate them. In a universe where warm inflation was followed by a long period of cold inflation, lasting tens of e-folds, the observed values of $n_{\rm s}$ and r would deviate significantly from our predictions. Fortunately, we do not expect to see such extreme amounts of cold inflation following the warm period. After 45–55 e-folds of warm inflation, the inflaton has already rolled far down its potential, so any subsequent period of cold inflation should end with the breakdown of slow roll within less than 10 e-folds. This extra period would not change the observables significantly, so that the results presented here still give a good indication of which parameter ranges lead to successful periods of warm inflation. Nevertheless, it would be interesting to conduct a detailed investigation of this added era of cold inflation, combined with concerted model-building efforts to keep it as short as possible.

3.5.1 Upper bound on $\mathbf{N_e}$ for monomial potentials

The number of e-folds of inflation is given by

$$N_{\rm e} = \int_{\phi_{\rm i}}^{\phi_{\rm f}} \frac{H}{\dot{\phi}} {\rm d}\phi = -\int_{\phi_{\rm i}}^{\phi_{\rm f}} \frac{V}{V_\phi} \frac{1+Q}{m_{\rm P}^2} {\rm d}\phi \,. \tag{3.25}$$

For many of our data points in monomial potentials, inflation ends with $\eta = 1 + Q_{\rm f}$ (cf. figure (3.10)), which fixes the final field value. If we assume constant $Q = Q_{\rm f} = Q_{\rm i}$, we can use the integral (3.25) to set an upper limit on the initial field value for a given number of e-foldings,

$$\phi_{\rm i} \leq \sqrt{\frac{2pN_{\rm e}m_{\rm P}^2}{1+Q_{\rm i}} + \phi_{\rm f}^2} \,. \tag{3.26}$$

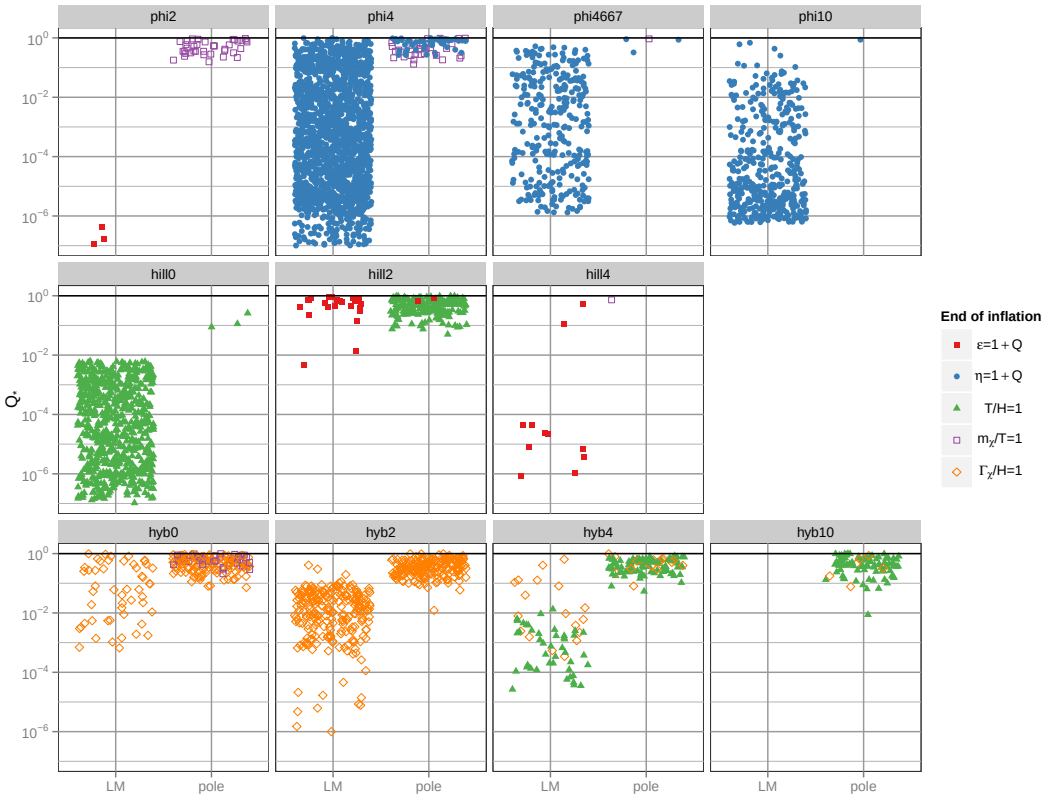

Figure 3.10: Reasons for the end of warm inflation in the pole and LM regimes. For all potentials, the pole regime is confined to relatively large $Q_\star$. All points lie between 45 and 55 e-folds and within 10σ of Planck's spectral index.

Field values below the upper limit are obtained if Q increases over the course of inflation, which is the case for monomial potentials with exponent $p < 14$ in the low-momentum regime (Bastero-Gil and Berera, 2009), and hence for all monomial potentials considered here. Since the slow-roll parameters for monomial potentials are functions of p and $1/\phi^2$ only, we can convert this into an upper limit on the low-Q spectral index $n_\mathrm{s} - 1 = -6\epsilon + 2\eta$,

$$n_\mathrm{s} - 1 \leq -\frac{2(p+2)(1+Q_\mathrm{i})}{p - 1 + 4N_\mathrm{e}} \,. \tag{3.27}$$

Even for the small values of Q assumed here, dissipation allows η to take greater values without slow roll breaking down, and hence the final field value is allowed to be smaller than without dissipation. Additionally, dissipation reduces $\mathrm{d}\phi/\mathrm{d}N_\mathrm{e}$, so a given number of e-folds can be produced by a smaller field excursion. Dissipation

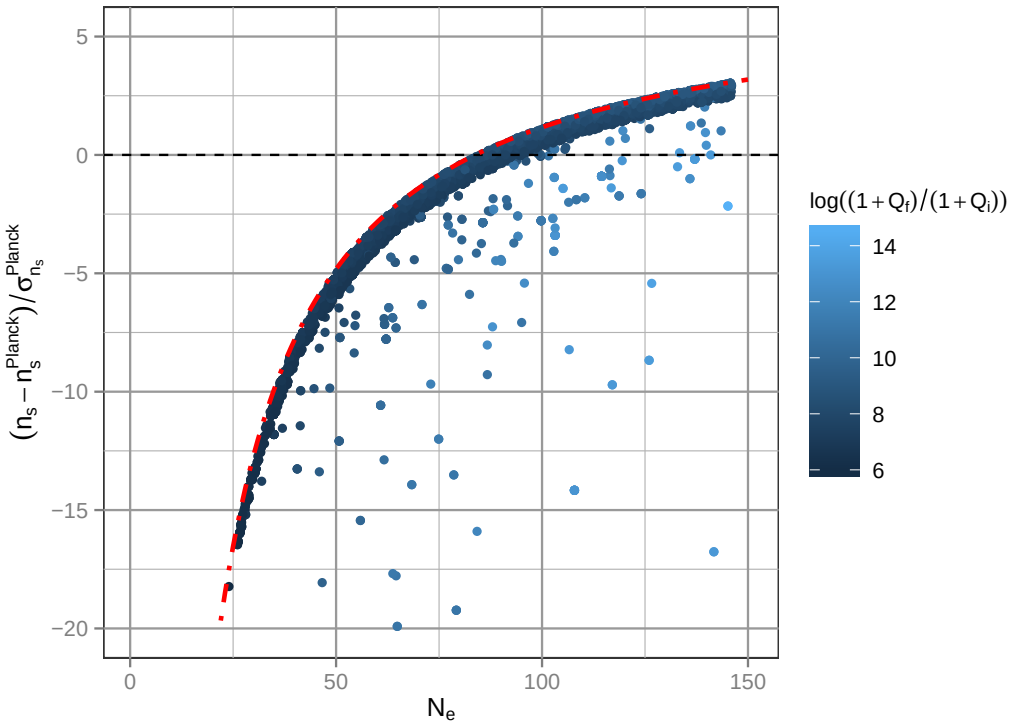

Figure 3.11: Spectral index (in standard deviations from Planck central value) vs e*-folds for low-Q, low-momentum data in the quartic monomial potential. We have selected points with $Q_\mathrm{i} < 10^{-6}$, where the spectral index has the form $n_\mathrm{s} - 1 = -6\epsilon + 2\eta$. The dot-dashed red line indicates the upper limit* (3.27) *on n_s if dissipation is negligible and inflation ends with $\eta = 1 + Q$.*

effectively compresses the inflaton field range and shifts it down to lower field values.

For $Q < 10^{-6}$, our data show the expected behaviour: the spectral index at any given N_e lies below the limit (3.27). For illustration, we include in figure (3.11) our low-momentum, low-Q data for the quartic monomial potential alongside the bound (3.27); this figure represents the low-Q limit of figure (3.7). The width of the densely populated band below the bound is given by the constraint $Q_\mathrm{i} < 10^{-6}$ we have imposed on the data in this plot. Scattered below the band are points with large $(1 + Q_\mathrm{f})/(1 + Q_\mathrm{i})$; for these points, Q changes dramatically over the course of inflation and has a significant impact on the integral (3.25) from the start.

It is interesting to note that, for monomial potentials with exponent $p =$

$\{2, 4, \frac{14}{3}, 10\}$, the low-$Q$ upper limit on n_s enters Planck's 2σ range at $N_\mathrm{e} = \{44, 65, 73, 130\}$, respectively—at least this many e-folds of low-Q warm inflation in the low-momentum regime are necessary for these potentials to produce an observationally-viable spectral index.

For $Q \gtrsim 10^{-3}$, the form of the spectral index (2.110) changes with the coefficients now functions of Q, as illustrated in figure (2.3). In this regime, the bound (3.27) no longer applies, and the slow-roll parameters in the spectral index no longer have their simple cold-inflation coefficients. For $Q > 10$, the coefficients decrease as $1/Q$ while maintaining fixed ratios $(1 : 3 : -\frac{1}{2})$ between the coefficients of ϵ, η, and σ.

3.6 Ideas for Future Work

The code we have developed could be extended in several interesting ways. First and most obvious, it would be straightforward to implement parameter scans in other inflaton potentials, for instance the one used by Shafi and Wickman (2011). It would be interesting to conduct a large-scale survey of single-field warm inflation along the lines of the Bayesian-model-selection study by Martin *et al.* (2013a) and Martin *et al.* (2013b) to assess how inflaton dissipation changes the overall landscape of inflationary model space. The computational obstacles to such a study are great, however. The rate at which our code generates data varies widely between potentials and can be prohibitive; the implementation of more complicated inflaton potentials and the extra parameters associated with them would likely require significantly improved performance.

More realistically, our code could easily be generalised to account for thermal corrections to the inflaton potential (Bastero-Gil *et al.*, 2014b), as well as the effects of viscosity (Bastero-Gil *et al.*, 2011b) and non-negligible inflaton occupation numbers (Bartrum *et al.*, 2014). All of these have already been examined independently for specific models, but our code would be well-suited to a broader study of the effects of these contributions on the parameter space accessible to warm inflation.

A further interesting extension would be the above-mentioned inclusion of a possible era of cold inflation following the end of warm inflation through any means other than the breakdown of slow roll. Such numerical studies could provide

valuable tests for any model-building attempts to remove the cold era entirely.

Ultimately, it would be instructive to assess the strength of evidence for warm over cold inflation. Again, the work of Martin *et al.* (2013b) could serve as a model. There, the authors present an efficient way to calculate the Bayesian evidences for 193 slow-roll single-field models of inflation given the Planck 2013 data. There is a risk that, in a Bayesian model comparison between cold- and warm-inflation implementations of the same inflaton potential, the latter might be put at a disadvantage due to the extra parameter volume necessary to parametrise the dissipation. On the other hand, Martin *et al.* (2013b) summarise the reheating history associated with a given model of cold inflation in just a single parameter $\theta_{\rm reh} = \ln(R)$. Note, however, that their prior is flat in the logarithm of $\theta_{\rm reh}$ between 10^{-46} and 10^{15}; for models with poorly constrained reheating predictions, such a large prior volume represents a significant penalty. If the parameters of warm inflation could be confined, by theoretical insight or by numerical study of the complicated web of constraints, to reasonably small ranges, certain models of warm inflation could conceivably be competitive with equivalent models of cold inflation.

Chapter 4

Conclusions

Warm inflation as an alternative dynamical implementation of exponential early-universe expansion has matured significantly in the twenty years since its inception. With dissipative inflationary dynamics derived from a thermal-field-theory description of the fluctuation–dissipation dynamics of a scalar field coupled to a thermal bath, warm inflation rests on sound theoretical footing. In recent years, further studies have investigated more and more aspects of the basic mechanism, so that it is now possible to account for the effects of thermal corrections to the inflaton potential, as well as the influence of viscosity and non-vanishing inflaton occupation numbers on the spectrum of density perturbations. There can be no doubt that warm inflation as a more general implementation of inflaton-field dynamics, allowing for the possibility of a radiation bath being produced and sustained alongside the exponential expansion, opens up exciting new possibilities for inflationary model building.

In this thesis, we have focused on low-temperature warm inflation using a two-stage decay model; our inflaton therefore couples to the light fields of the radiation bath only via heavy mediator fields χ. We were interested in finding parameter regimes where the number N_χ of such mediator fields can be reduced compared to previous studies. To that end, we used the general expression for the low-temperature dissipation coefficient. Previous studies have focussed on the low-momentum regime alone, where dissipation is mediated by virtual χ modes; here, we have included the pole regime, where real, on-shell χ modes dominate instead. The pole term had previously been ignored because on-shell production of χ modes in the low-T regime suffers from Boltzmann suppression

by a factor $\exp(-m_\chi/T)$ and was therefore thought to be negligible. It has been shown, however, that for sufficiently small values of the effective coupling $\hat{h}$ between mediators and light fields, the pole contribution can significantly enhance dissipation. It has to be noted that $\hat{h}$ cannot be lowered arbitrarily, however; consistency of the approximations made when deriving the dissipation coefficient requires that the system remain close to thermal equilibrium. This implies that the decay rate of mediators into light degrees of freedom be greater than the Hubble rate, which imposes a lower limit on $\hat{h}$, as we described at the end of section 2.4.

One of the motivations for this thesis was to investigate whether the enhanced dissipation and the different parametric dependences in the pole regime would allow for warm inflation with a smaller number of mediator fields. In the low-momentum regime, the full set of constraints needed for a successful period of warm inflation typically requires $N_\chi \sim \mathcal{O}(10^6)$. It is the main result of this work that pole-dominated dissipation can indeed make lower-N_χ ranges accessible to warm inflation. We showed in figure (3.8) that the pole and the low-momentum regimes occupy distinct regions in the N_χ–g plane, where g is the coupling between the inflaton and the χ fields. Pole-dominated solutions prefer smaller couplings around $g \sim \mathcal{O}(10^{-6} \dots 10^{-4})$ compared to typical values $g \sim \mathcal{O}(10^{-3} \dots 1)$ in the low-momentum regime. We also found that, as we had hoped, the pole regime can work with fewer mediator fields; where low-momentum dissipation requires $N_\chi > \mathcal{O}(10^6)$, the pole contribution can reach values as low as $N_\chi \sim \mathcal{O}(10^4)$. This regime holds great promise for future numerical and analytical work trying to reduce the field content of warm inflation even further.

Additionally, the pole regime contains some of the most observationally promising regions of warm-inflationary parameter space in our data. In equation (2.110), we gave an expression for the spectral index of the primordial power spectrum resulting from warm inflation with a general dissipation coefficient in the weak dissipative regime, and we used this to compare our numerical results to CMB observations. We showed in figure (3.5) that not only is the pole regime populated with points that require low N_χ, many of these points are in excellent agreement with Planck constraints on the spectral tilt and the tensor-to-scalar ratio. The quadratic hilltop potential is particularly noteworthy. Not only does it achieve the lowest values of N_χ in our sample, precisely those points with smallest

N_χ also lie in the preferred range for n_s and exhibit very small values of r.

We showed in figure (3.6) that pole-dominated dissipation can also bring chaotic potentials back into agreement with observations, all the while requiring fewer mediator fields than low-momentum-dominated dissipation. It has previously been shown that the quartic chaotic potential is consistent with Planck constraints in weak dissipative warm inflation that includes nearly-thermal inflaton occupation numbers at horizon crossing (Bartrum *et al.*, 2014); here, we accomplish the same with negligible inflaton occupation numbers.

This work has shown that pole-dominated inflaton dissipation is well worth studying for the favourable parameter regions it opens up and the better agreement with CMB observation it allows. Next to further analytical work, codes like ours will certainly be a valuable tool for advancing our understanding of the dynamics of warm inflation.

Bibliography

Abbott, L. F., Farhi, E., and Wise, M. B., *Particle Production in the New Inflationary Cosmology*, Phys. Lett. **B117** (1982):29. *(Cited on page 26)*

Ade, P. *et al.* (BICEP2, Planck), *Joint Analysis of BICEP2/KeckArray and Planck Data*, Phys. Rev. Lett. **114** (2015a):101301, arXiv:1502.00612. *(Cited on page 25)*

Ade, P. *et al.* (Planck Collaboration), *Planck 2015 results. XIII. Cosmological parameters* (2015b), arXiv:1502.01589. *(Cited on pages 4, 6, 9, 24, and 75)*

Ade, P. A. R. *et al.* (Planck), *Planck 2015 results. XX. Constraints on inflation* (2015c), arXiv:1502.02114. *(Cited on pages ix, x, 22, 25, 76, 77, 78, and 80)*

Aitchison, I. J., *Supersymmetry and the MSSM: An Elementary introduction* (2005), arXiv:hep-ph/0505105. *(Cited on page 17)*

Albrecht, A. and Steinhardt, P. J., *Cosmology for Grand Unified Theories with Radiatively Induced Symmetry Breaking*, Phys.Rev.Lett. **48** (1982):1220–1223. *(Cited on page 15)*

Albrecht, A., *et al.*, *Reheating an Inflationary Universe*, Phys. Rev. Lett. **48** (1982):1437. *(Cited on page 26)*

Albrecht, A., *et al.*, *Causality and the microwave background*, Phys. Rev. Lett. **76** (1996):1413–1416, arXiv:astro-ph/9505030. *(Cited on page 24)*

Bartrum, S., Berera, A., and Rosa, J. G., *Gravitino cosmology in supersymmetric warm inflation*, Phys. Rev. **D86** (2012):123525, arXiv:1208.4276. *(Cited on page 33)*

Bartrum, S., *et al.*, *The importance of being warm (during inflation)*, Phys.Lett. **B732** (2014):116–121, arXiv:1307.5868. *(Cited on pages 26, 34, 62, 63, 65, 76, 85, and 89)*

Bassett, B. A., Tsujikawa, S., and Wands, D., *Inflation dynamics and reheating*, Rev.Mod.Phys. **78** (2006):537–589, arXiv:astro-ph/0507632. *(Cited on pages 26, 28, and 30)*

Bastero-Gil, M. and Berera, A., *Warm inflation model building*, Int.J.Mod.Phys. **A24** (2009):2207–2240, arXiv:0902.0521. *(Cited on page 83)*

Bastero-Gil, M., Berera, A., and Kronberg, N., *Exploring the Parameter Space of Warm-Inflation Models* (2015), arXiv:1509.07604. *(Cited on pages ix and 63)*

Bastero-Gil, M., Berera, A., and Ramos, R. O., *Dissipation coefficients from scalar and fermion quantum field interactions*, JCAP **1109** (2011a):033, arXiv:1008.1929. *(Cited on pages 56 and 57)*

Bastero-Gil, M., Berera, A., and Ramos, R. O., *Shear viscous effects on the primordial power spectrum from warm inflation*, JCAP **1107** (2011b):030, arXiv:1106.0701. *(Cited on pages 34, 62, and 85)*

Bastero-Gil, M., Berera, A., and Rosa, J. G., *Warming up brane-antibrane inflation*, Physical Review D **84** (2011c)(10):103503, arXiv:1103.5623. *(Cited on page 52)*

Bastero-Gil, M., King, S., and Shafi, Q., *Supersymmetric Hybrid Inflation with Non-Minimal Kahler potential*, Phys.Lett. **B651** (2007):345–351, arXiv:hep-ph/0604198. *(Cited on pages 18, 20, and 21)*

Bastero-Gil, M., *et al.*, *Warm baryogenesis*, Phys. Lett. **B712** (2012):425–429, arXiv:1110.3971. *(Cited on page 35)*

Bastero-Gil, M., *et al.*, *General dissipation coefficient in low-temperature warm inflation*, JCAP **1301** (2013):016, arXiv:1207.0445. *(Cited on pages ix, x, 34, 55, 56, 57, 58, 74, 75, and 76)*

Bastero-Gil, M., *et al.*, *Cosmological fluctuations of a random field and radiation fluid*, JCAP **1405** (2014a):004, arXiv:1401.1149. *(Cited on pages 34, 62, and 63)*

Bastero-Gil, M., *et al.*, *Delaying the waterfall transition in warm hybrid inflation*, JCAP **1403** (2014b):023, arXiv:1312.2961. *(Cited on pages 54 and 85)*

Bastero-Gil, M., *et al.*, *Observational implications of mattergenesis during inflation*, JCAP **1410** (2014c)(10):053, arXiv:1404.4976. *(Cited on page 76)*

Baumann, D., *TASI Lectures on Inflation* (2009), arXiv:0907.5424. *(Cited on pages 8 and 12)*

Bellac, M., *Thermal Field Theory*, Cambridge Monographs on Mathematical Physics, Cambridge University Press, 1996. *(Cited on page 44)*

Berera, A., *Warm inflation*, Phys.Rev.Lett. **75** (1995):3218–3221, arXiv:astro-ph/9509049. *(Cited on pages 32 and 36)*

Berera, A., *Thermal properties of an inflationary universe*, Phys. Rev. **D54** (1996):2519–2534, arXiv:hep-th/9601134. *(Cited on pages 32 and 42)*

Berera, A., *Interpolating the stage of exponential expansion in the early universe: A Possible alternative with no reheating*, Phys. Rev. **D55** (1997):3346–3357, arXiv:hep-ph/9612239. *(Cited on pages 31 and 33)*

Berera, A., *Warm inflation at arbitrary adiabaticity: A Model, an existence proof for inflationary dynamics in quantum field theory*, Nucl.Phys. **B585** (2000):666–714, arXiv:hep-ph/9904409. *(Cited on page 61)*

Berera, A. and Fang, L.-Z., *Thermally induced density perturbations in the inflation era*, Phys.Rev.Lett. **74** (1995):1912–1915, arXiv:astro-ph/9501024. *(Cited on pages 32, 36, and 61)*

Berera, A., Gleiser, M., and Ramos, R. O., *Strong dissipative behavior in quantum field theory*, Phys. Rev. **D58** (1998):123508, arXiv:hep-ph/9803394. *(Cited on pages 33 and 39)*

Berera, A., Gleiser, M., and Ramos, R. O., *A First principles warm inflation model that solves the cosmological horizon / flatness problems*, Phys. Rev. Lett. **83** (1999):264–267, arXiv:hep-ph/9809583. *(Cited on pages 33 and 39)*

Berera, A., Moss, I. G., and Ramos, R. O., *Local Approximations for Effective Scalar Field Equations of Motion*, Phys. Rev. **D76** (2007):083520, arXiv:0706.2793. *(Cited on page 49)*

Berera, A., Moss, I. G., and Ramos, R. O., *Warm Inflation and its Microphysical Basis*, Rept.Prog.Phys. **72** (2009):026901, arXiv:0808.1855. *(Cited on pages 35, 51, and 56)*

Berera, A. and Ramos, R. O., *The Affinity for scalar fields to dissipate*, Phys. Rev. **D63** (2001):103509, arXiv:hep-ph/0101049. *(Cited on pages 34, 49, and 50)*

Bezrukov, F. and Shaposhnikov, M., *The Standard Model Higgs boson as the inflaton*, Phys.Lett. **B659** (2008):703–706, arXiv:0710.3755. *(Cited on page 17)*

Brout, R., Englert, F., and Gunzig, E., *The Creation of the Universe as a Quantum Phenomenon*, Annals Phys. **115** (1978):78. *(Cited on page 7)*

Bueno Sanchez, J. C., *et al.*, *The gravitino problem in supersymmetric warm inflation*, JCAP **1103** (2011):020, arXiv:1011.2398. *(Cited on page 33)*

Burgess, C. P., *et al.*, *The Inflationary brane anti-brane universe*, JHEP **07** (2001):047, arXiv:hep-th/0105204. *(Cited on page 77)*

Caldwell, R. R., Kamionkowski, M., and Weinberg, N. N., *Phantom Energy and Cosmic Doomsday*, Phys. Rev. Lett. **91** (2003):071301, arXiv:astro-ph/0302506. *(Cited on page 6)*

Chevallier, M. and Polarski, D., *Accelerating universes with scaling dark matter*, Int. J. Mod. Phys. **D10** (2001):213–224, arXiv:gr-qc/0009008. *(Cited on page 6)*

Coleman, S. R. and Weinberg, E. J., *Radiative Corrections as the Origin of Spontaneous Symmetry Breaking*, Phys.Rev. **D7** (1973):1888–1910. *(Cited on pages 19 and 54)*

Copeland, E. J., *et al.*, *False vacuum inflation with Einstein gravity*, Phys.Rev. **D49** (1994):6410–6433, arXiv:astro-ph/9401011. *(Cited on pages 16 and 18)*

de Sitter, W., *On the relativity of inertia. Remarks concerning Einstein's latest hypothesis*, Koninklijke Nederlandse Akademie van Weteschappen Proceedings Series B Physical Sciences **19** (1917):1217–1225. *(Cited on page 5)*

Dodelson, S., *Coherent phase argument for inflation*, AIP Conf.Proc. **689** (2003):184–196, arXiv:hep-ph/0309057. *(Cited on pages ix and 23)*

Dolgov, A. and Kirilova, D., *On particle creation by a time-dependent scalar field*, Sov.J.Nucl.Phys. **51** (1990):172–177. *(Cited on page 27)*

Dolgov, A. D. and Linde, A. D., *Baryon Asymmetry in Inflationary Universe*, Phys. Lett. **B116** (1982):329. *(Cited on page 26)*

Drees, M., *An Introduction to supersymmetry* (1996), arXiv:hep-ph/9611409. *(Cited on page 17)*

Dvali, G., Shafi, Q., and Schaefer, R. K., *Large scale structure and supersymmetric inflation without fine tuning*, Phys.Rev.Lett. **73** (1994):1886–1889, arXiv:hep-ph/9406319. *(Cited on page 19)*

Eisenstein, D. J. *et al.* (SDSS), *Detection of the Baryon Acoustic Peak in the Large-Scale Correlation Function of SDSS Luminous Red Galaxies*, Astrophys. J. **633** (2005):560–574, arXiv:astro-ph/0501171. *(Cited on page 24)*

Fang, L. Z., *Entropy Generation in the Early Universe by Dissipative Processes Near the Higgs' Phase Transitions*, Phys. Lett. **B95** (1980):154–156. *(Cited on pages 7 and 32)*

Finelli, F., *et al.*, *Single-field inflation constraints from CMB and SDSS data*, JCAP **1004** (2010):011, arXiv:0912.0522. *(Cited on page 15)*

Frieman, J., Turner, M., and Huterer, D., *Dark Energy and the Accelerating Universe*, Ann. Rev. Astron. Astrophys. **46** (2008):385–432, arXiv:0803.0982. *(Cited on pages ix and 7)*

Graham, C. and Moss, I. G., *Density fluctuations from warm inflation*, JCAP **0907** (2009):013, arXiv:0905.3500. *(Cited on pages 34 and 61)*

Green, D., *et al.*, *Trapped inflation*, Physical Review D - Particles, Fields, Gravitation and Cosmology **80** (2009)(6):32, arXiv:0902.1006. *(Cited on page 30)*

Guth, A. H., *The Inflationary Universe: A Possible Solution to the Horizon and Flatness Problems*, Phys.Rev. **D23** (1981):347–356. *(Cited on pages 7 and 14)*

Hall, L., Moss, I., and Berera, A., *Scalar perturbation spectra from warm inflation*, Physical Review D **69** (2004)(8):083525, arXiv:0305015. *(Cited on page 37)*

Hall, L. M. H. and Moss, I. G., *Thermal effects on pure and hybrid inflation*, Phys. Rev. **D71** (2005):023514, arXiv:hep-ph/0408323. *(Cited on pages 54 and 55)*

Harrison, E. R., *Fluctuations at the threshold of classical cosmology*, Phys. Rev. **D1** (1970):2726–2730. *(Cited on page 24)*

Hiebert, K. L. and Shampine, L. F., *Implicitly defined output points for solutions of ODEs*, Tech. rep., Sandia Labs., Albuquerque, NM (USA), 1980. *(Cited on page 72)*

Hindmarsh, A. C., *et al.*, *SUNDIALS: Suite of nonlinear and differential/algebraic equation solvers*, ACM Transactions on Mathematical Software (TOMS) **31** (2005)(3):363–396. *(Cited on page 71)*

Hindmarsh, M. B. and Kibble, T. W. B., *Cosmic strings*, Rept. Prog. Phys. **58** (1995):477–562, arXiv:hep-ph/9411342. *(Cited on page 24)*

Hubbard, J., *Calculation of Partition Functions*, Phys. Rev. Lett. **3** (1959):77–78. *(Cited on page 47)*

Kinney, W. H., *et al.*, *Latest inflation model constraints from cosmic microwave background measurements*, Phys.Rev. **D78** (2008):087302, arXiv:0805.2966. *(Cited on page 15)*

Kofman, L., Linde, A. D., and Starobinsky, A. A., *Reheating after inflation*, Phys. Rev. Lett. **73** (1994):3195–3198, arXiv:hep-th/9405187. *(Cited on page 27)*

Kofman, L., Linde, A. D., and Starobinsky, A. A., *Towards the theory of reheating after inflation*, Phys.Rev. **D56** (1997):3258–3295, arXiv:hep-ph/9704452. *(Cited on page 29)*

Kofman, L., *et al.*, *Beauty is Attractive: Moduli Trapping at Enhanced Symmetry Points* **05** (2004):50, arXiv:0403001. *(Cited on page 30)*

Krauss, L. M. and Scherrer, R. J., *The return of a static universe and the end of cosmology*, General Relativity and Gravitation **39** (2007):1545–1550, arXiv:0704.0221. *(Cited on page 6)*

Kubo, R., *The fluctuation-dissipation theorem*, Reports on Progress in Physics **29** (1966)(1):255. *(Cited on pages 40 and 42)*

Lazarides, G., *Inflationary cosmology*, Lect.Notes Phys. **592** (2002):351–391, arXiv:hep-ph/0111328. *(Cited on pages 18 and 19)*

Liddle, A. R., *Inflation as the unique causal mechanism for generating density perturbations on scales well above the Hubble radius*, Phys. Rev. **D51** (1995):5347–5351, arXiv:astro-ph/9410083. *(Cited on page 24)*

Linde, A. D., *A New Inflationary Universe Scenario: A Possible Solution of the Horizon, Flatness, Homogeneity, Isotropy and Primordial Monopole Problems*, Phys.Lett. **B108** (1982):389–393. *(Cited on page 15)*

Linde, A. D., *Chaotic Inflation*, Phys.Lett. **B129** (1983):177–181. *(Cited on page 15)*

Linde, A. D., *Axions in inflationary cosmology*, Phys.Lett. **B259** (1991):38–47. *(Cited on page 16)*

Linde, A. D., *Particle physics and inflationary cosmology* (2005), arXiv:hep-th/0503203. *(Cited on page 8)*

Linde, A. D. and Riotto, A., *Hybrid inflation in supergravity*, Phys.Rev. **D56** (1997):1841–1844, arXiv:hep-ph/9703209. *(Cited on page 18)*

Linder, E. V., *Exploring the expansion history of the universe*, Phys. Rev. Lett. **90** (2003):091301, arXiv:astro-ph/0208512. *(Cited on page 6)*

Lyth, D. H., *What would we learn by detecting a gravitational wave signal in the cosmic microwave background anisotropy?*, Phys.Rev.Lett. **78** (1997):1861–1863, arXiv:hep-ph/9606387. *(Cited on pages 14 and 65)*

Lyth, D. H. and Liddle, A. R., *The primordial density perturbation: Cosmology, inflation and the origin of structure*, 2009. *(Cited on page 14)*

Lyth, D. H. and Riotto, A., *Particle physics models of inflation and the cosmological density perturbation*, Phys.Rept. **314** (1999):1–146, arXiv:hep-ph/9807278. *(Cited on pages 12 and 14)*

Maartens, R., *Causal thermodynamics in relativity* (1996), arXiv:astro-ph/9609119. *(Cited on page 62)*

Martin, J., Ringeval, C., and Vennin, V., *Encyclopaedia Inflationaris* (2013a):368, arXiv:1303.3787. *(Cited on page 85)*

Martin, J., Ringeval, C., and Vennin, V., *Observing the Inflationary Reheating* (2014), arXiv:1410.7958. *(Cited on page 31)*

Martin, J., *et al.*, *The Best Inflationary Models After Planck* (2013b):62, arXiv:1312.3529. *(Cited on pages 85 and 86)*

Martin, S. P., *A Supersymmetry primer* (1997), arXiv:hep-ph/9709356. *(Cited on page 17)*

Moss, I. G., *Primordial Inflation With Spontaneous Symmetry Breaking*, Phys. Lett. **B154** (1985):120. *(Cited on page 32)*

Moss, I. G. and Xiong, C., *Dissipation coefficients for supersymmetric inflatonary models* (2006), arXiv:hep-ph/0603266. *(Cited on pages 34, 49, 50, 51, and 58)*

Moss, I. G. and Xiong, C., *On the consistency of warm inflation*, Journal of Cosmology and Astroparticle Physics **2008** (2008)(11):023, arXiv:0808.0261. *(Cited on pages 38 and 61)*

Nilles, H. P., *Supersymmetry, Supergravity and Particle Physics*, Phys.Rept. **110** (1984):1–162. *(Cited on pages 17 and 20)*

Peebles, P. J. E. and Yu, J. T., *Primeval adiabatic perturbation in an expanding universe*, Astrophys. J. **162** (1970):815–836. *(Cited on page 24)*

Perlmutter, S. *et al.* (Supernova Cosmology Project), *Measurements of Omega and Lambda from 42 high redshift supernovae*, Astrophys.J. **517** (1999):565–586, arXiv:astro-ph/9812133. *(Cited on page 6)*

Rehman, M. U., Shafi, Q., and Wickman, J. R., *Supersymmetric Hybrid Inflation Redux*, Phys.Lett. **B683** (2010):191–195, arXiv:0908.3896. *(Cited on page 20)*

Riess, A. G. *et al.* (Supernova Search Team), *Observational evidence from supernovae for an accelerating universe and a cosmological constant*, Astron.J. **116** (1998):1009–1038, arXiv:astro-ph/9805201. *(Cited on page 6)*

Sakharov, A. D., *Violation of CP Invariance, c Asymmetry, and Baryon Asymmetry of the Universe*, Pisma Zh. Eksp. Teor. Fiz. **5** (1967):32–35, [Usp. Fiz. Nauk161,61(1991)]. *(Cited on page 35)*

Sato, K., *Cosmological Baryon Number Domain Structure and the First Order Phase Transition of a Vacuum*, Phys. Lett. **B99** (1981):66–70. *(Cited on page 7)*

Serban, R. and Hindmarsh, A. C., *CVODES: the sensitivity-enabled ODE solver in SUNDIALS*, in *ASME 2005 International Design Engineering Technical Conferences and Computers and Information in Engineering Conference*, American Society of Mechanical Engineers, 2005 257–269. *(Cited on page 71)*

Shafi, Q. and Wickman, J. R., *Observable Gravity Waves From Supersymmetric Hybrid Inflation*, Phys.Lett. **B696** (2011):438–446, arXiv:1009.5340. *(Cited on pages 18 and 85)*

Shtanov, Y., Traschen, J. H., and Brandenberger, R. H., *Universe reheating after inflation*, Phys. Rev. **D51** (1995):5438–5455, arXiv:hep-ph/9407247. *(Cited on page 27)*

Smoot, G. F., *et al.*, *Structure in the COBE differential microwave radiometer first year maps*, Astrophys.J. **396** (1992):L1–L5. *(Cited on page 9)*

Starobinsky, A. A., *A New Type of Isotropic Cosmological Models Without Singularity*, Phys.Lett. **B91** (1980):99–102. *(Cited on pages 7, 14, and 25)*

Stratonovich, R., *On a method of calculating quantum distribution functions* **2** (1957):416. *(Cited on page 47)*

Traschen, J. H. and Brandenberger, R. H., *Particle Production During Out-of-equilibrium Phase Transitions*, Phys. Rev. **D42** (1990):2491–2504. *(Cited on page 27)*

Vilenkin, A., *Cosmic Strings and Domain Walls*, Phys. Rept. **121** (1985):263–315. *(Cited on page 24)*

Vilenkin, A. and Shellard, E. P. S., *Cosmic Strings and Other Topological Defects*, Cambridge University Press, 2000. *(Cited on page 24)*

Watari, T. and Yanagida, T., *N=2 supersymmetry in a hybrid inflation model*, Phys.Lett. **B499** (2001):297–304, arXiv:hep-ph/0011389. *(Cited on page 21)*

Weinberg, S., *Gravitation and Cosmology*, John Wiley & Sons, 1972. *(Cited on page 3)*

Weinberg, S., *The cosmological constant problem*, Rev. Mod. Phys. **61** (1989):1–23. *(Cited on page 6)*

Weinberg, S., *The quantum theory of fields. Vol. 3: Supersymmetry*, 2000. *(Cited on page 17)*

Wess, J. and Bagger, J., *Supersymmetry and supergravity*, 1992. *(Cited on page 17)*

Yokoyama, J. and Linde, A. D., *Is warm inflation possible?*, Phys. Rev. **D60** (1999):083509, arXiv:hep-ph/9809409. *(Cited on pages 33 and 39)*

Yokoyama, J. and Maeda, K.-i., *On the Dynamics of the Power Law Inflation Due to an Exponential Potential*, Phys. Lett. **B207** (1988):31. *(Cited on page 32)*

Zeldovich, Y., Kobzarev, I. Y., and Okun, L., *Cosmological Consequences of the Spontaneous Breakdown of Discrete Symmetry*, Zh.Eksp.Teor.Fiz. **67** (1974):3–11. *(Cited on page 9)*

Zeldovich, Ya. B., *A Hypothesis, unifying the structure and the entropy of the universe*, Mon. Not. Roy. Astron. Soc. **160** (1972):1P–3P. *(Cited on page 24)*

Zimdahl, W., *'Understanding' cosmological bulk viscosity*, Monthly Notices of the Royal Astronomical Society **280** (1996):1239–1243. *(Cited on page 62)*